STRUCTURAL SYSTEMS
RESEARCH PROJECT

Report No.
SSRP 09-02
Final

Experimental evaluation of the in-plane seismic behavior of store-front window systems

By

C. Eva and T. C. Hutchinson

Final Report.

April 11, 2009

Department of Structural Engineering
University of California, San Diego
La Jolla, California 92093-0085

University of California, San Diego

Department of Structural Engineering

Structural Systems Research Project

Report No. SSRP 09-02

Experimental evaluation of the in-plane seismic behavior of store-front window systems

By

C. Eva

Graduate Researcher

T. C. Hutchinson

Associate Professor

Submitted to

Department of Structural Engineering

University of California, San Diego

La Jolla, California 92093-0085

April 11, 2009

DISCLAIMER

The opinions, recommendations and conclusions contained within this report are solely those of the authors, and do not necessarily reflect the views or policies of the project sponsors. This report does not constitute a standard, specification, or regulation.

ABSTRACT

Glass window systems have been shown to suffer significant damage during earthquake loading, resulting in the potential for human injuries and significant economic losses. Film-coated windows are recognized to hold potential for mitigating these adverse affects. However, despite its potential, limited study has been conducted to evaluate the benefits of film-coated window systems under seismic loading. Of those studies undertaken, the focus has been on anchored film, which is less common in practice. Furthermore, no thorough study of the effects of loading histories on window system performance as related to envisioned scenario earthquakes, has been performed to-date. It is unclear if previously used loading protocols are representative of demands induced on window systems used in buildings in the California seismic environment. Finally, previous studies have been limited in terms of their variation of window system geometry, with the largest experimental studies focused on a single 0.83 aspect ratio (height/width) specimen.

In this work, three variables of interest were studied through in-plane seismic racking experiments of store-front window systems: (i) loading protocol, (ii) window film type and attachment, and (iii) aspect ratio. The baseline window system was a 5’x5’ unit, constructed of ¼” annealed single pane glass supported by an aluminum frame, with detailing typical of mid-rise (store-front) window systems. This report presents the overall experimental program, the identified damage modes and associated drift limits, and trends associated with variation of the aforementioned test variables.

ACKNOWLEDGEMENTS

The authors wish to gratefully acknowledge the financial support and technical guidance extended by the Association of Industrial Metallizers, Coaters and Laminators (AIMCAL) – Window Film Committee, where Mr. Darrell Smith is the program manager and Mr. Andres Vasquez is the technical adviser. Dr. George Mavroeidis assisted with processing the ground motions and conducted the seismic hazard analysis for the load protocol study. In addition, the writers wish to acknowledge the testing assistance of the Charles Lee Powell Laboratory staff and in particular Dr. Christopher Latham, Mr. Andrew Gunthardt, and Mr. Charley Stearns. This report contributes to the Masters Thesis of the first author, Mr. Charles Eva, where Professor Tara Hutchinson served as the chair. Helpful suggestions of the committee members, Professors José Restrepo and Chia-Ming Uang, are greatly appreciated.

TABLE OF CONTENTS

DISCLAIMER iii

ABSTRACT viv

ACKNOWLEDGEMENTS ix

TABLE OF CONTENTS xiii

LIST OF FIGURES iv

LIST OF TABLES iv

Chapter 1: Introduction 1

1.1 Motivation 1

1.2 Previous work and State-of-Practice 2

1.2.1 Damage States 8

1.2.2 Design Code Prescriptions 8

1.3 Scope of this Work 9

1.3.1 Report organization 11

Chapter 2: Experimental Program 12

2.1 Small Scale Pilot Tests 12

2.1.1 Introduction and Scope 12

2.1.2 Out of Plane Test 12

2.1.3 In-plane tension tests 13

2.1.4 Camera setup 14

2.1.5 Results 14

2.1.6 Physical observations 16

2.1.7 Measured Results 17

2.1.8 Comparison to Previous Work 18

2.1.9 Small Scale Test Conclusions 19
2.2 Full Scale Test Setup 19
2.3 Test Matrix 22
2.3.1 Loading Protocol (LP) Series 24
2.3.2 Window Film (WF) Series 25
2.3.3 Aspect Ratio (AR) Series 25
2.4 Specimen Assembly and Construction 25
2.4.1 Window Film Installation 27
2.4.3 Wet Glazing Attachment System Installation 27
2.5 Instrumentation 29
2.5.1 Instrumentation Support Frames 30
2.5.2 Strain Gauge Setup 32
2.5.3 Accelerometer Setup 32
2.5.4 Load Cell Setup 33
2.5.5 Camera Setup 33
2.6 Load protocols 36
2.6.1 Monotonic (static) Load Protocol 36
2.6.2 Crescendo (Dynamic) Load Protocol 36
2.6.3 FEMA 461(quasi-static) Load Protocol 37
2.6.4 Mid- and Low-Rise protocol 38
Chapter 3: Experimental Results 40
3.1 Introduction 40
3.2 Damage State Observations 40
3.3 Global Response 44
3.3.1 Individual Specimen Load 46

Chapter 4: Results Analysis 51
4.1 Correlation between Small Scale and Full Scale Testing 51
4.2 Effect of Film and Attachment System 53
4.3 Effect of Load Protocol 58
4.4 Effect of Aspect Ratio 61
4.5 Glass Freedom 64
4.6 Comparison to Previous Work 65
Chapter 5: Conclusions 68
5.1 Motivation 68
5.2 Scope of Work 69
5.3 Findings 70
5.3.1 Identified Damage States 70
5.3.3 Film and Attachment System Effects 71
5.3.4 Aspect Ratio effects 73
5.4 Future Work 73
References 75
Appendices 78
Appendix A: Drawings and Details 78
Appendix B: Load-Deflection Response Curves 104
Appendix C: Summary of Previous Experiments 112
Appendix D: Glass Specifications 118
Appendix E: Calculations 120

LIST OF FIGURES

Figure 1.1 Damage to window systems observed during the Palm springs, 1986 earthquake. (Courtesy of the National Information Service for Earthquake Engineering, EERC, University of California, Berkeley)..... 1
Figure 1.2 Damage to window systems observed during the Puget Sound, Washington, 1965 earthquake. (Courtesy of the National Information Service for Earthquake Engineering, EERC, University of California, Berkeley) 2
Figure 1.3 Facility at UMR used for dynamic racking tests of full-size curtain wall panels (Courtesy of Behr, 1996). 4
Figure 1.4 Crescendo protocol used at UMR and Penn State for testing of full-size curtain wall panels and adopted by AAMA (2001b) (Behr, 1996)..... 5
Figure 1.5 Serviceability Damage State: Minor Cracking..... 8
Figure 1.6 Ultimate Damage State: Extensive Cracking 8
Figure 2.1 - Panel 0 - Crack tracking through shadows..... 12
Figure 2.2 – 12”x12” Tension Test Setup..... 13
Figure 2.3 - Panel 1: 0mil Film..... 14
Figure 2.4 - Panel 2: 0mil Film..... 15
Figure 2.5 - Panel 3: 0mil Film..... 15
Figure 2.6 - Panel 4: 2mil Film..... 15
Figure 2.7 - Panel 5: 2mil Film..... 16
Figure 2.8 - Panel 6: 2mil Film..... 16
Figure 2.9 - Panel 7: 8mil Film..... 16
Figure 2.10 - Force vs. displacement and stiffness vs. time profiles..... 18
Figure 2.11 System elevation view..... 20
Figure 2.12 5'x5' window size setup 20
Figure 2.13 4'x8' window size setup 21
Figure 2.14 6'x4' window size setup 21
Figure 2.15 Store-Front Window Detail 26
Figure 2.16 Rubber blocks in window units: (a) schematic of general locations and (b) photograph of rubber stop. 26

Figure 2.17 Window film Installation 27
Figure 2.18 Wet Glazing Attachment System Installation 28
Figure 2.19 Wet glazing attachment system detail 29
Figure 2.20 Elevation view of potentiometer, accelerometer and inclinometer setup 30
Figure 2.21 Drill and tap to attach potentiometers (D03, D05, D06) 31
Figure 2.22 Cables installed on D17 and D18 for vibration and deflection reinforcement 31
Figure 2.23 Aluminum angle glued to reaction frame and table for accelerometer installation .. 32
Figure 2.24 Load cell installation setup 33
Figure 2.25 Basler camera placement 34
Figure 2.26 Video camera placement 35
Figure 2.27 Two inch square grid pattern spray painted into each corner of the glass to aid damage tracking 35
Figure 2.28 Overall test setup (two 5'x5' specimen setup) 36
Figure 2.29 Crescendo load protocol 37
Figure 2.30 FEMA 461 drift-sensitive load protocol 38
Figure 2.31 Mid-Rise Load Protocol (Hutchinson et al., 2008) 39
Figure 2.32 Low-Rise Load Protocol (Hutchinson et al., 2008) 39
Figure 3.1 (SDS-1) Gasket Damage and displacement 41
Figure 3.2 (SDS-2) Minor Cracking 41
Figure 3.3 (SDS-3) Wet Glazing Attachment System detachment 42
Figure 3.4 (UDS-1) Extensive glass cracking 43
Figure 3.5 (UDS-2) Glass Fallout 43
Figure 3.6 Global response from tests (a) Monotonic 4 and (b) Crescendo 3 –Two-5'x5' specimens with 2mil of film unattached. 45
Figure 3.7 Global response from tests (a) Jian IV (*low-rise load protocol*) and (b) NewLP 1 (*mid-rise load protocol*) - 5'x5' specimen with 2mil of film unattached 45
Figure 3.8 Global response plot from test FEMA 2 (FEMA 461 load protocol) - 5'x5' specimen with 2mil of film unattached 46
Figure 3.9 System Load versus Drift Ratio % (Two 5'x5' specimens both with 4 mil film) 46
Figure 3.10 Load per panel versus drift ratio: (a) Load in north panel. (b) Load in south panel overlaid with system load envelope (5'x5' specimens – 4 mil film, test FEMA 2**)** 47

Figure 3.11 Equal load distribution when table is moving in positive direction 48
Figure 3.12 Unequal load distribution when table is moving in positive direction. (a) North panel with larger force contribution. (b) South panel with larger force contribution**.** 48
Figure 3.13 Detail of section I for members A-D and E-H 49
Figure 3.14 South Panel falls from system at 7.7% drift ratio (two 5'x5'specimens both without film, test Monotonic 11) 50
Figure 4.1 Small Scale at failure displacement– Typical Failure Mode: Buckling (12"x12" specimen with 2 mil film) 51
Figure 4.2 Full Scale at failure displacement – Typical Failure Mode: Buckling (5'x5' specimen with 8 mil film – un-attached) 51
Figure 4.3 Correlation of Load between small scale testing and full scale testing (AR: 1.0 - Monotonic Load) 53
Figure 4.4 Effects of Film on all applicable damage states (all 5'x5' specimens subjected to the Monotonic load protocol) 54
Figure 4.5 Effects of attachment system on the secant stiffness at specified drift ratios (all 5'x5' specimens subjected to the Monotonic load protocol)..... 55
Figure 4.6 Effects of film and attachment system on serviceability limit states: (a) gasket damage and (b) first crack (AR 1.0 specimens subjected to the FEMA 461 load protocol)..... 56
Figure 4.7 Effects of film on attachment system failure (AR 1.0 specimens subjected to the FEMA 461 load protocol) 56
Figure 4.8 Effects of film and attachment system on ultimate damage states: (a) extensive cracking and (b) glass fallout (AR 1.0 specimens subjected to the FEMA 461 load protocol).... 57
Figure 4.9 Stress concentrations along the top edge of the glass (5'x5' panel with 2-ply 8mil film and wet glazing attachment system subjected to Monotonic load protocol) 57
Figure 4.10 Effects of film on percent area of glass fallout (AR 1.0 specimens subjected to the Monotonic load proto col) 58
Figure 4.11 Force versus displacement response comparing the Crescendo to the FEMA 461 protocol 59
Figure 4.12 Force versus displacement response comparing the Mid-rise to the FEMA 461 Protocol 59

Figure 4.13 Force versus displacement response comparing the Low-rise to the FEMA 461 protocol 59
Figure 4.14 Force versus displacement response comparing the Low-rise to the Mid-rise protocol 59
Figure 4.15 Force versus displacement response comparing the Mid-rise to the Crescendo protocol 60
Figure 4.16 Effects of Load protocol on the Serviceability Damage States (5'x5' specimens with 2mil unattached film – 10 specimens total). 61
Figure 4.17 Effects of Load protocol on the Ultimate Damage States. (5'x5'specimens with 2mil unattached film – 10 specimens total). 61
Figure 4.18 Effects of aspect ratio on serviceability damage states: (a) gasket damage and (b) first crack (All specimens tested using FEMA 461 loading protocol)..... 62
Figure 4.19 Effects of aspect ratio on the serviceability damage state SDS-3: wet glazing attachment system (All specimens tested using FEMA 461 loading protocol) 63
Figure 4.20 Effects of aspect ratio on ultimate damage states: (a) extensive cracking and (b) glass fallout (All specimens tested using FEMA 461 loading protocol) 63
Figure 4.21 Intensity of glass rotation for each tested aspect ratio in attached and un-attached setups (All specimens tested using FEMA 461 loading protocol)..... 64

LIST OF TABLES

Table 1.1 Summary of related window system tests in literature 6
Table 1.2 Summary of design prescriptions for window systems 9
Table 2.1 Testing matrix 23
Table 2.2 Mapping between test name and specimen type 24
Table 4.1 Characteristics of the 5'x5' window specimens tested 61
Table 4.2 Slope of rotation as aspect ratio changes under FEMA 461 loading protocol 65
Table 4.3 Serviceability limit state drift ratio summary of previous and present study testing ... 66
Table 4.4 Ultimate limit state drift ratio summary of previous and present study testing 67
Table 5.1 Summary of load protocol effects 71
Table 5.2 Summary of film and attachment drift ratios 73

Chapter 1: Introduction

1.1 Motivation

Previous earthquakes have confirmed that window systems can sustain substantial damage, in spite of observed good performance of other nonstructural elements, within the same structure [1964 Alaska (Lagorio, 1990); 1971 San Fernando (Ayres and Sun, 1973); 1978 Off-Miyaga (Sakamoto et al., 1984); 1985 Mexico City (Evan and Ramirez, 1989); 1989 Loma Prieta, 1994 Northridge, 1995 Kobe, 2001 Nisqually (EERI 1990, 1995a, b, 2001; Lingell, 1994)]. Earthquake-induced damage to window systems has the potential to cause human injuries and result in significant economic losses due to business disruptions and loss of functionality (Figures 1.1 and 1.2).

Figure 1.1 Damage to window systems observed during the Palm springs, 1986 earthquake. (Courtesy of the National Information Service for Earthquake Engineering, EERC, University of California, Berkeley)

Figure 1.2 Damage to window systems observed during the Puget Sound, Washington, 1965 earthquake. (Courtesy of the National Information Service for Earthquake Engineering, EERC, University of California, Berkeley)

1.2 Previous work and State-of-Practice

Perhaps the earliest work on this subject in the United States is that reported by Boukamp and Meehen (1960) at the University of California, Berkeley. The authors conducted 33 monotonic, two reversed cyclic, and four impact tests on windows with glass panels ranging in thickness from 1/8" to 1/4". Variables considered included window glass-to-sash clearance, sash type and size, and location of the glass fixity. The authors find that the frame type has a marked impact on the behavior of the units, and that large deformation capacities are achieved by the specimens (up to an interstory drift ratio of 8%). The later finding was attributed to the large glass-to-mullion clearances provided in common practice. The tests of Boukamp and Meehan (1960) were the only such experiments to-date to systematically test specimens of varying (Height:Width) aspect ratios, ranging from 0.5, 1.0, and 2.0 (sizes of 2'x4', 4'x4', 8'x4'). Conclusions from this study indicate that although the overall limit state displacement increases with increasing aspect ratio

of the window panel, drift ratios (displacement limit divided by height) may increase or decrease, depending on the hardness of the bedding mastic. Soft mastic resulted in limit state drift ratios that decreased with increasing aspect ratio, whereas hard mastic resulted in limit state drift ratios that increased with increasing aspect ratio. Although these conclusions are valuable, modern window detailing may vary considerably and it is not known how damage modes and associated drift limits are affected by the window system's aspect ratio.

Between the late 1980s and early 1990s, the BRANZ laboratory in New Zealand conducted testing on single window specimens of 4.6' x 4' and 9.2' x 4' (1/4" thick), primarily in an effort to evaluate serviceability drift limits (Thurston and King, 1992). Specimens were loaded with monotonic, static and incremental cyclic loading. Of interest in the tests were displacement rates, boundary conditions, and cycle count per amplitude. The authors find that rotation of the glass, within the window system is the largest contributor to the deformation capacity of the system.

The most extensive testing programs performed on glass panel systems to-date have been those at the University Missouri-Rolla (UMR) and Penn State (Behr and Belarbi, 1995, 1996; Behr, 1998; Memari et al., 2003, 2004). These tests consistently involved 5'x6' sized windows (AR = 0.83), tested in an in-plane loading rig, designed specifically for the window systems (Figure 1.3). Testing performed at both UMR and Penn State involved use of a single loading protocol throughout the investigations. The protocol adopted (termed *crescendo*) is a variation of the Applied Technology Council - 24 (ATC) (1992) protocol for steel moment frames and their components, and it is now recommended by American Architectural Manufactures Association (AAMA) (2001a) for testing of window systems (Figure 1.4). Variables in these tests have been extensive, including, glass type (annealed, tempered, and laminated) and glass thickness (1/4" to 1", with single and multi-pane glazing).

The focus of these experiments was to document the drift limits associated with these two key damage states, which are described in more detail in section 1.2.1. Table 1.1 summarizes the drift ratios in which glass was observed to first crack (serviceability limit state), and then fall-out (ultimate limit state) during the experiments conducted by others. This Table includes only previous work, where the glass thickness matches that considered in the present study; i.e. ¼" annealed monolithic glass, aluminum framing (additional data may be found in Appendix C). From the previous data, monotonic testing resulted in an average serviceability drift ratio of

3.1% with an average standard deviation of 40%. Cyclic testing averages 4.1% with an average standard deviation of 30%. Ultimate drift ratios were not studied in previous monotonic tests however the average cyclic drift ratio was 5.6% with an average standard deviation of 23%. The high standard deviations can be attributed to the variations of glass and mullion types.

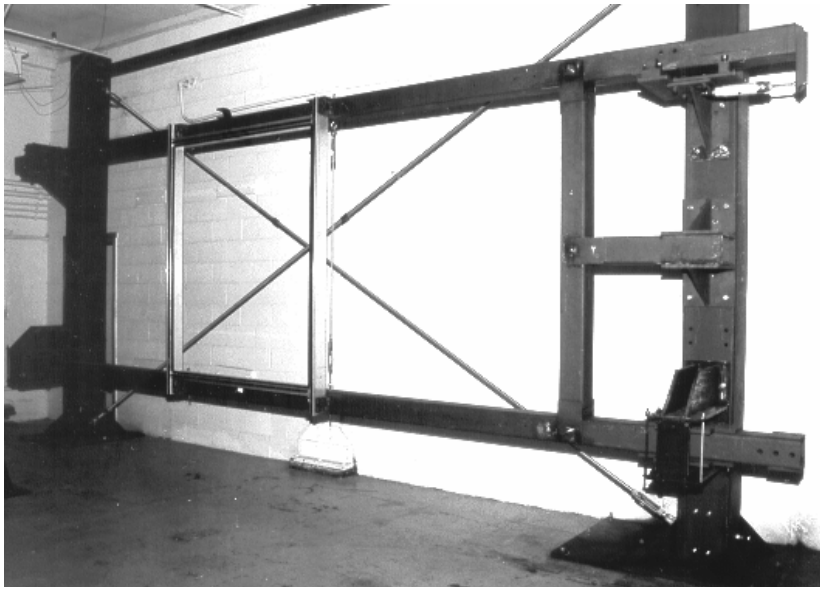

Figure 1.3 Facility at UMR used for dynamic racking tests of full-size curtain wall panels (Courtesy of Behr, 1996).

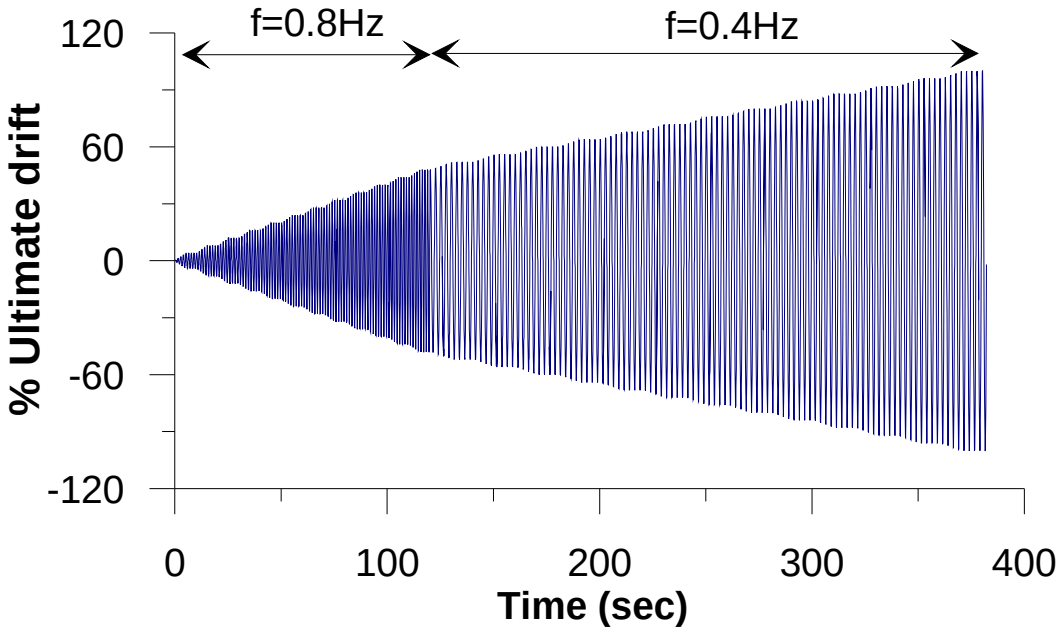

(a) Full record

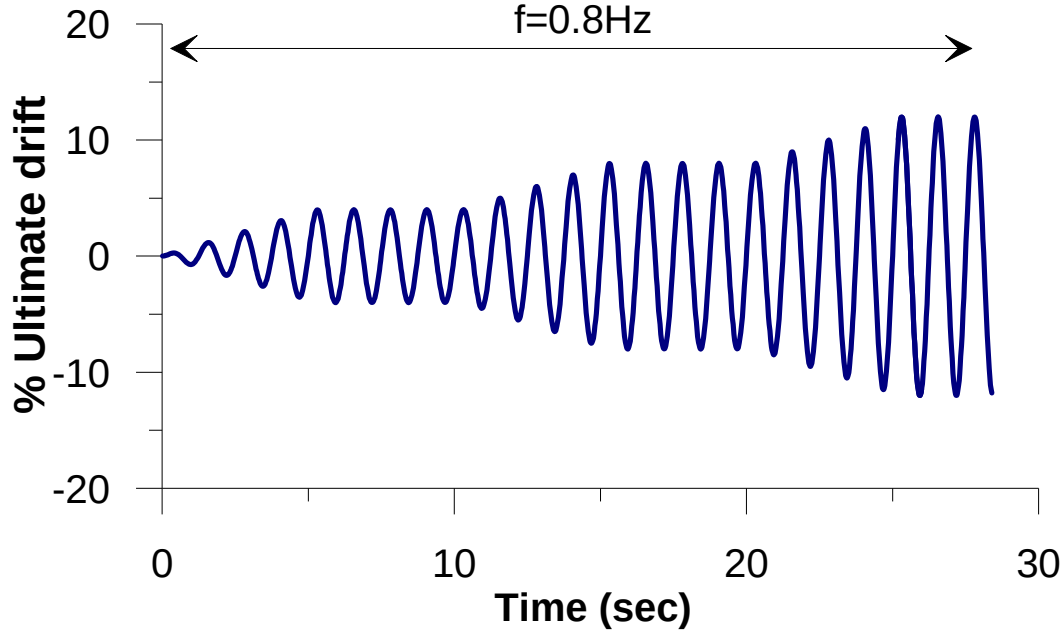

(b) First 30 seconds of the protocol

Figure 1.4 Crescendo protocol used at UMR and Penn State for testing of full-size curtain wall panels and adopted by AAMA (2001b) (Behr, 1996)

Experiment condition					Experiment results			
Glass size $H \times L$ (ft)	Glass thick (inch)	Glass type	Load type	Number of specimens	Glass cracking		Glass fallout	
					Drift (inch)	Drift ratio (%)	Drift (inch)	Drift ratio(%)
Bouwkamp (1960) Objective: To study the effect of sash material and panel attachment								
4X8	0.25	plate glass, aluminum sash, all around attachment of the sash to the boards, 1/4 clearance, soft putty	monotonic	1	1.46	1.52	N/O[1]	N/O
4X8	0.25	plate glass, aluminum sash, head-and-sill attachment of the sash to the boards, 1/4 clearance, soft putty	monotonic	1	2.36	2.46	N/O	N/O
4X8	0.25	plate glass, steel sash, all around attachment of the sash to the boards, 3/8 clearance, soft putty	monotonic	1	2.26	2.35	N/O	N/O
4X8	0.25	plate glass, steel sash, head-and-sill attachment of the sash to the boards, 3/8 clearance, soft putty	monotonic	1	1.84	1.92	N/O	N/O
4X8	0.25	plate glass, wood sash, all around attachment of the sash to the boards, 1/4 clearance, soft putty	monotonic	1	3.52	3.67	N/O	N/O
4X8	0.25	plate glass, wood sash, all around attachment of the sash to the boards, 1/4 clearance, soft putty	monotonic	1	3.83	3.99	N/O	N/O
4X8	0.25	plate glass, aluminum sash, all around attachment of the sash to the boards, 1/4 clearance, soft putty	monotonic	1	2.06	2.15	N/O	N/O
4X8	0.25	plate glass, aluminum sash, all around attachment of the sash to the boards, 1/2 clearance, soft putty	monotonic	1	2.8	2.92	N/O	N/O
4X8	0.25	plate glass, aluminum sash, all around attachment of the sash to the boards, 1/4 clearance, hard putty	monotonic	1	1.01	1.05	N/O	N/O
4X8	0.25	plate glass, aluminum sash, all around attachment of the sash to the boards, 1/2 clearance, hard putty	monotonic	1	2.20	2.29	N/O	N/O
4X8	0.25	plate glass, aluminum sash, panel subdivided horizontally, all around attachment of the sash to the boards, 1/4 clearance, soft putty	monotonic	1	4.31	4.49	N/O	N/O
4X8	0.25	aluminum sash, panel subdivided horizontally, all around attachment of the sash to the boards, 1/2 clearance, soft putty	monotonic	1	6.06	6.31	N/O	N/O
4X8	0.25	plate glass, aluminum sash, panel subdivided vertically, all around attachment of the sash to the boards, 1/4 clearance, soft putty	monotonic	1	2.49	2.59	N/O	N/O
4X8	0.25	plate glass, aluminum sash, panel subdivided vertically, all around attachment of the sash to the boards, 1/2 clearance, soft putty	monotonic	1	5.41	5.64	N/O	N/O

[1]N/O – Not Observed

Table 1.1 Summary of related window system tests in literature

Experiment condition					Experiment results			
Glass size $H \times L$ (ft)	Glass thick (inch)	Glass type	Load type	Number of specimens	Glass cracking		Glass fallout	
					Drift (inch)	Drift ratio (%)	Drift (inch)	Drift ratio(%)
Behr et al. (1996) Objective: Evaluate performance of architectural glass								
5X6	0.25	Annealed monolithic (Store front)	crescendo	12	3.02	4.23	4.21	5.90
5X6	0.25	Fully tempered monolithic	crescendo	16	3.98	5.57	3.98	5.57
5X6	0.25	Annealed Laminate	crescendo	12	5.71	8.00	5.71	8.00
Behr et al. (1998) Objective: Evaluate various glass types								
5X6	0.25	Annealed monolithic (Curtain wall)	crescendo	6	1.97	2.80	2.17	3.08
5X6	0.25	Heat-strengthened monolithic	crescendo	5	3.39	4.82	3.39	4.82
5X6	0.25	Fully tempered monolithic	crescendo	5	2.95	4.19	2.95	4.19
5X6	0.25	Annealed laminated	crescendo	6	1.81	2.58	5.59	7.95
5X6	0.25	Annealed monolithic with 0.1mm PET film	crescendo	6	1.97	2.80	3.98	5.66
5X6	0.25	Heat-strengthened monolithic spandrel	crescendo	6	2.40	3.42	2.48	3.53
5X6	0.25	Heat-strengthened laminated	crescendo	6	2.13	3.02	5.12	7.28
Memari et al. (2004) Objective: To study glass fitted with anchored pet film								
5X6	0.25	clear annealed monolithic glass, with film (edge grip)	crescendo	2	2.6	3.30	4.7	5.97

Table 1.1 Continued

1.2.1 Damage States

Previous work has identified two predominant damage states associated with (i) serviceability (Figure 1.5) and (ii) ultimate condition of the window system post-earthquake (Figure 1.6). Serviceability refers to the condition whereby the window system is repairable and does not pose any safety hazards post-event (e.g. minor cracking or gasket damage only). In contrast, the ultimate damage state refers to the condition whereby the window system is not repairable and does pose safety hazards post-event (e.g. large region of glass has cracked or fallen from the unit). The first studies on damage states were conducted by Behr et al. (1995) at the University of Missouri-Rolla. Behr et al. (1995) describe an ultimate limit state as glass damage that poses a threat to life safety because of glass breakage and glass fallout. Behr et al. also describes serviceability damage states or thresholds as system repairs that become necessary due to problems that include visual degradation, risk of future glass breakage due to thermal and wind effects, and loss of building envelope seal integrity.

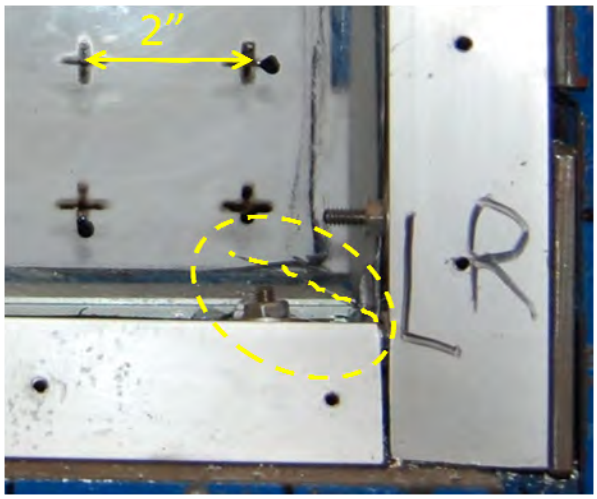

Figure 1.5 Serviceability Damage State: Minor Cracking

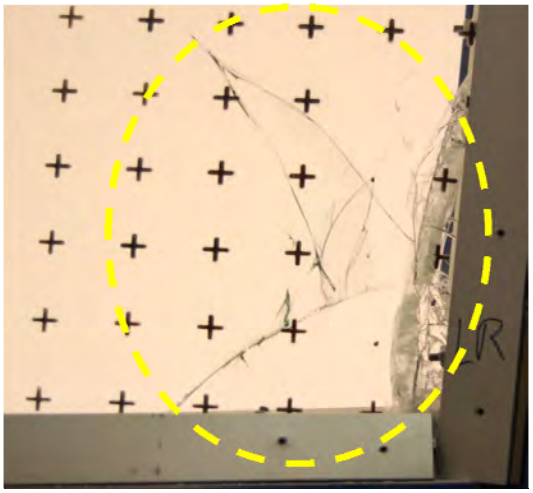

Figure 1.6 Ultimate Damage State: Extensive Cracking

1.2.2 Design Code Prescriptions

The Federal Emergency Management Agency (FEMA) design documents indicate that at a drift ratio of 1%, there is a 50% chance that the glass within a window system will crack (FEMA 461 2006). This recommendation is inconsistent with previous observations, which largely indicate that glass cracking occurs at a minimum drift ratio of 2.5%. A much more conservative value can

be found in the Canadian Standards Association (CSA 2005). CSA indicate that the deflection shall not exceed 1/16 inch per foot of height of the glazed opening or 0.5% drift ratio, to minimize window system damage. At the time of this report, the only code which took into account any seismic relation in predicting/preventing glazing damage was the Uniform Building Code (UBC 1994). The UBC states that the allowed maximum drift ratio for buildings with a period of less than 0.7 seconds was 1.5% or $0.0019R_w$, and for buildings with a period greater than 0.7 seconds the maximum allowable drift ratio was 1.1% or $0.0015R_w$. Table 1.2 summarizes this information. All drift ratio values were quite conservative, which exposes the lack of data to accurately predict when glazing damage might occur.

Reference	Drift Criteria
FEMA 461 (2006) (Federal Emergency Management Agency)	At **1% drift ratio**, there is a 50% chance that glazing will crack
CSA (2005) (Canadian Standards Association)	Deflection shall not exceed 1/16 inch per foot of height of the glazed opening. (**0.5% drift ratio**)
UBC (1994) (Uniform building code)	The allowed maximum drift ratio is **1.5%** or 0.0019Rw (T<0.7s), **1.1%** or 0.0015Rw (T>0.7s)

Table 1.2 Summary of design prescriptions for window systems

1.3 Scope of this Work

In this work, three variables of interest are studied through in-plane seismic racking experiments of window systems, namely: (i) loading protocol, (ii) window film type and attachment, and (iii) aspect ratio. In addition, specimen repeatability is evaluated by testing three specimens of select types during the program. The baseline window systems is a 5'x5 unit, constructed of ¼" annealed single pane glass supported by an aluminum frame, with detailing typical of store-front window systems. A total of 53 window systems were tested. The justification for the three variables of interest is as follows:

(i) Loading History – Various loading protocols exist in the literature for simulating seismic demands on structural and nonstructural components [see e.g. for bridge piers – FHWA (2004); for timber components – Krawinkler et al. (2000) or sequential phased displacement (SPD) – e.g.

Shepard (1995, 1996); for steel components – ATC (1992); for cladding systems – AAMA (2001a)]. Such protocols are either displacement or load-controlled, include (or not) reversed cycles of equal or unequal amplitude, and may be at static or dynamic rates. A common characteristic pervasive amongst the types of load protocols representative of seismic loading is the desire to consider reversed cyclic loading conditions due to the reversed cyclic nature of earthquake loading. However, the actual quantity and amplitude of reversed cycles for different components is still under debate. Speculation regarding loading protocol effects has further been increased due to the poor performance of various types of structural components [e.g. Dinehart and Shenton (1998), Ficcadenti et al. (1998), Gatto and Uang (2003)]. Such speculation is no less for nonstructural components [e.g. piping work by Malhotra et al. (2003), Hoehler et al. (2009)]. These and other studies have pointed out the now well recognized fact that to evaluate the performance of a component or system, damage in a component is cumulative and this level of damage depends on the history of deformations or loads that the component undergoes (Krawinkler, 1996).

At present, the accepted protocol for testing window systems is that developed by UMR and Penn State researchers, the aforementioned Crescendo protocol (AAMA, 2001a). The crescendo protocol, shown in Figure 1.4, represents two frequencies of input (0.4 Hz and 0.8 Hz) and incurs ramp up cycles prior to four cycles at each maximum deformation demand. Furthermore, it imposes nearly 200 cycles of displacement to the specimens. It is unclear if such a protocol is representative of demands induced on window systems used in buildings in the California seismic environment. Further, it is unclear what effect other loading protocols will have on seismic drift limits and damage modes of window specimens. Parallel to this study, two new protocols were developed with emphasis on low- and mid-rise building structure drift response. This study indicated that cyclic drift counts on the order of 30-40 were more representative for typical building structures (Hutchinson et al., 2008).

To investigate the effects of load history, it is important to define baseline capacity and damage modes of the window specimens, prior to cyclic degradation. To perform such an assessment, a series of monotonic, displacement-controlled tests are performed first in this study to identify baseline conditions.

(ii) Window Film and Attachment – Film-coated glazing, although not specifically designed to withstand anticipated earthquake events (it's original intent being for safety or thermal purposes), is recognized to hold potential for mitigating the adverse effects in building and other structures under seismic loading conditions. However, to-date, only one study considered film-coated systems (Memari et al., 2004). This study focused on anchored film, which is less common in daily practice.

(iii) Window Aspect Ratio – As noted, the only systematic study of window aspect ratio was that conducted by Boukamp and Meeham (1960). Systematic study of the effects of window aspect ratio on damage modes and associated drift ratios is needed.

1.3.1 Report organization

This report is organized into the following chapters:

- Chapter 2 presents the experimental program, including the test matrix, set-up, instrumentation, and protocol for test execution.
- Chapter 3 presents a summary of experimental results; including identified damage states, physical observations, and a summary of global response characteristics of the window systems.
- Chapter 4 synthesizes results from the experiments, considering the effects of the three variables of interest in this study, namely load protocol, film thickness, and aspect ratio. In addition, comparison with previous work is discussed.
- Chapter 5 presents conclusions and findings of the study.
- Appendices are included to summarize the load rig design, individual test damage reports, and additional experimental data.

Chapter 2: Experimental Program

2.1 Small Scale Pilot Tests

2.1.1 Introduction and Scope

Tests were conducted on 12” square ¼” thick annealed glass panels. The goal of this experiment was to determine the effects of window film on glass fracture type, load at failure and the feasibility of capturing crack propagation on video. Eight panels were tested, with three different film thicknesses: 0mil (uncoated), 2 mil and two (2) 4 mil plies together (8 mil total). An initial test in out of plane bending was used to determine the capabilities of tracking crack propagation through video images. The second test was an in-plane tension test through compression of the specimen. This test was to further examine video capture capabilities of crack propagation and attempt to correlate this with load.

2.1.2 Out of Plane Test

Panel 0, with no film, was tested by a simple out of plane test as a first step in determining the crack tracking possibilities. The base of the glass panel was secured to a stiff mounting bar, then a clamp was placed near the top of the panel and tightened manually until failure in bending. The best imaging result is found using a shadowing effect, where a white backdrop is placed behind the glass unit (Figure 2.1).

(a) (b) (c)

Figure 2.1 - Panel 0 - Crack tracking through shadows

As seen in Figure 2.1 (b) the shadows of the cracks are much more defined than the cracks themselves. The shadows stand out more as the crack thickens as seen in Figure 2.1 (c).

2.1.3 In-plane tension tests

This test was designed to further test the crack propagation detection using video and correlate the onset of cracks to a load. The panel was tested in plane diagonally to concentrate the loads down the center of the panel. This loading causes tension cracks to form parallel to loading. A back light projection was used with paper backing the glass panel to allow shadows to form as cracks form. The panel was held in place using two stiff steel mounting frames (the design plans for the mounting frames can be found in Appendix A). The stiff frames were in turn secured by the clamps of the MTS testing machine. Rubber stoppers similar to those found in full scale window construction to separate the mullion and window glass were used in between the stiff steel frame and glass to prevent concentrated load buildup. The specimens were loaded monotonically at a rate of 2 in/sec.

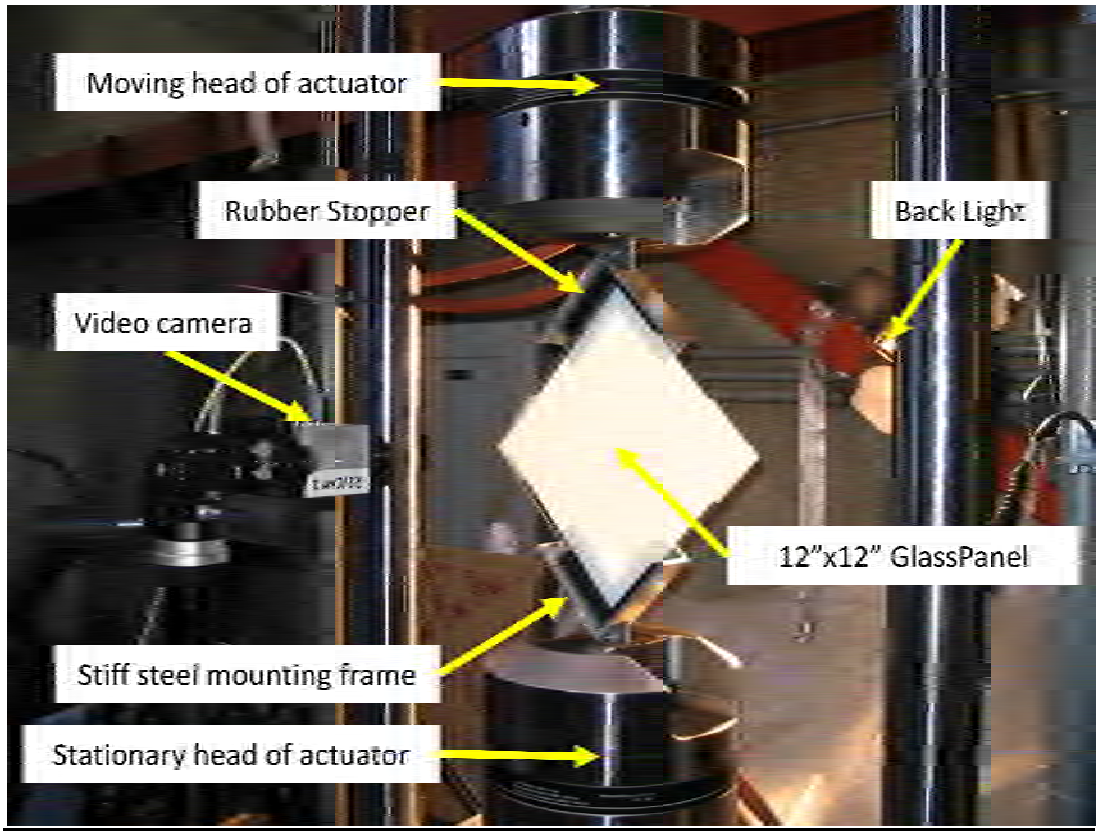

Figure 2.2 – 12”x12” Tension Test Setup

2.1.4 Camera setup

One Basler camera was used to capture the crack propagation (model: A301fc). The camera was set at its maximum capture rate to best observe the onset and propagation of the cracks (80 frames per second). The camera was placed approximately 18 inches from the glass surface which gave an approximate resolution of one megapixel. After the tests, each frame of the video was extracted to analyze the cracking.

2.1.5 Results

Crack propagation through the specimen's entire height was observed to be faster than 0.0125 seconds (maximum camera frame rate - 80hertz). Therefore only one frame of the video for each specimen shows the crack orientations just prior to failure. Figures 2.3 - 2.5 show a series of photographs of un-filmed specimens showing the video frame in which the first crack can be seen (b), the prior video frame (a) and following video frame (c). Figures 2.6 - 2.9 show a series of photographs of filmed speciemens showing the video frame in which the first crack can be seen (a) and the following two video frames (b and c). Notice that the film holds the glass fragments together.

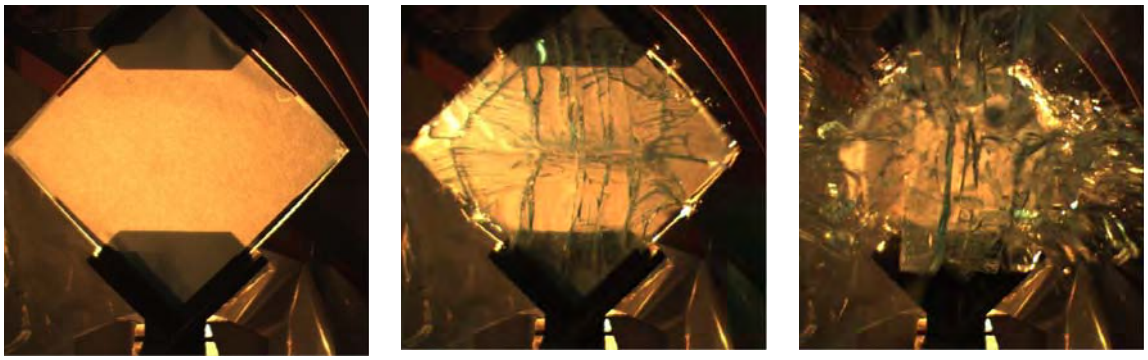

(a) Cracking minus one video frame

(b) Onset of cracking

(c) Cracking plus one video frame

Figure 2.3 - Panel 1: 0mil Film

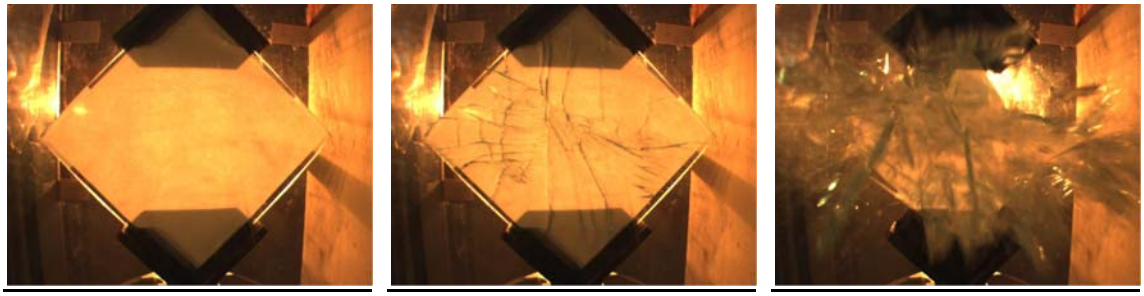

(a)
Cracking minus one video frame

(b)
Onset of cracking

(c)
Cracking plus one video frame

Figure 2.4 - Panel 2: 0mil Film

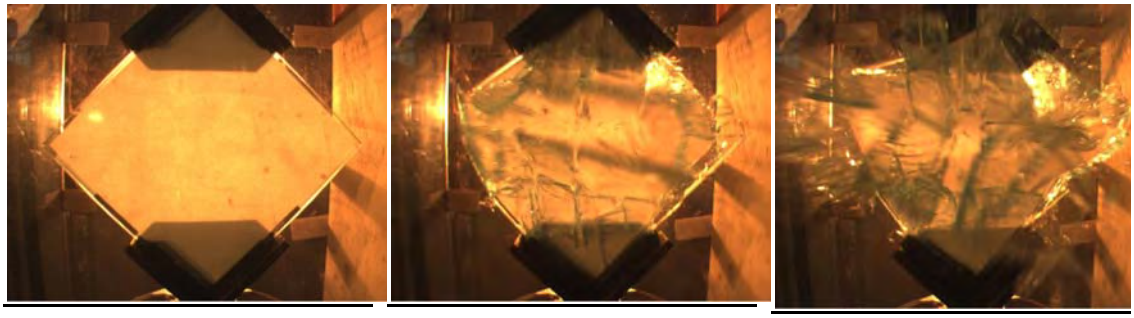

(a)
Cracking minus one video frame

(b)
Onset of cracking

(c)
Cracking plus one video frame

Figure 2.5 - Panel 3: 0mil Film

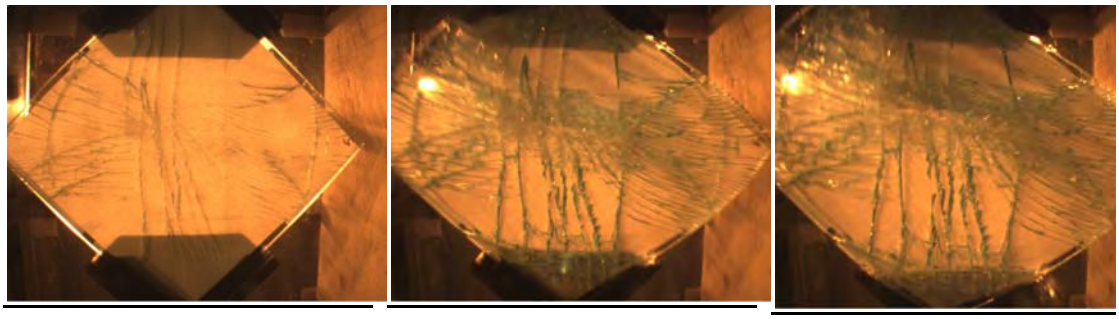

(a)
Onset of cracking

(b)
Cracking plus one video frame

(c)
Cracking plus two video frames

Figure 2.6 - Panel 4: 2mil Film

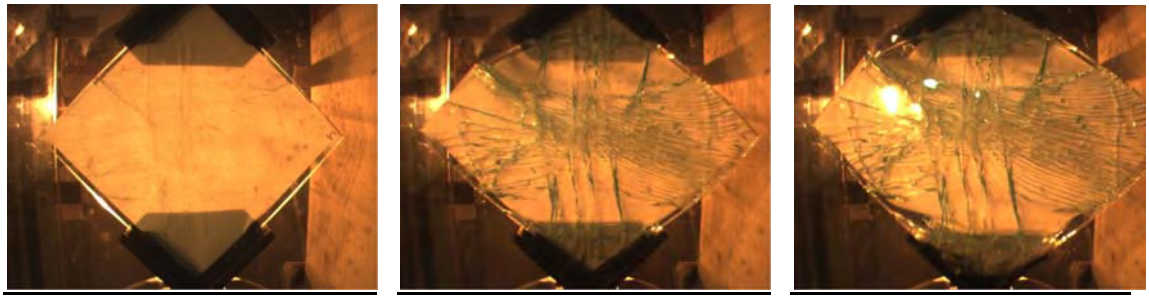

(a)
Onset of cracking

(b)
Cracking plus one video frame

(c)
Cracking plus two video frames

Figure 2.7 - Panel 5: 2mil Film

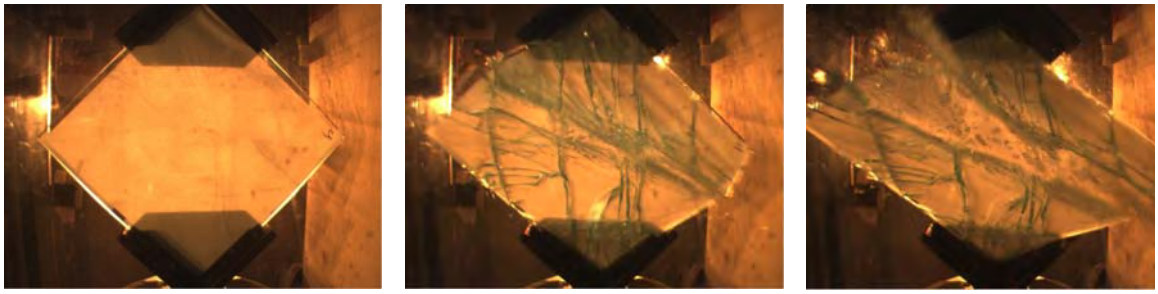

(a)
Onset of cracking

(b)
Cracking plus one video frame

(c)
Cracking plus two video frames

Figure 2.8 - Panel 6: 2mil Film

(a)
Onset of cracking

(b)
Cracking plus one video frame

(c)
Cracking plus two video frames

Figure 2.9 - Panel 7: 8mil Film

2.1.6 Physical observations

Observations presented in Figures 2.3 - 2.9 indicate that primary tensile stress cracks formed parallel to the loading direction and secondary/buckling cracks formed perpendicular to the loading direction. Failure was attributed to the secondary cracks causing the glass to buckle. Figure 2.9 shows photographs of Panel 7, which was the only glass panel to not fall from the

testing apparatus after failure. This happened because the thicker film (2-ply 8 mil) was able to remain stable despite the outward potential of the panel. However, the cracking pattern (parallel tensile stress cracks and perpendicular buckling cracks) was not affected by the application or thickness of the film.

The effect of the film was limited to the amount of shrapnel that was produced. The panel with no film produced a large volume of shrapnel. As the thickness of the film was increased, the amount of loose glass after failure was greatly reduced. A panel with 2 mil film preserved approximately 75% - 85% of the shrapnel on the glass itself, while a panel with 4mil film contained approximately 95% of the shrapnel. The panel with 2-ply 8 mil coating contained near 100% of the shrapnel.

2.1.7 Measured Results

Figure 2.10 shows the resulting force-displacement and stiffness-time response measured during the experiments. The average peak load for all tests was 10.5 kips with no correlation between peak load and film thickness. The total displacement capacity of the assembly was between 0.7 - 0.8 inches. The one curve that stands out from the rest is the first panel tested. This panel observes a stiffer initial response, with subsequent softening matching the early displacement behavior of subsequent panel tests. This is attributed to the re-use of the rubber stoppers placed in the reaction set-up, which resulted in an initial plastic deformation of the rubber stopper during test one. As a result, the following tests show a slightly smaller maximum displacement, and softer initial load behavior. The glass panel specimens with no film had a much lower final stiffness (~8 k/in) just prior to failure than the filmed panels (~11 k/in).

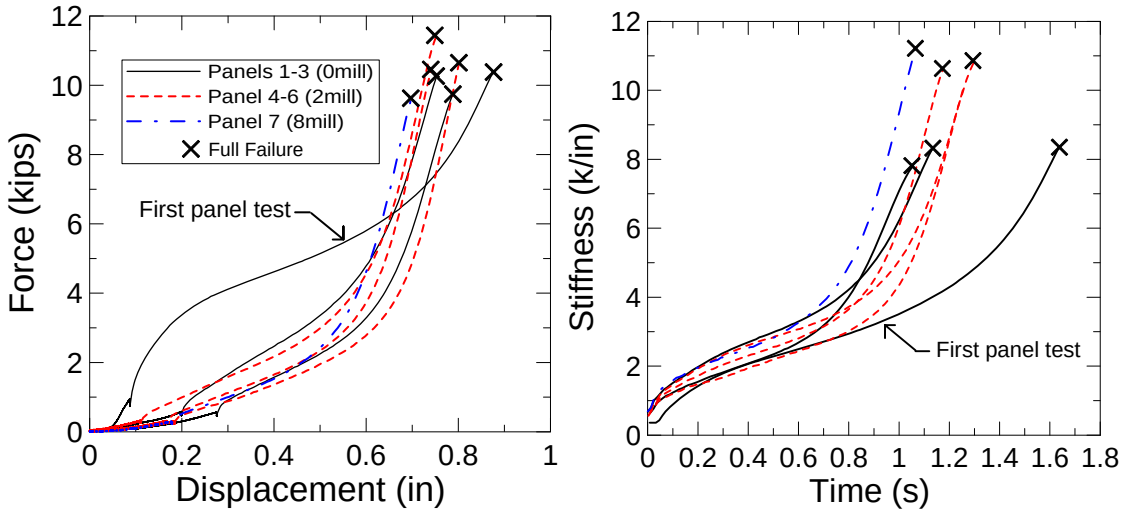

Figure 2.10 - Force vs. displacement and stiffness vs. time profiles

The glass material used follows the guidelines set forth in the ASTM specification C1036, clear float glass. According to the material data sheet provided by Pittsburgh Plate Glass Co. (PPG) for float glass (Appendix D) the tensile strength of the glass specimens (modulus of rupture) is 6000 lbs/in^2. Assuming a compressive strut loading area of 3 in^2, the compression force expected to fail the specimens was approximately 18,000 lbs. It is believed that the maximum tensile load was not reached because the panels failed in buckling. This conclusion is consistent with observations of the full scale testing as well. For more details comparing small scale results to full scale results refer to Section 4.1 Correlation between Small Scale and Full Scale Testing.

2.1.8 Comparison to Previous Work

The only other set of testing on small (12”x12”) panels was performed by Memari et al. (2007). The focus of their studies was to correlate small scale to full scale through the stiffness of each component of a window system (glass, mullion, etc). They reported no buckling failure (however noted that somewhat less than pure in-plane loading was observed in full-scale tests) and peak loads ranging from 9 kips to 14 kips (average 11 kips). Converting this pure diagonal loading to its (45 degree) horizontal and vertical components the peak loads range from 6.4 kips to 9.9 kips (average 8.2 kips). The small panels tested in this report all failed in buckling with a peak load ranging from 6.8 kips to 8.1 kips (45 degree component) with an average of 7.5 kips. The peak load difference (9% increase in load capacity) can be attributed to the difference in failure mechanisms. Drift ratio capacity could not be compared due to testing setups. Previous work included a specialized testing frame which had metal to glass loading contacts where as this

report inserted the stiff rubber blocks, found in the full scale specimens, between the steel loading rig and the glass to reduce load concentrations.

2.1.9 Small Scale Test Conclusions

It was possible to track the onset and propagation of cracking through shadowing of the cracks from video data. It was also possible to correlate the load to ultimate failure. Despite similar ultimate failure loads and displacements for film and non filmed panels, secant stiffness values were found to be 37% higher in filmed specimens than un-filmed panels. Cracking patterns were, however, also not affected by the thickness or application of film.

2.2 Full Scale Test Setup

Window specimens were loaded in pure shear in an in-plane racking frame similar in concept to that used at Pennsylvania State University and the University of Missouri-Rolla, and denoted in the AAMA (2001b) specifications. The lateral racking system was designed to support pure shear loading and minimize out-of-plane excursions.

The testing rig was composed of an outer moment frame that surrounds an inner racking frame (Figure 2.11). The reaction frame system at UCSD was different than that at Penn State or UMR primarily via the incorporation of pivot points at the lower line of the window. The UCSD modified design allows for flexible height adjustment and accommodates three different specimen sizes: two side by side 5’x5’ windows (Figure 2.12), one 4’x8’ window (Figure 2.13) and one 6’x4’ window (Figure 2.14). The outer frame sandwiches the inner frame preventing out-of-plane movement. Each component of the testing frame was composed of steel tube members (HSS 4”x4”x1/4”). The outer moment frame was reinforced using diagonal members (HSS 2.5”x2.5”x1/4”) to increase its stiffness. This provided optimal load transfer between the shake table and the windows. Variable specimen size is easily adjustable through the movement of the lower horizontal and vertical support members (Figure 2.11). Detailed construction plans for the reaction frame can be found in Appendix A. Note that the reaction frame is mounted onto the UCSD Powell Laboratory shake table. The shake table provides the input loading, while the upper inner frame is anchored, with a load cell placed in parallel, to a reaction wall. In this sense, the design is inverted (loading incoming from the base of the window), as observed when the window system is in the field.

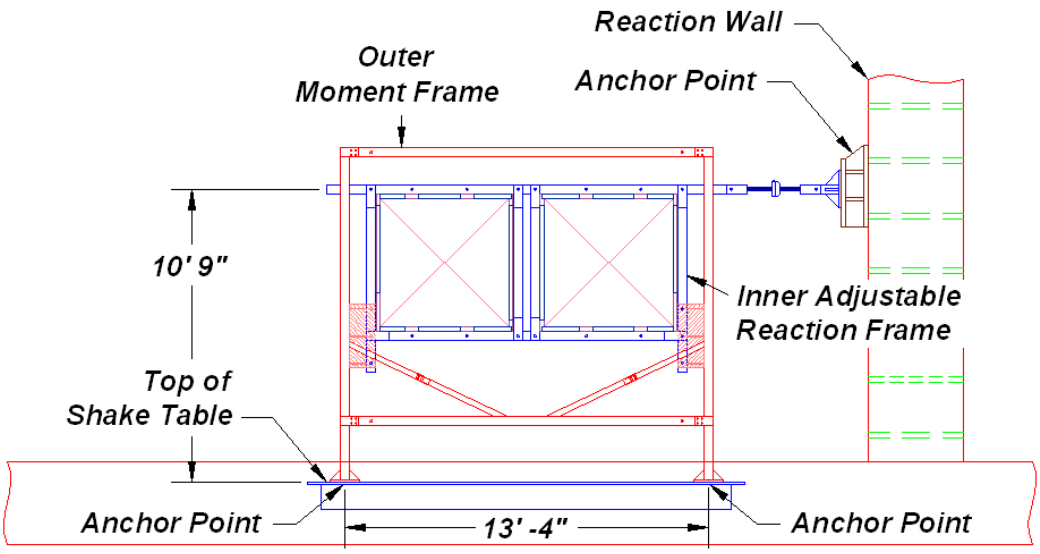

Figure 2.11 System elevation view

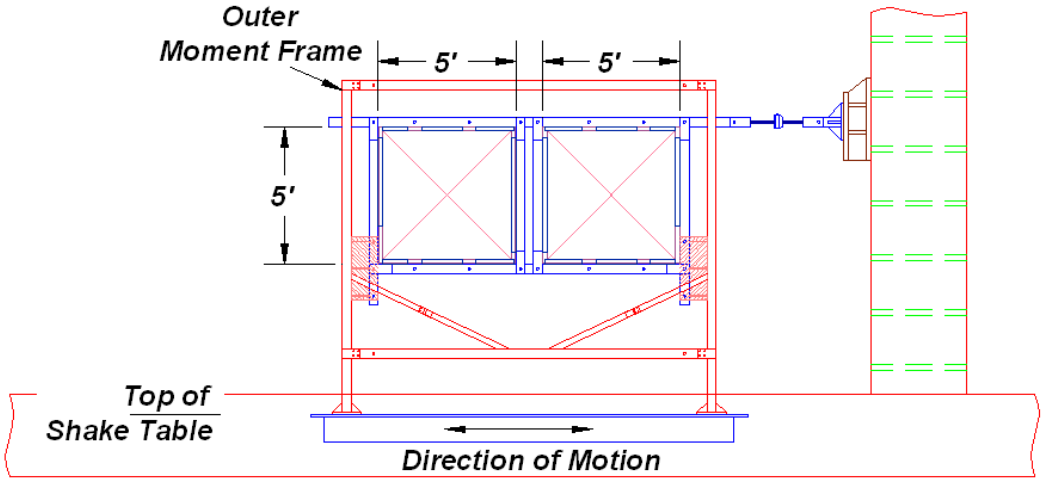

Figure 2.12 5'x5' window size setup

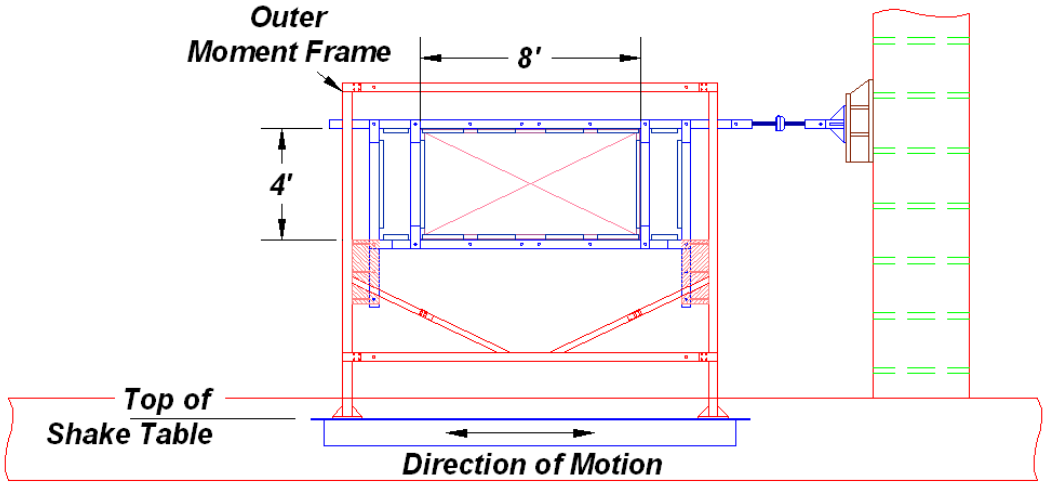

Figure 2.13 4'x8' window size setup

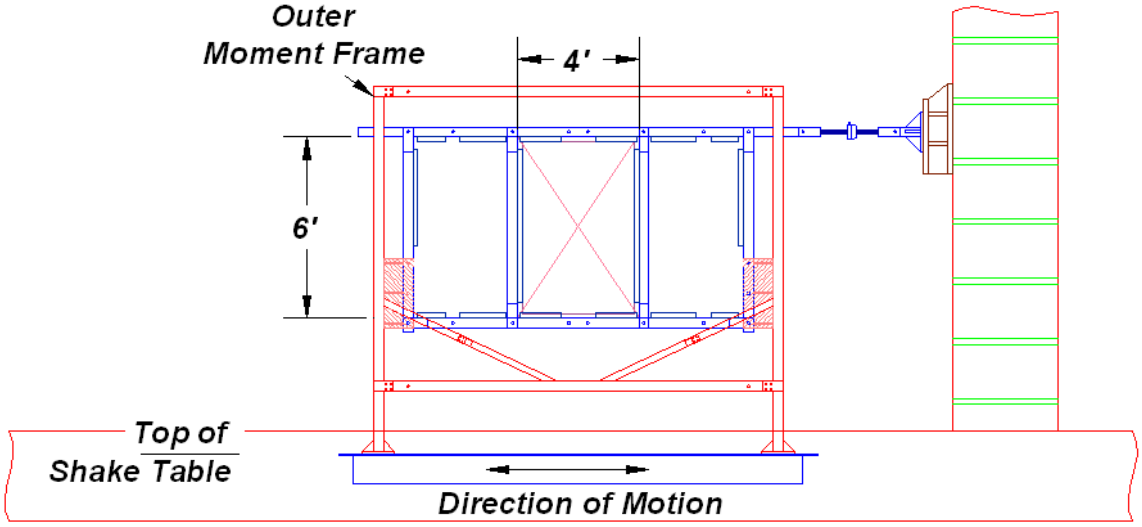

Figure 2.14 6'x4' window size setup

2.3 Test Matrix

Table 2.1 outlines the testing matrix for the in-plane racking experiments conducted at UCSD. The testing matrix investigates three variables of interest: (a) Loading protocol (group LP), (b) window film type and attachment system (group WF), and (c) aspect ratio (group AR). Window systems have the following baseline properties, unless otherwise noted in table 2.1.

- Size: 5'x 5'
- ¼" annealed single pane glass
- Store-front window system, Aluminum frame

Testing of a single specimen provides insufficient information since the level at which strength degradation occurs has significant scatter, and is rapid (ATC, 1992). Glass cracking or fallout is a brittle, rapid failure mode; therefore, investigation into the repeatability of specimen response is inherently built into the matrix by testing multiple specimens of select individual specimen types. In total, 53 specimens were tested during the program. It should be noted that conducting multiple tests per specimen type would provide enhanced confidence and thorough validation of repeatability, for a given variable. Table 2.2 shows the mapping between test name and specimen type.

Group		Specimen No.			Aspect Ratio[1]	Window Film Type	Attachment System	Load Protocol	Notes
LP	LP-01[2]	a	b	c	1.0	None	None	Monotonic (Static)	Control
	LP-02	a	b	c	1.0	Single Ply 2 mil	None	Monotonic (Static)	
	LP-03	a	b	c	1.0	Single Ply 4 mil	None	Monotonic (Static)`	
	LP-04	a	b	c	1.0	Two Ply 8 mil	None	Monotonic (Static)	
	LP-05	a	b	-	1.0	Single Ply 2 mil	Wet Glazed	Monotonic (Static)	
	LP-06	a	b	c	1.0	Single Ply 4 mil	Wet Glazed	Monotonic (Static)	
	LP-07	a	b	c	1.0	Two Ply 8 mil	Wet Glazed	Monotonic (Static)	
	LP-08	a	b	c	1.0	None	None	Crescendo (Dynamic)	
	LP-09[2]	a	b	c	1.0	2 mil (a,b) - 4 mil (c,d)	None	FEMA 461 (Quasi-static)	
	LP-10	a	b	-	1.0	2 mil (a) - 4 mil (b)	None	Crescendo (Dynamic)	
	LP-11	a	b	-	1.0	Single Ply 2 mil	None	Mid-Rise Load Protocol	
	LP-12	a	b	-	1.0	Single Ply 2 mil	None	Low-Rise Load Protocol	
WF	WF-1	a	b	-	1.0	None	None	Mid-Rise Load Protocol	Control
	WF-2	a	b	-	1.0	Single Ply 2 mil	None	FEMA 461 (Quasi-static)	
	WF-4	a	b	-	1.0	Two Ply 8 mil	None	FEMA 461 (Quasi-static)	
	WF-5	a	b	-	1.0	Single Ply 2 mil	Wet Glazed	FEMA 461 (Quasi-static)	
	WF-6	a	b	-	1.0	Single Ply 4 mil	Wet Glazed	FEMA 461 (Quasi-static)	
	WF-7	a	b	-	1.0	Two Ply 8 mil	Wet Glazed	FEMA 461 (Quasi-static)	
AR[3]	AR-01	a	-	-	0.5	None	None	FEMA 461 (Quasi-static)	
	AR-02	a	-	-	1.5	None	None	FEMA 461 (Quasi-static)	
	AR-03	a	-	-	0.5	Single Ply 4 mil	None	FEMA 461 (Quasi-static)	
	AR-04	a	-	-	1.5	Single Ply 4 mil	None	FEMA 461 (Quasi-static)	
	AR-05	a	-	-	0.5	Single Ply 4 mil	Wet Glazed	FEMA 461 (Quasi-static)	
	AR-06	a	-	-	1.5	Single Ply 4 mil	Wet Glazed	FEMA 461 (Quasi-static)	

[1] Aspect ratio = H = height x W = width, 1.5 = 6'x4', 1.0 = 5'x5', 0.5 = 4'x8'

[2] Two more specimens for LP-01(a-e) included for 5 total; one more specimen for LP-09(a-d) included for 4 total.

[3] Note that single specimens of series AR were tested

Table 2.1 Testing matrix

Group	Test Name	Loading	South Slot	North Slot	Date
LP	Monotonic 1	Monotonic	LP-01a	LP-01b	9/20/2007
	Crescendo 1	Crescendo	LP-01a	LP-01b	9/24/2007
	Crescendo 2	Crescendo	LP-08a	LP-08b	9/27/2007
	Monotonic 2	Monotonic	LP-02a	LP-01c	3/6/2008
	Monotonic 3	Monotonic	LP-02c	LP-02b	3/11/2008
	Monotonic 4	Monotonic	LP-03a	LP-03b	3/14/2008
	Monotonic 5	Monotonic	LP-04a	LP-03c	3/27/2008
	Monotonic 6	Monotonic	LP-04c	LP-04b	4/3/2008
	Monotonic 7	Monotonic	LP-05a	LP-05b	4/7/2008
	Monotonic 8	Monotonic	LP-06a	LP-06b	5/8/2008
	Monotonic 9	Monotonic	LP-07a	LP-06c	5/14/2008
	Monotonic 10	Monotonic	LP-07c	LP-07b	5/16/2008
	Monotonic 11	Monotonic	LP-01e	LP-01d	6/5/2008
	FEMA 1	FEMA 461	LP-09a	LP-09b	6/26/2008
	FEMA 2	FEMA 461	LP-09c	LP-09d	7/1/2008
	Crescendo 3	Crescendo	LP-10a	LP-10b	7/15/2008
	Jian II (NewLP 1)	Mid-Rise	LP-11a	LP-11b	7/23/2008
	Jian IV	Low-Rise	LP-12a	LP-11a	7/25/2008
WF	NewLP 2	Mid-Rise	WF-01a	WF-01b	8/6/2008
	NewLP 3	FEMA 461	WF-04a	WF-04b	8/8/2008
	NewLP 4	FEMA 461	WF-05a	WF-05b	8/12/2008
	NewLP 5	FEMA 461	WF-06a	WF-06b	8/14/2008
	NewLP 6	FEMA 461	WF-07a	WF-07b	8/18/2008
AR	AR 1	FEMA 461	AR 1 - 0 mil		8/21/2008
	AR 3	FEMA 461	AR 3 - 4 mil		8/26/2008
	AR 2	FEMA 461	AR 2 - 0 mil		8/29/2008
	AR 4	FEMA 461	AR 4 - 4 mil		9/2/2008
	AR 6	FEMA 461	AR 6 - 4 mil (WG attach)		9/3/2008
	AR 5	FEMA 461	AR 5 - 4 mil (WG attach)		9/9/2008

Table 2.2 Mapping between test name and specimen type

2.3.1 Loading Protocol (LP) Series

The loading protocol series is made up of five different protocols: Monotonic, Crescendo, FEMA 461, Mid-Rise and Low-Rise Protocol. A total of 18 tests (36 specimens) were conducted in the LP series. Refer to section 2.6 for protocol definitions.

2.3.2 Window Film (WF) Series

A group of specimens, denoted WF, were used to investigate the effect of (a) single ply 2 mil, (b) single ply 4 mil, and (c) two plies of 4 mil film to create a 2 ply 8 mil film, each either attached with wet glazing at the top or unattached. Wet glazing attachment involves use of a silicon-based material placed via an injection gun between the glass, film, and aluminum frame. Refer to section 2.4.3 for wet glazing attachment details. A total of 12 tests were performed in the WF series.

2.3.3 Aspect Ratio (AR) Series

The testing program of table 1.1 systematically varies the window aspect ratio for a controlled group of specimens denoted as AR. Aspect ratios of 0.5, 1.0, and 1.5, resulting in window sizes of (H x W) 4'x8', 5'x5', and 6'x4', are considered. These sizes are based on discussions with commercial manufacturers of window systems for mid- and low-rise building structures in California, who identified these to be the most common. A total of 6 tests were performed in the AR series.

2.4 Specimen Assembly and Construction

The window specimens were manufactured offsite by Pacific Skyline Glass and Mirror in San Diego, California. The specimens were constructed of an aluminum mullion frame surrounding a single layer of ¼" thick annealed glass. Rubber gaskets surround the connection between the mullion and glass on all sides. Figure 2.15 shows the mullion detail. Rubber blocks were installed around the perimeter of the glass. These were used as centering spacers and gravity support for the glass. The blocks were 2 inches long, 5/8 inches wide, by ½ inches thick, and installed about the perimeter with structural silicone, as shown in Figure 2.16. The specimen details incorporated those common to store-front and mid-rise curtain window systems.

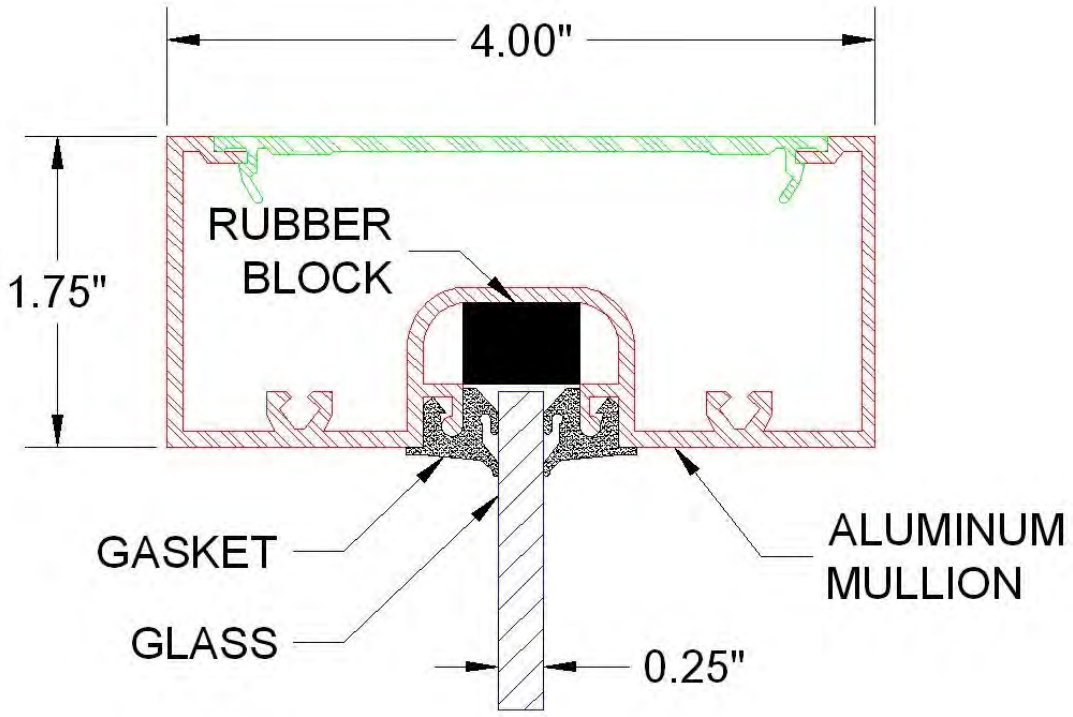

Figure 2.15 Store-Front Window Detail

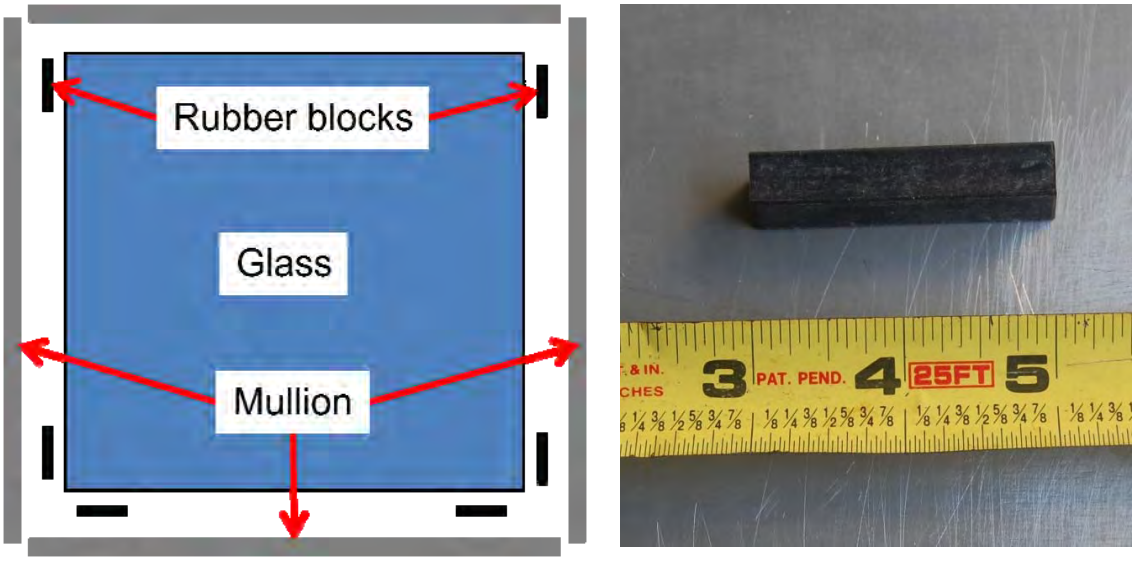

(a) (b)

Figure 2.16 Rubber blocks in window units: (a) schematic of general locations and (b) photograph of rubber stop.

2.4.1 Window Film Installation

Window film is traditionally placed for safety and thermal purposes. In this study, its additional benefits, to reduce seismic damage, were of interest. The windows were filmed onsite using window filming procedures used in practice (Figure 2.17). The process for film installation is as follows: (i) the window is first cleaned thoroughly, (ii) a soapy solution is sprayed on the surface of the glass so that the film can be slid easily into place, (iii) the film is applied and cut to fit the window dimensions, and (iv) then, using a stiff rubber squeegee, the soapy solution is squeezed out which causes the film to stick to the glass. The windows were stored and allowed to cure for a minimum of 20 days. For the dual layer 8 mil specimens, each layer was applied using the standard window filming procedure and cured for 20 days.

(a) (b)

(c) (d)

Figure 2.17 Window film Installation

2.4.3 Wet Glazing Attachment System Installation

The wet glazing attachment system is designed to secure the top edge of the film to the mullion (window film and attachment system are installed on the inside of the building envelope). Wet glazing is used in practice to provide added security of the film for the following applications:

wind-borne debris protection, personal safety (including spontaneous glass failure), and forced entry protection. While there are a number of film attachment (mechanical and other) methods, the wet glazing method is simplest and least expensive. The installation of the wet glazing attachment system was performed according to standard installation guidelines. A brief description of the process follows (Figure 2.18): (i) the top portion of the glass and mullion were taped off approximately 0.5 inches from both sides of the corner, (ii) the rubber gasket was removed using a razor knife and structural silicone was applied in the exposed groove, and (iii) after the silicone was dry to the touch, the tape is removed. Figure 2.19 shows a detail of the wet glazing attachment system. Sixteen windows had the wet glazing attachment system installed.

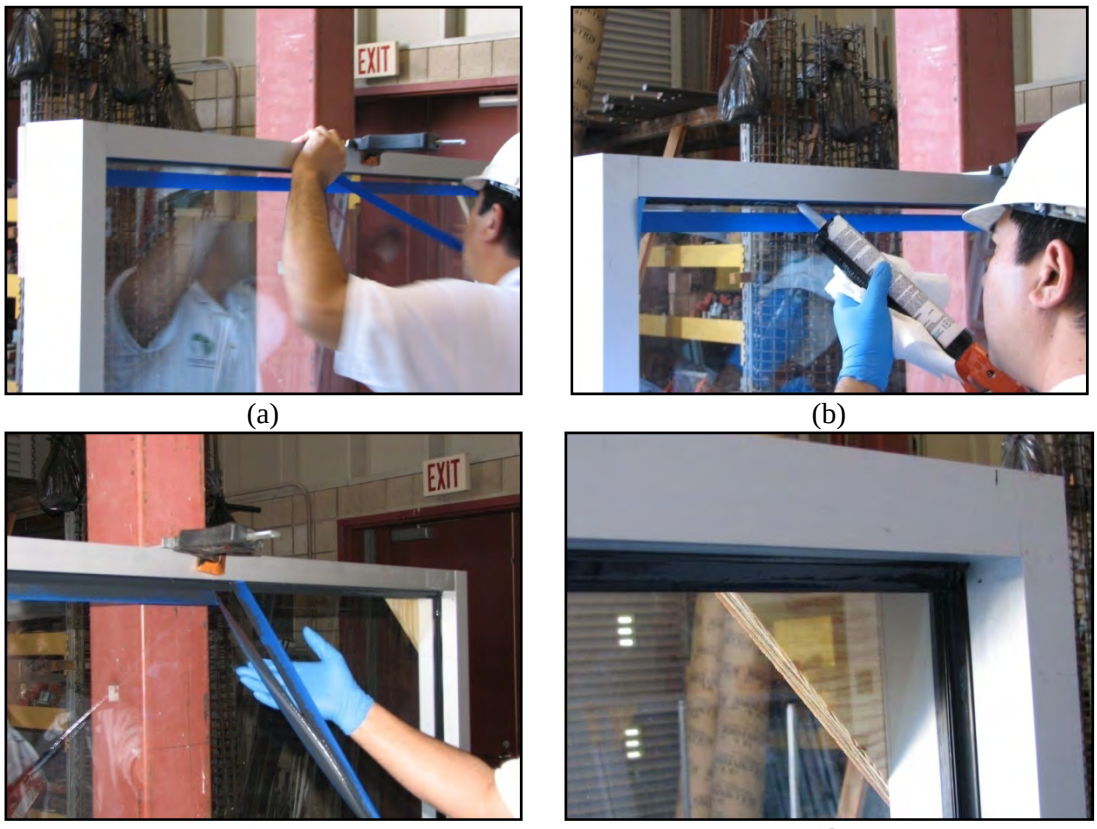

(a) (b)

(c) (d)

Figure 2.18 Wet Glazing Attachment System Installation

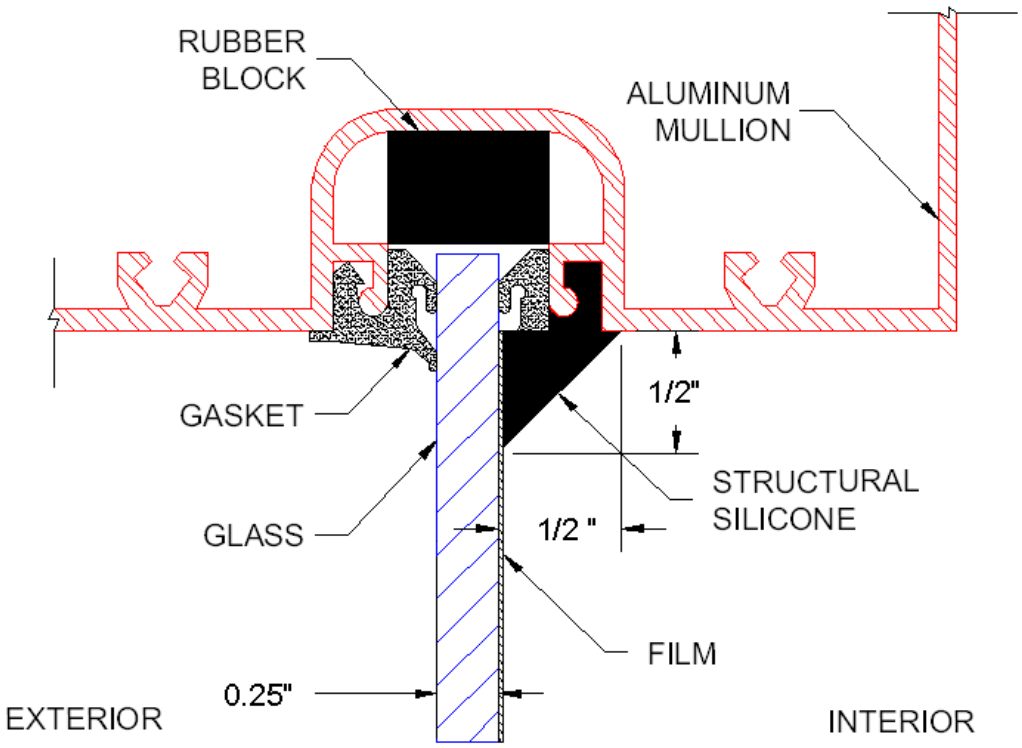

Figure 2.19 Wet glazing attachment system detail

2.5 Instrumentation

A total of 100 instruments were placed throughout the specimens to monitor displacements, rotations, strains, accelerations, and load. Conventional linear potentiometers and video cameras monitored the displacement field of the specimen and glass within the window system. Strain gauges were placed on the reaction frame to determine loads in the frame, while accelerometers measured the table and frame accelerations (Figure 2.20).

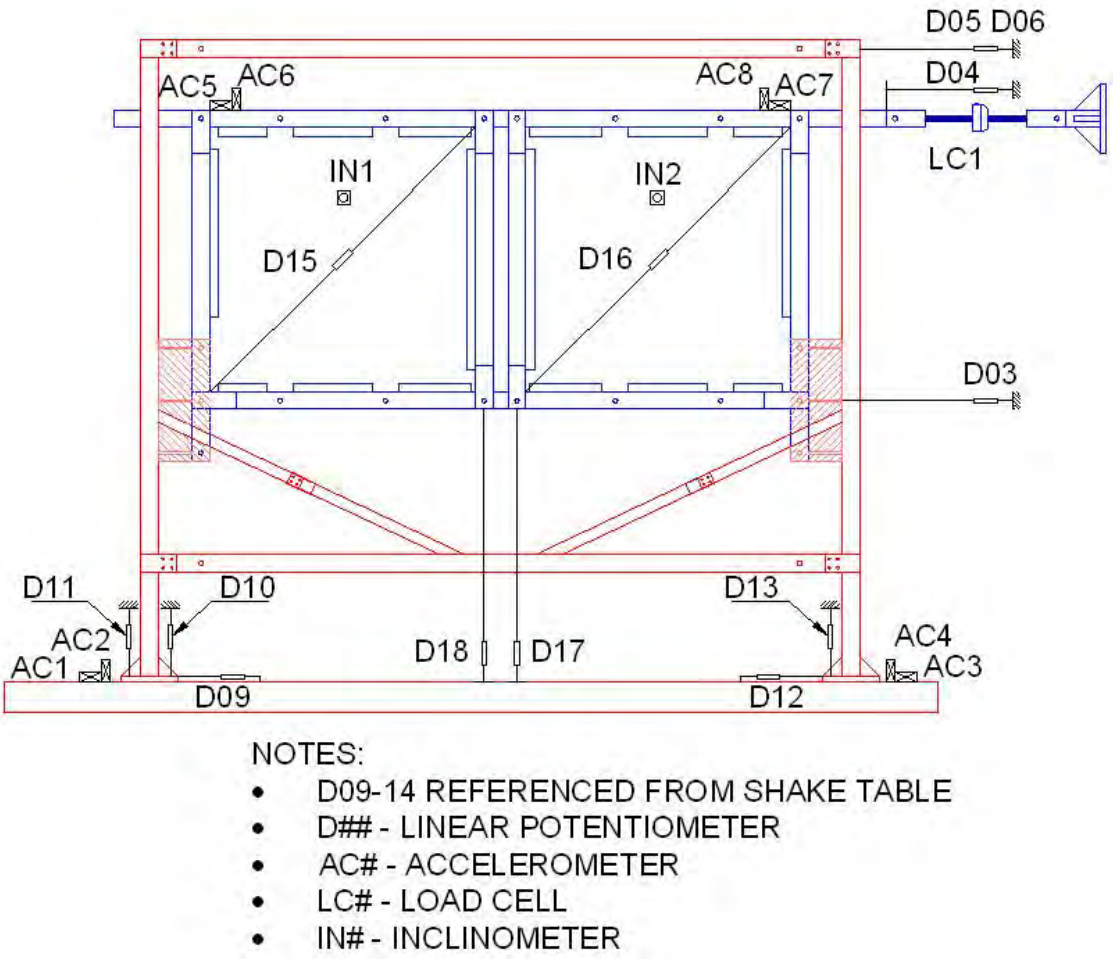

Figure 2.20 Elevation view of potentiometer, accelerometer and inclinometer setup

2.5.1 Instrumentation Support Frames

Stiff unistrut support frames were used to support instrumentation surrounding the reaction frame and specimens. Around each reaction frame footing two in plane and two out of plane supports were built 8 inches above the shake table floor. Linear potentiometers (LPs) were installed on the support frame at their target position. The center support frame for D17/18 was reinforced with cables leading away from the corners of the frame (Figure 2.22) to increase its rigidity. Instruments D02, D03, D05 and D06 are all attached to the window frame (Figure 2.21). An aluminum plate was installed (hot glue) as a joint target for D17 and D18. All data cables were run either through a single path along the top side of the shake table or up over the top of the window frame along a single path over the load cell and down the strong wall.

Figure 2.21 Drill and tap to attach potentiometers (D03, D05, D06)

Figure 2.22 Cables installed on D17 and D18 for vibration and deflection reinforcement

2.5.2 Strain Gauge Setup

The strain gauge setup required the surface preparation of grinding all paint from the areas where they were to be installed. Surfaces were then cleaned, gauges glued, protected with m-coat and finally a thick mastic tape was used to fully protect the installed gauge from mechanical damage. All gauge wires along the bottom horizontal member were run south along the member then up along the connecting vertical member. From that point the wires were run up over the load cell and down along the strong wall to a coffin (Figure 2.24). All other gauges were run directly up to the stationary horizontal member, then run south towards the load cell and down along the strong wall to a coffin. See Appendix A for strain gauge layout.

2.5.3 Accelerometer Setup

Accelerometers were installed using 90 degree aluminum angles hot glued to a mounting point (Figure 2.23). One was placed on the horizontal plane to measure the acceleration of the table and one was placed on the vertical section of the bracket to measure acceleration in the vertical direction. All accelerometer mounts were secured to the table using hot glue. The direction of sensitivity of the gauges AC6 and AC8 allowed the direct attachment to the window frame without the use of angle brackets.

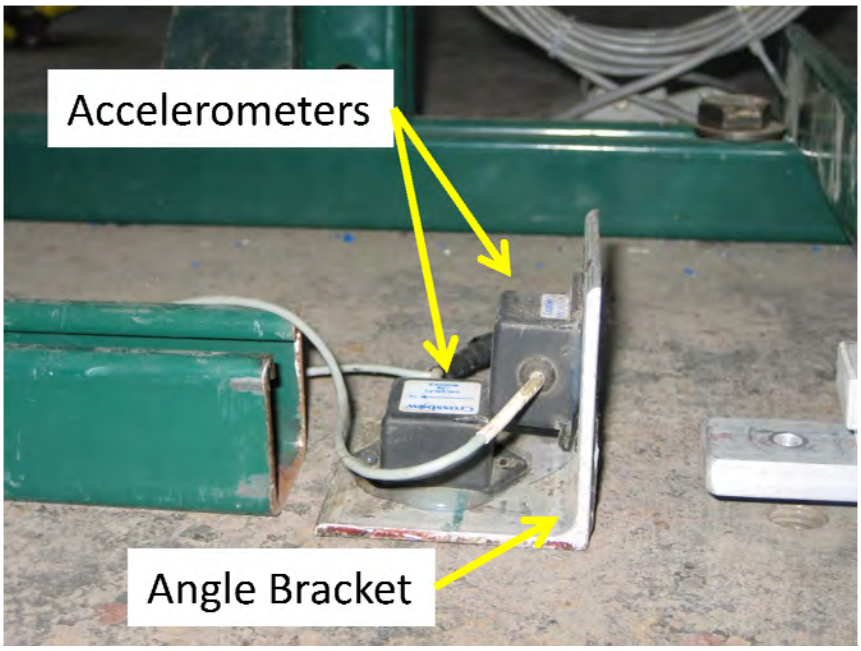

Figure 2.23 Aluminum angle glued to reaction frame and table for accelerometer installation

2.5.4 Load Cell Setup

The 50 kip load cell was calibrated using a MTS 810 Machine and placed in-line with the reaction frame and the strong wall. The load cell assembly is made up of two thread rods extending from either end of the load cell (Figure 2.24). These thread rods are then screwed into a plate-pin bracket to be attached via pin to the reaction wall and frame. The installation of the load cell was achieved as follows: The outer moment reaction frame was moved to the exact zero position and held with a crane. This was achieved by leveling the inner racking frame so that the outer members were perfectly vertical. Then the load cell was attached to the inner racking frame via pin connection. The large screws holding the load cell in place were then spun to align the pin hole located on the reaction wall.

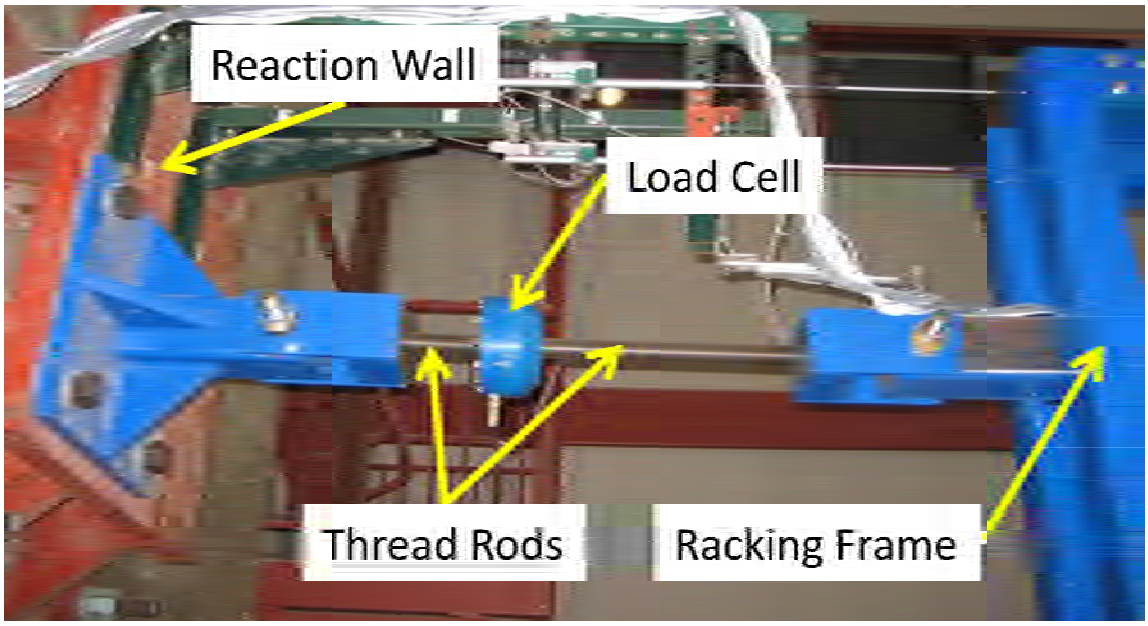

Figure 2.24 Load cell installation setup

2.5.5 Camera Setup

High speed video cameras were placed in each corner of a specimen to monitor the damage progression (Figure 2.25). The cameras used were of type Basler A301-FC. Each camera was mounted on a unistrut support placing the lens of the camera 18 inches from the glass and stabilized using lateral support cables (Figure 2.26). The horizontal and vertical placement dimension of the camera from the nearest pin connection in the racking frame was 13 inches and

18 inches. A two inch grid pattern of crosses was painted on the glass in each corner to aide damage tracking and scaling (Figure 2.27).

Backdrops were placed behind the specimens and backlit using two 1000 watt flood lamps (Figure 2.28). The backdrop was built out of a 2-ply bed sheet pulled taught over a wood frame much like a painter's canvas. The backdrop was attached to the top of the inner racking frame, which stayed stationary through the testing, therefore creating a stable non-moving backdrop.

Figure 2.25 Basler camera placement

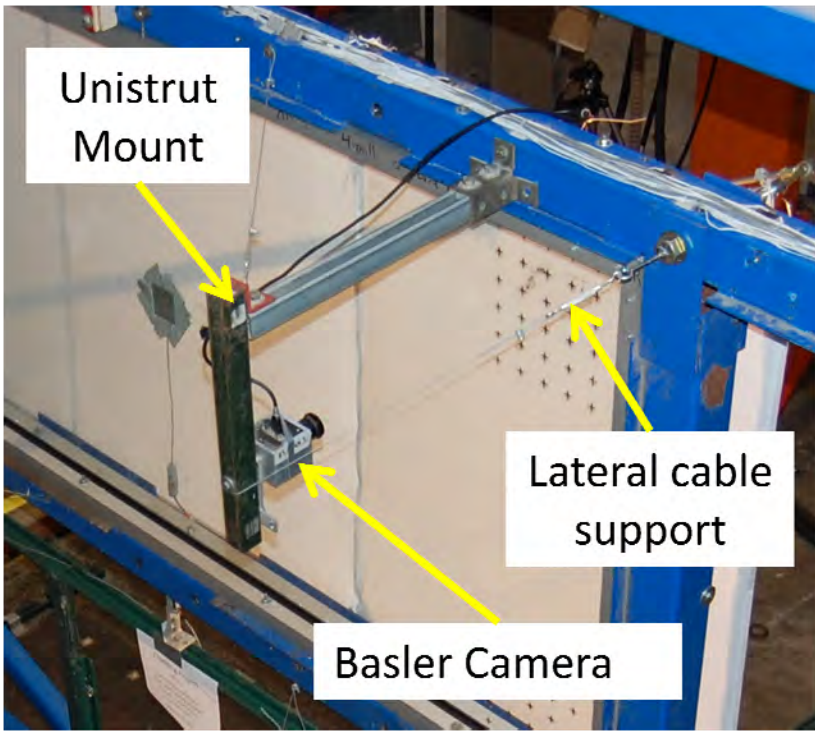

Figure 2.26 Video camera placement

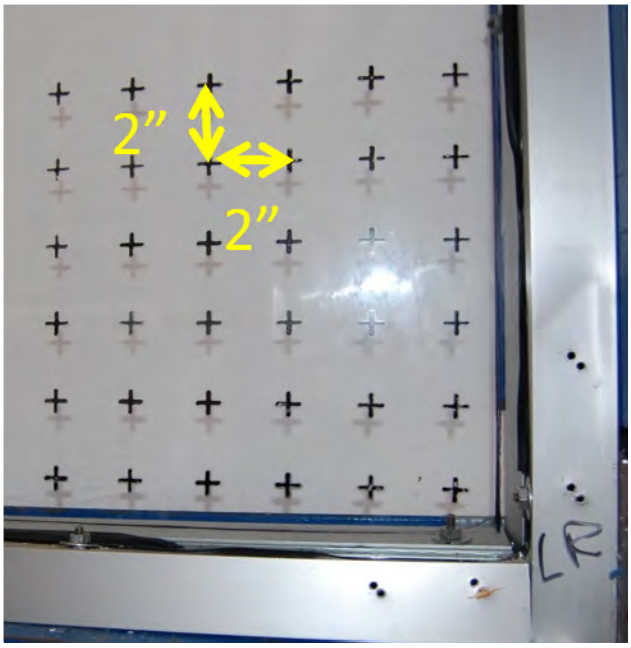

Figure 2.27 Two inch square grid pattern spray painted into each corner of the glass to aid damage tracking

Figure 2.28 Overall test setup (two 5'x5' specimen setup)

2.6 Load protocols

A group of specimens, denoted LP, were used to investigate the effect of loading protocols on the seismic response of glass panel systems. The following loading protocols were evaluated in the course of this study:

2.6.1 Monotonic (static) Load Protocol

Prior to cyclic degradation, it was desirable to characterize the monotonic behavior of the window specimens. This behavior defines the baseline capacity and damage modes of the window specimens. To achieve the monotonic load protocol, specimens were loaded in one direction at a rate of 0.03 in/sec (to ensure no inertial effects) until failure.

2.6.2 Crescendo (Dynamic) Load Protocol

This loading protocol was proposed by Behr and Memari (1996) in an effort to move towards a standard test method for evaluating the seismic performance of architectural glass and window systems. It is characterized by progressively increasing racking amplitudes. The "crescendo" test is a step-wise increasing amplitude swept sine function that has a total duration of six minutes. It

consists of a continuous series of alternating ramp-up and constant-amplitude intervals; each step is comprised of four sinusoidal cycles at a frequency of 0.8 Hz. A modification to the standard "crescendo" test was introduced by Brueggeman et al. (2000) to simplify the protocol and address limitations related to the hydraulic power supply and servoactuator volumetric flow requirements. The adopted protocol involves a racking frequency adjustment from 0.8 to 0.4 Hz to achieve the target dynamic drift amplitudes. Each drift amplitude step is 0.25''. It should be noted that the "crescendo test" is similar in configuration to the "multiple step test" described in ATC (1992). The "crescendo" load protocol has been adopted by the AAMA (2001b) (Figure 2.29) for determining the seismic drift that causes glass fallout from curtain wall and store-front system mock-ups, and for providing design guidance for the acceptable seismic performance of such wall systems.

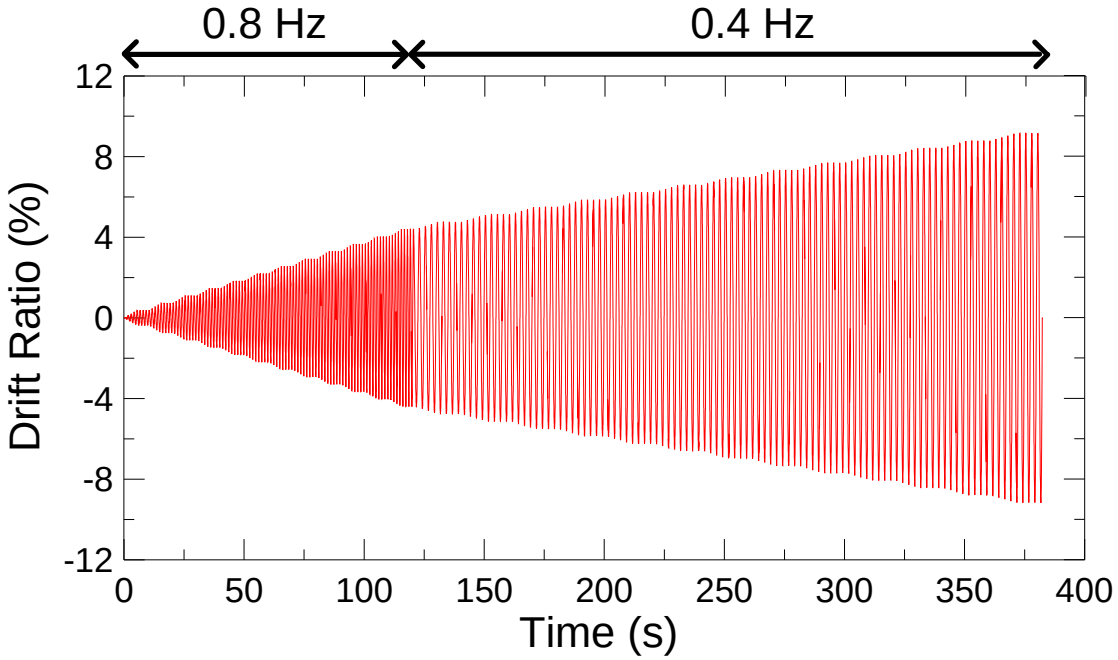

Figure 2.29 Crescendo load protocol

2.6.3 FEMA 461(quasi-static) Load Protocol

This loading protocol is characterized by increasing amplitude, reversed cyclic displacement-controlled loading (Figure 2.30). Two cycles per amplitude are selected to represent significant enough accumulation of damage per amplitude. Three different loading rates were chosen to ensure no inertial effects, while minimizing test length, and assuring sufficient time for physical inspection: 0.067 in/sec for the first three time steps, 0.134 in/sec for the next four time steps, and 0.268 in/sec for the final three time steps. The FEMA 461 (2006) load protocol contains less

cumulative cycles than the “crescendo” protocol. Therefore failure modes and associated drift limits that are sensitive to cumulative cycles may be observed when comparing like specimens tested under these two protocols. This loading protocol was developed by considering an ensemble of 20 earthquake ground motions propagated through numerical models of single-degree-of-freedom and multi-degree-of-freedom frame building structures, with periods ranging from T = 0.2 to 3.6 seconds. The FEMA 461 load protocol considered herein is targeted for application to drift sensitive nonstructural components.

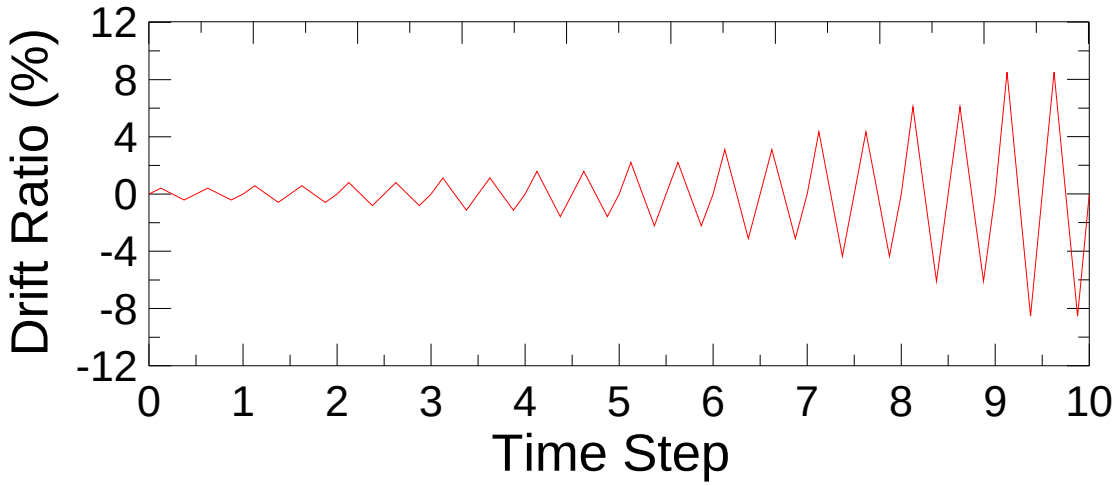

Figure 2.30 FEMA 461 drift-sensitive load protocol

2.6.4 Mid- and Low-Rise protocol

It is unclear if the “crescendo” load protocol is representative of demands induced on cladding systems used in buildings in the California seismic environment. In addition, while the FEMA 461 load protocol was specifically designed for drift-sensitive nonstructural components, the hysteretic response of drift sensitive nonstructural components varies broadly. For this purpose, in-structure drift time histories for two representative building structures were generated and used to develop two new load protocols for considering during these experiments (Hutchinson et al., 2008). These were referred to as the *Mid-Rise Load Protocol* (Figure 2.31) and the *Low-Rise Load Protocol* (Figure 2.32). The *Mid-Rise load protocol* was developed using interstory drift time histories generated from a 12-story building structure, while the *Low-Rise load protocol* was developed using interstory drift time histories from a four-story building model.

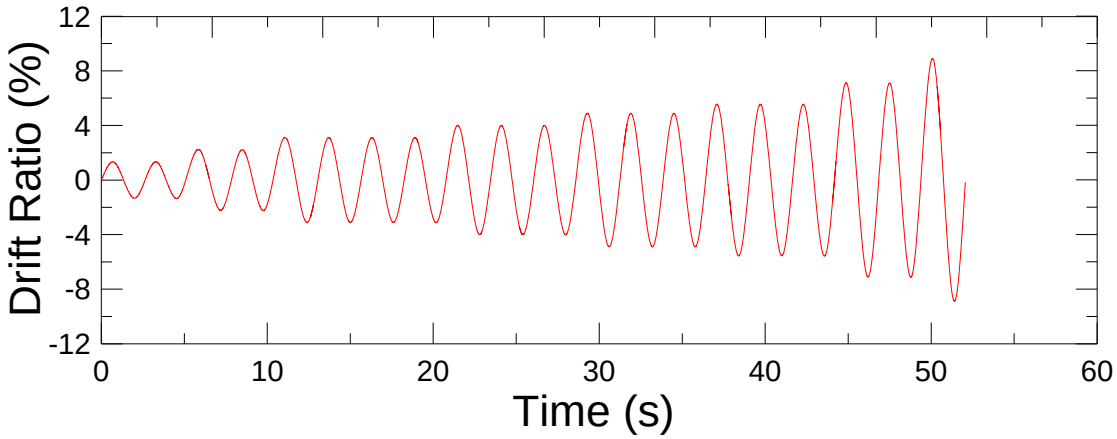

Figure 2.31 Mid-Rise Load Protocol (Hutchinson et al., 2008)

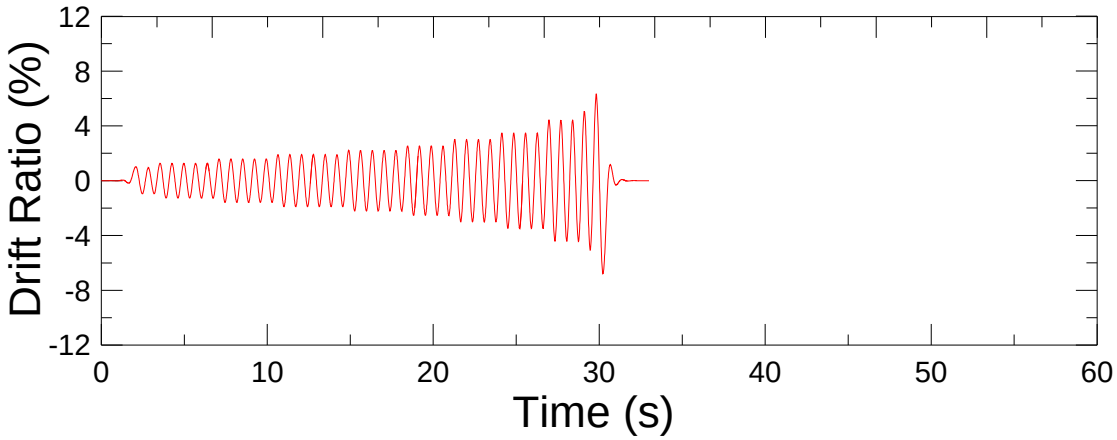

Figure 2.32 Low-Rise Load Protocol (Hutchinson et al., 2008)

Chapter 3: Experimental Results

3.1 Introduction

Experimental results are presented in terms of physical observations, global and local response and a comparative sense. First, observed modes of damage are described in the context of these systems. These damage states are then related to the interstory drift ratio of the specimens. Interstory drift ratio in this context is defined as the differential in-plane shear displacement divided by the vertical distance between the inner racking frame pins above and below the specimen. Finally, the global response, peak load and displacement, are evaluated. Like specimen groups are cross-compared to assess the effects of the variables considered in the program.

3.2 Damage State Observations

Damage to the window units is categorized into two main groups: (i) Serviceability Damage States (SDS) and (ii) Ultimate Damage States (UDS). SDS are damage modes, which results in the inability to immediately continue normal (service), however, the window system can be repaired with minimal cost and returned to its original serviceability state. UDS are damage modes, which are not repairable and pose an immediate safety hazard. Upon achieving an UDS, the window system must be completely replaced. Physical damage modes associated with SDS and UDS are described as follows:

Serviceability Damage States (SDS):

(SDS-1) Gasket Damage (Figure 3.1)

- Drift at which the perimeter gasket shows damage, this includes visible unseating (pullout or compression into mullion), tears, or shredded regions of gasket. Unseating, tears, or shredded lengths of more than 1” length of gasket was designated as the threshold for this damage state.

(SDS-2) Minor Glass Cracking (Figure 3.2)

- Drift at which a crack in the glass of less than 6 inches in length forms.

(SDS-3) Wet Glazing Attachment System Detachment (Figure 3.3)

- Drift at which a gap or tear large enough to see through (day-lighting) forms at the wet glazing attachment.

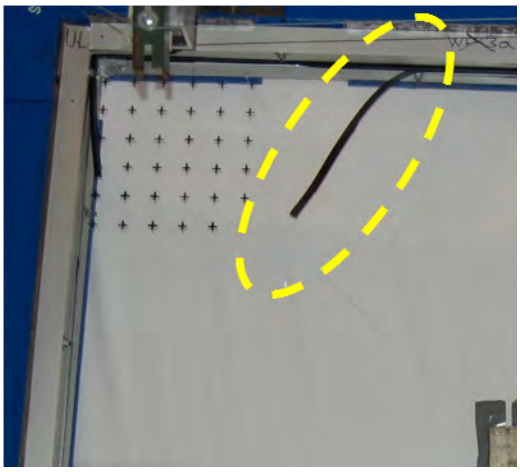

Figure 3.1 (SDS-1) Gasket Damage and displacement

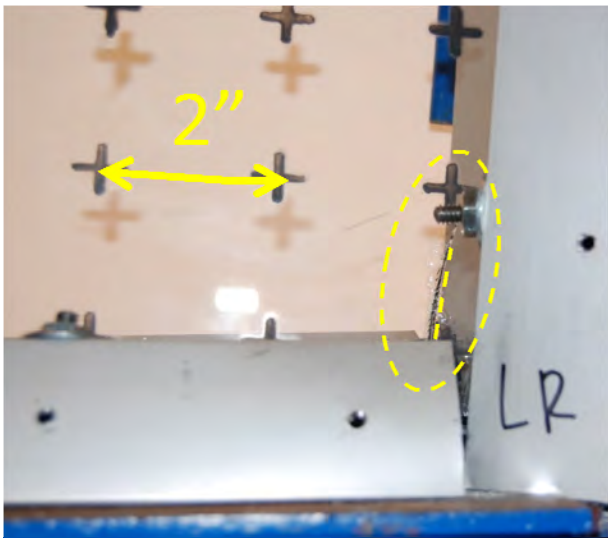

Figure 3.2 (SDS-2) Minor Cracking

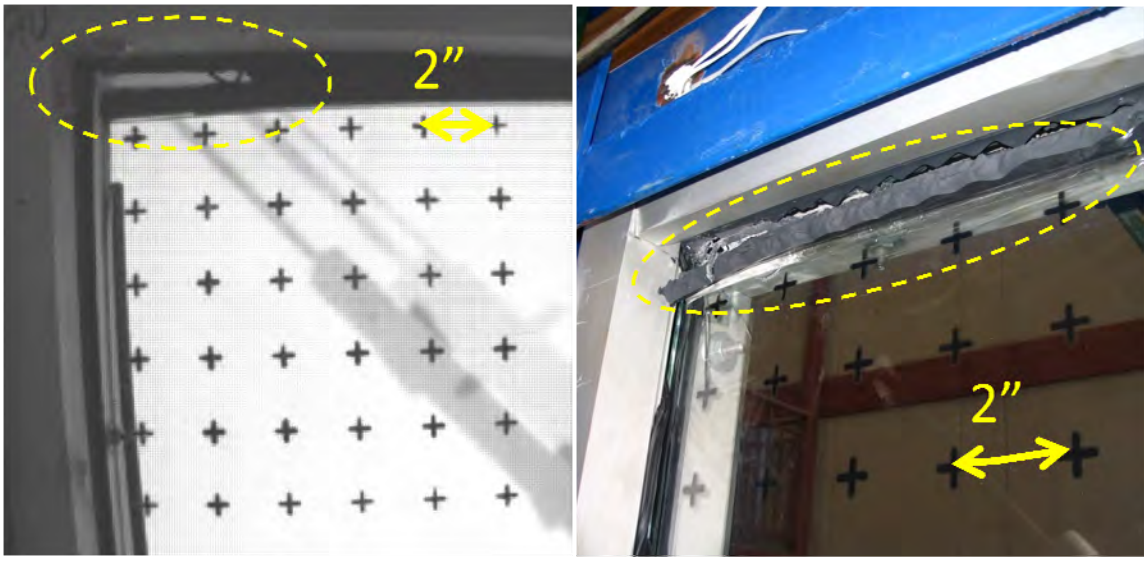

Figure 3.3 (SDS-3) Wet Glazing Attachment System detachment

Ultimate Damage State (UDS):

(UDS-1) Extensive Glass Cracking (Figure 3.4)

- Drift at which a crack in the glass extends beyond 6 inches in length

(UDS-2) Glass Fallout (Figure 3.5)

- Drift at which an area of glass larger than 1 square inch falls from the window system.

Figure 3.4 (UDS-1) Extensive glass cracking

Figure 3.5 (UDS-2) Glass Fallout

3.3 Global Response

Samples of the global response for each of the load protocols considered in the LP series are presented in Figures 3.6-3.8. Each plot presents the system load (kips) versus the interstory drift ratio (%) for specimens with 2 mil film, where the film is unattached. All other global response plots can be found in Appendix B. The system cyclic behavior indicates dominance by the characteristics of the aluminum frame at the early drift ratios, as seen by the relatively soft behavior at 3% to 4% drift ratio. Subsequently, contact of the glass with the boundaries and sufficient compression of the surrounding rubber blocks results in a hardening behavior. These characteristics of the hysteretic response were consistent for all specimens. Similar global response characteristics can be observed in the various global response plots, including a generally pinched-style hysteresis, subsequent hardening upon attainment of large drift ratios (up to 4%). Pinched hysteresis behavior is attributed to the glass moving through a gap in contact with the frame as it rotates in the window.

Due to various system limitations imposed drift ratios for each protocol differs. Large drift ratios were achieved with the monotonic protocol by detaching the load cell anchor point, moving the shake table to the maximum negative position, reattaching the load cell then pushing through zero to the maximum positive stroke of the table. Peak drift ratio input was reduced in the *low-rise load protocol* due to system maximum velocity limitations. *Crescendo*, *FEMA 461* and *low-rise load protocols* were able to be pushed to peak cyclic system displacements in both positive directions of 8.5% for the 5'x5' window systems.

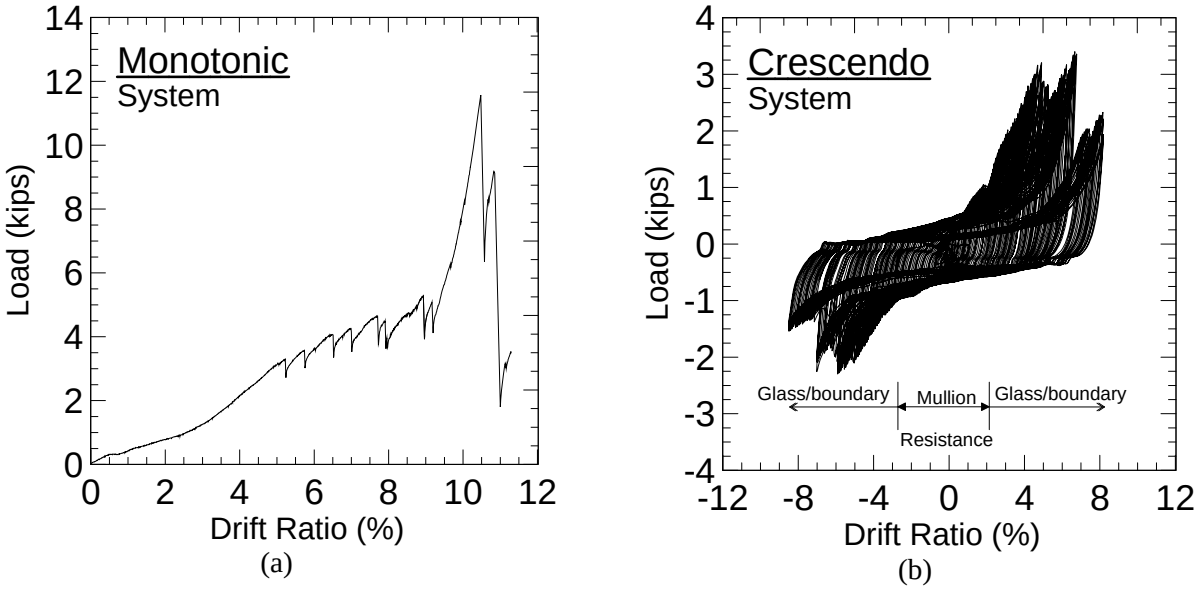

(a) (b)

Figure 3.6 Global response from tests (a) Monotonic 4 and (b) Crescendo 3 –Two-5'x5' specimens with 2mil of film unattached.

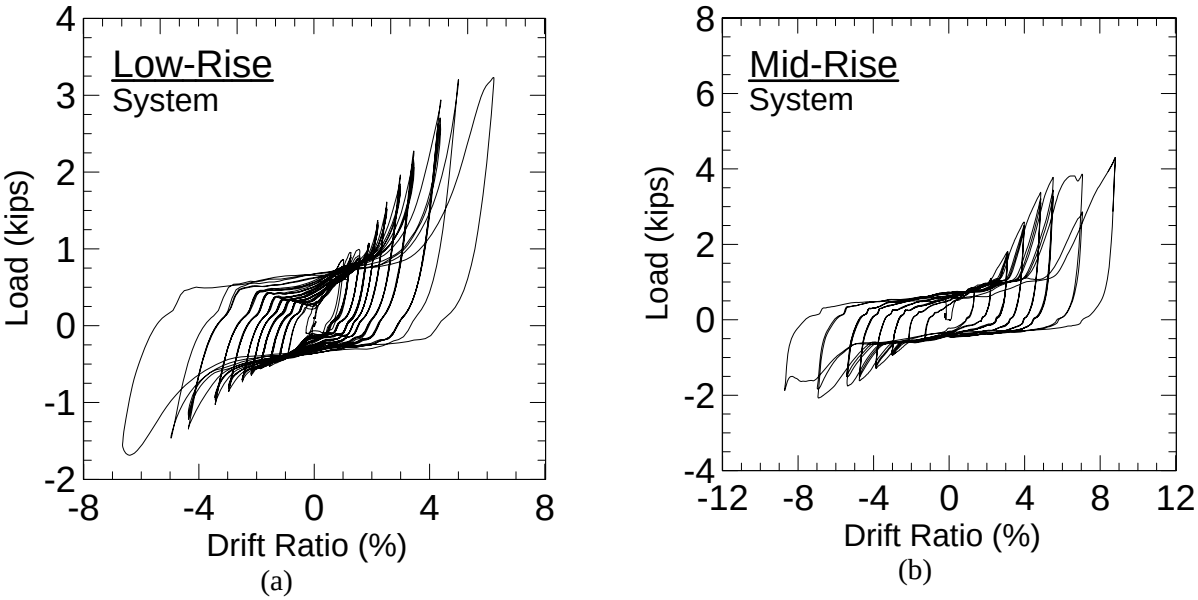

(a) (b)

Figure 3.7 Global response from tests (a) Jian IV (*low-rise load protocol*) and (b) NewLP 1 (*mid-rise load protocol*) - 5'x5' specimen with 2mil of film unattached

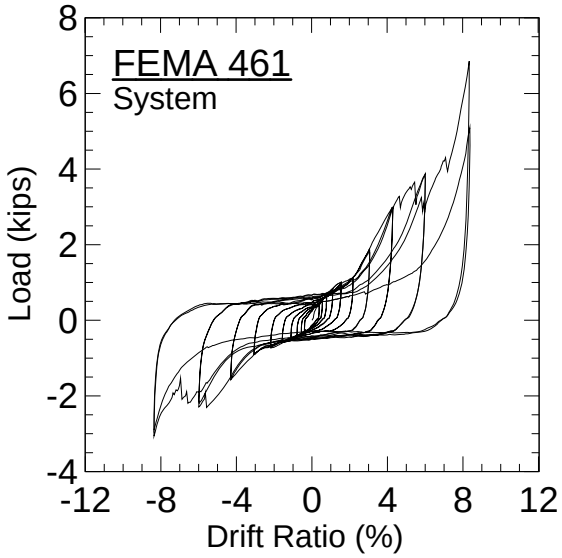

Figure 3.8 Global response plot from test FEMA 2 (FEMA 461 load protocol) - 5'x5' specimen with 2mil of film unattached

3.3.1 Individual Specimen Load

The baseline specimens (5'x5' panel size) were tested in pairs, placed in parallel. Given that a single load cell measured the system load, this meant that the individual panel load had to be extracted on a test-by-test basis. Figure 3.9 is an example of the system load of one test (FEMA 2 – LP09c_LP09d) composed of two 5'x5' specimens dissected into its associated panel loads (Figure 3.10).

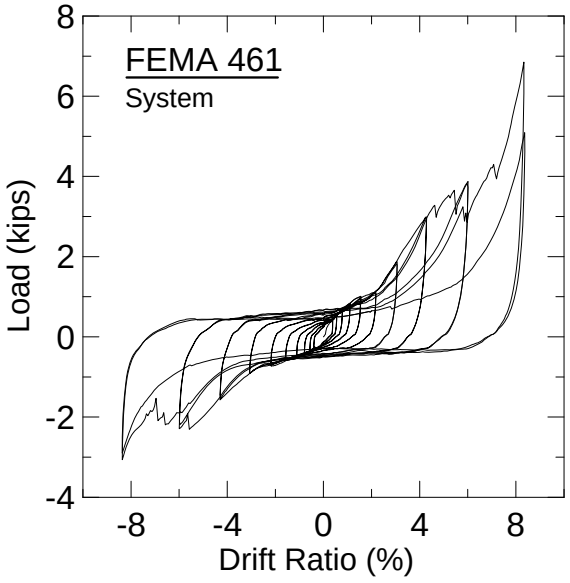

Figure 3.9 System Load versus Drift Ratio % (Two 5'x5' specimens both with 4 mil film)

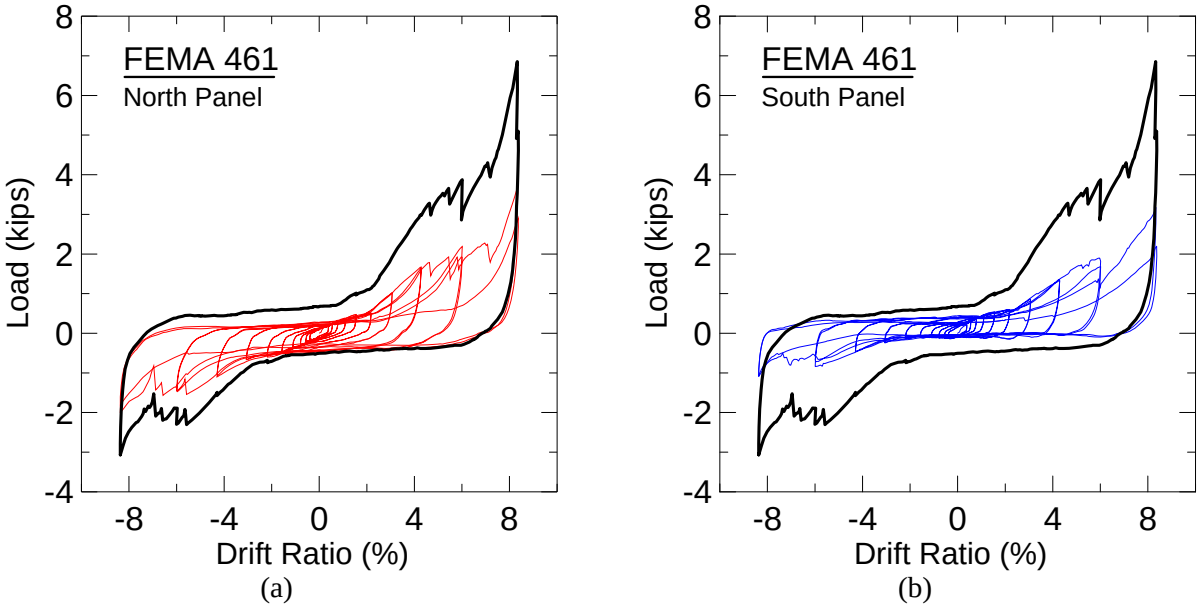

Figure 3.10 Load per panel versus drift ratio: (a) Load in north panel. (b) Load in south panel overlaid with system load envelope (5'x5' specimens – 4 mil film, test FEMA 2**)**

The separation of the Panel Loads from the System Load was achieved as follows. When the panels are subject to a positive drift ratio (Shake table moving to left in Figure 3.11) the upper left and lower right corners of both windows will contact the inner reaction frame. From the north panel this will cause a downward component force at point F and an upward component force at point G from the south panel (Figure 3.11). When these forces (F-North and F-South) are equal the system load measured through the load cell is evenly distributed between the panels. However if F-North and F-South are not equal then the load distribution between the panels is not equal. Uneven forces in the panels will cause members A-D and E-H to deform either upwards or downwards. Figure 3.12 (left) shows that when F-North is larger than F-South, members A-D and E-H deform downwards. Figure 3.12 (right) shows the opposite.

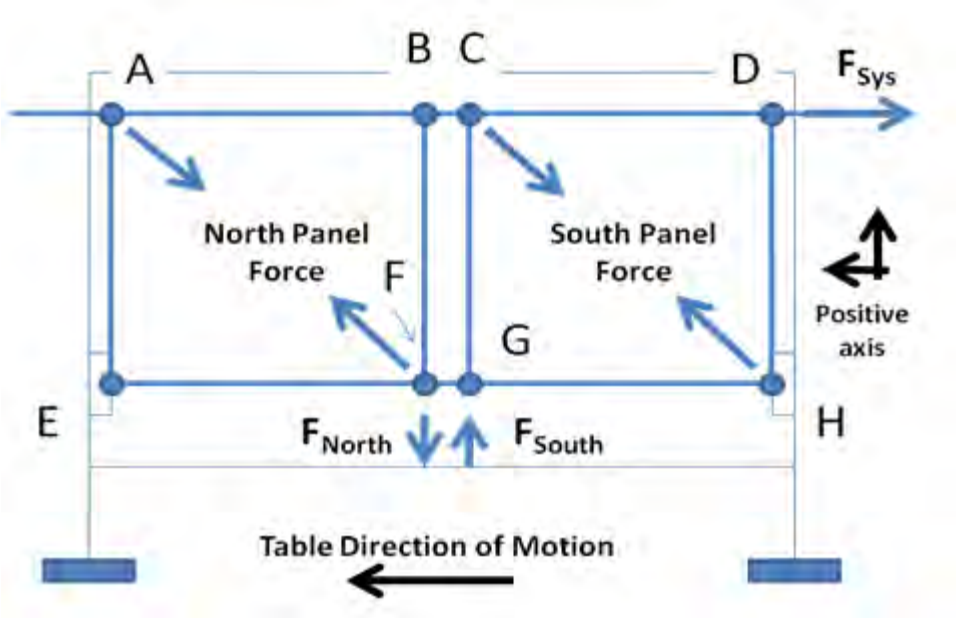

Figure 3.11 Equal load distribution when table is moving in positive direction

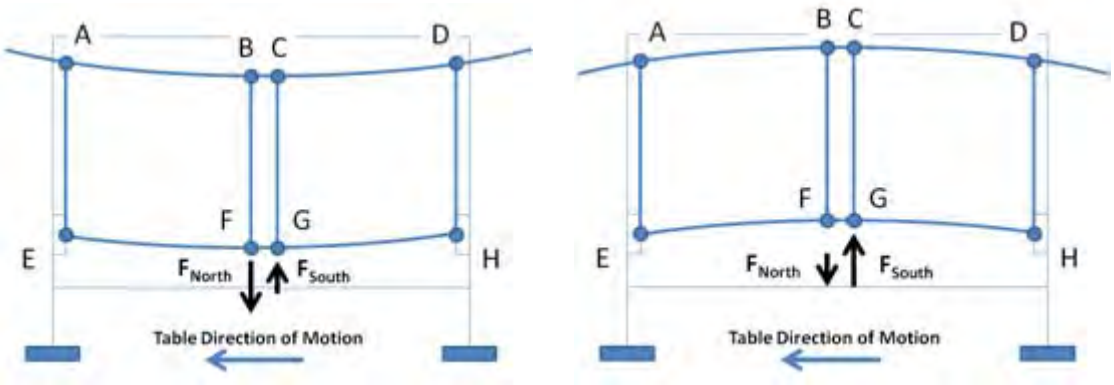

(a) (b)

Figure 3.12 Unequal load distribution when table is moving in positive direction. (a) North panel with larger force contribution. (b) South panel with larger force contribution**.**

The displacement at points F and G are captured with the gauges D17 and D18 (Figure 2.20). D17 and D18 are averaged to obtain D_{avg}, and assume a mid-span deflection. Then using the equation for max displacement of a simple beam under a concentrated point load in the center ((3.1) the required load (F_{net}) to achieve D_{avg} can be back-calculated.

$$F_{net} = \frac{D_{avg} 48EI}{L^3} \tag{3.1}$$

Where L = length of members A-D or E-H (which are equal), E = Modulus of Elasticity of the members A-D and E-H, and I = weighted average moment of inertia of members A-D and E-H.

The weighted average moment of inertia is calculated as follows: Both members were composed of two different cross sections along their length. Section I is a built-up section, as shown in Figure 3.13, whereas Section II is just the HSS 4”x4”x1/4” part of section I. The moment of inertia of section I is 16.26 in^4, while the moment of inertia of section II (HSS section alone) is 7.80 in^4. Section I is used for 91 inches of the total length, while Section II is used for 45.5 inches. The weighted average of the moment of inertia is calculated by taking the sum of the moment of inertias multiplied by their corresponding length divided by the total length. For sections A-D and E-H the weighted moment of inertia is 13.44in^4. Since both members resist the bending forces, the total moment of inertia used in equation 3.1 was 26.88in^4.

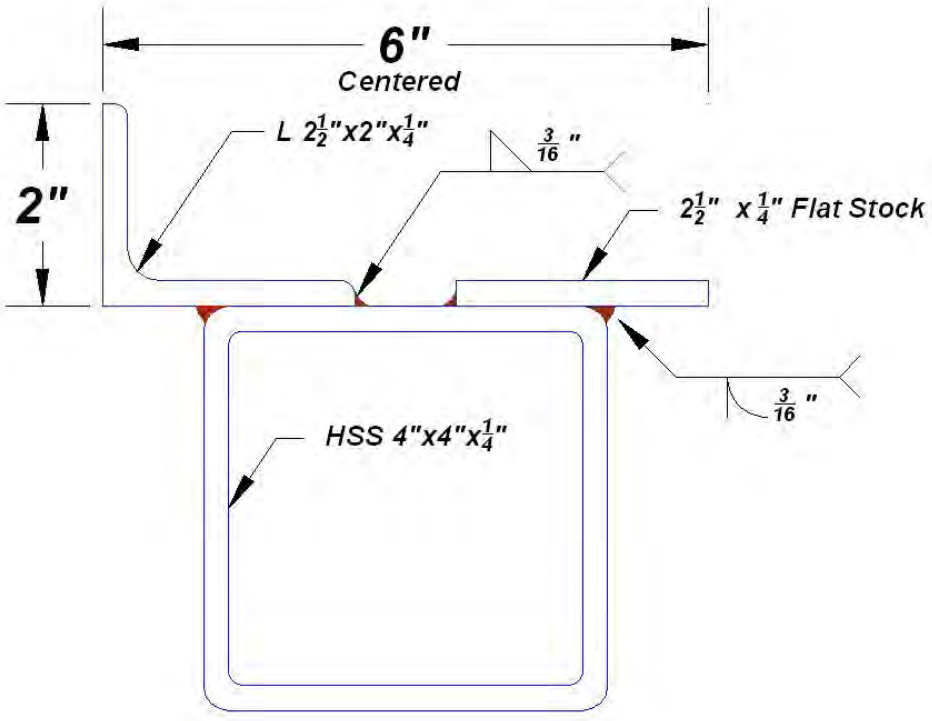

Figure 3.13 Detail of section I for members A-D and E-H

Since the component forces of F_{north} and F_{south} are equal due to a 45 degree angle component breakdown it can be concluded that the sum of F_{north} and F_{south} equals F_{sys}. Assuming the difference between the north and south panel forces equals F_{net} ($F_{net} = F_{South} - F_{North}$) the load in the south panel at any given time can be calculated:

$$F_{North} = \frac{F_{sys} - F_{net}}{2} \tag{3.2}$$

Substituting 3.1into 3.2 we get:

$$F_{North} = \frac{F_{sys}}{2} - \frac{D_{avg} 48EI}{2L^3} \tag{3.3}$$

To verify this method it was applied to a specific test where one panel had completely shattered and fell from the system. Upon failure, zero load will be carried by the shattered window unit, while the measured total system load will be carried by the intact panel. Figure 3.14 (Test Monotonic 11) represents a typical test case in which this occurred. First the system is loaded and a plateau reached (point A) where all gaps (glass to mullion and mullion to frame) closed. Stiffening of the system is attributed to the transfer of load to the rubber stops at contact locations (region B). For Test Monotonic 11, the first minor crack occurs in the South panel at a peak load of 4.5 kips (point C - 6.5% Drift ratio). The South panel then develops a major crack (C^1) and the load redistributes to the North Panel. This causes local stress concentrations in the north panel which subsequently cracked (C^2). Finally at a drift ratio of 7.68% (point C^3), the south panel fully shatters and falls from the system. Subsequently, the system load should equal that of the North panel. Figure 3.14 indicates this to be true (region D). Beyond 7.68% drift ratio all load measured through the load cell is registering only in the north (intact) panel.

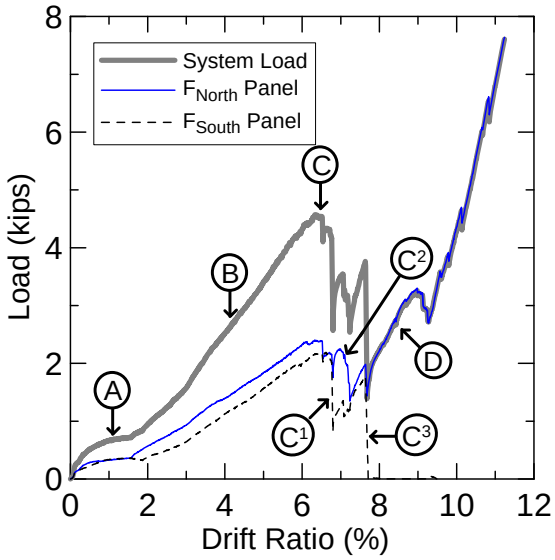

Figure 3.14 South Panel falls from system at 7.7% drift ratio (two 5'x5'specimens both without film, test Monotonic 11)

Chapter 4: Results Analysis

4.1 Correlation between Small Scale and Full Scale Testing

Correlation between full scale behavior and small scale testing results is extremely valuable, primarily due to the lower cost of testing smaller specimens. Similar failure modes between small and full scale testing were crucial for this correlation. As noted in Section 2.1 Small Scale Pilot Tests the application and thickness of film does not affect the cracking pattern of the specimen. The small scale test results showed that the primary failure mode was buckling. Each of the panels failed in this manner. From full scale testing, it is observed that 73% (15) of those panels that failed in a manner attributed to buckling. The remaining failures are attributed to local stress concentrations due to variable rubber block placement or wet glazing attachment system. Figure 4.1 (2 mil film) and Figure 4.2 (8 mil film) show photographs of a typical ultimate failure mode as observed in both a small scale and full scale test. The solid line overlays represent primary stress cracking caused by the in-plane loading. The dashed lines represent the buckling plane in which the specimen failed. Note the similarities between the two tests: Both tests showed a buckling plane perpendicular to the loading plane through opposite corners of loading. Both tests also showed primary tensile stress fracture cracks forming parallel to the loading plane.

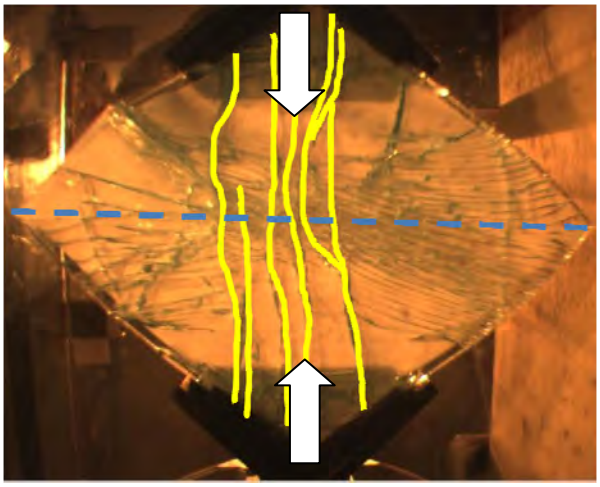

Figure 4.1 Small Scale at failure displacement– Typical Failure Mode: Buckling (12”x12” specimen with 2 mil film) – direction of loading indicated by white arrows.

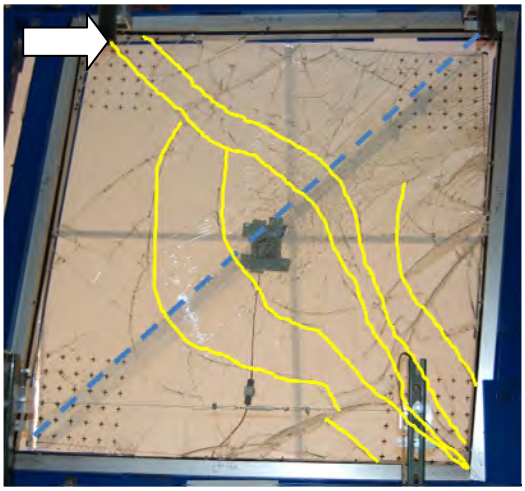

Figure 4.2 Full Scale at failure displacement – Typical Failure Mode: Buckling (5’x5’ specimen with 8 mil film – un-attached) – direction of loading indicated by white arrows.

The vertical ultimate load (peak load obtained) applied to the small scale specimens can be converted to horizontal shear load for direct comparison to the loads applied to the full scale specimens:

$$Load_{full\ scale} = Load_{Small\ Scale} * \sin(45°) \tag{4.1}$$

Figure 4.3 compares the measured ultimate loads obtained by the small scale (solid bar) and full scale (hatched bar) tests. The average ultimate failure loads from the small scale tests were within 4% of the average full scale loads for any film arrangement. This observation can be attributed to the buckling failure mode.

Theoretical buckling loads were calculated based on the panel loading configurations. Little to no moment resistance was expected at the ends of the small scale panel, therefore the buckling load was calculated using an effective length factor (K) of 1.0. The length of one side (12 inches) was used for the width portion of the moment of inertia and the unsupported length was estimated as the distance between the rubber block supports where the panel was loaded. In the small scale testing the un-braced diagonal length was approximately 75% of the total diagonal length. Using a modulus of elasticity of 10.6×10^6 psi for the glass, a critical buckling load of 7.14 kips was estimated for the small scale tests. Full scale calculations varied slightly from the small scale where the effective length factor (K) was believed to be in between 1.0 and 0.5 because some moment resistance (yet not perfectly rigid) can be anticipated due to the flexibility of the mullion. A value of 0.75 for K was therefore chosen. The un-braced length was calculated using visual observations of the extent of damage, from the experimental results. When the full scale panels buckle there were portions of the glass which stayed in plane and sections that left that plane. The diagonal length of the glass parallel to loading that was no longer in plane was assumed to be the un-braced length. The average un-braced length was 45% of the total diagonal length. Calculations can be found in appendix E.

The above calculations resulted in a theoretical critical buckling load of 7.14 kips for small scale and 7.29 kips for the full scale tests. Experimental results are plotted in Figure 4.3 overlaid with calculated critical buckling loads.

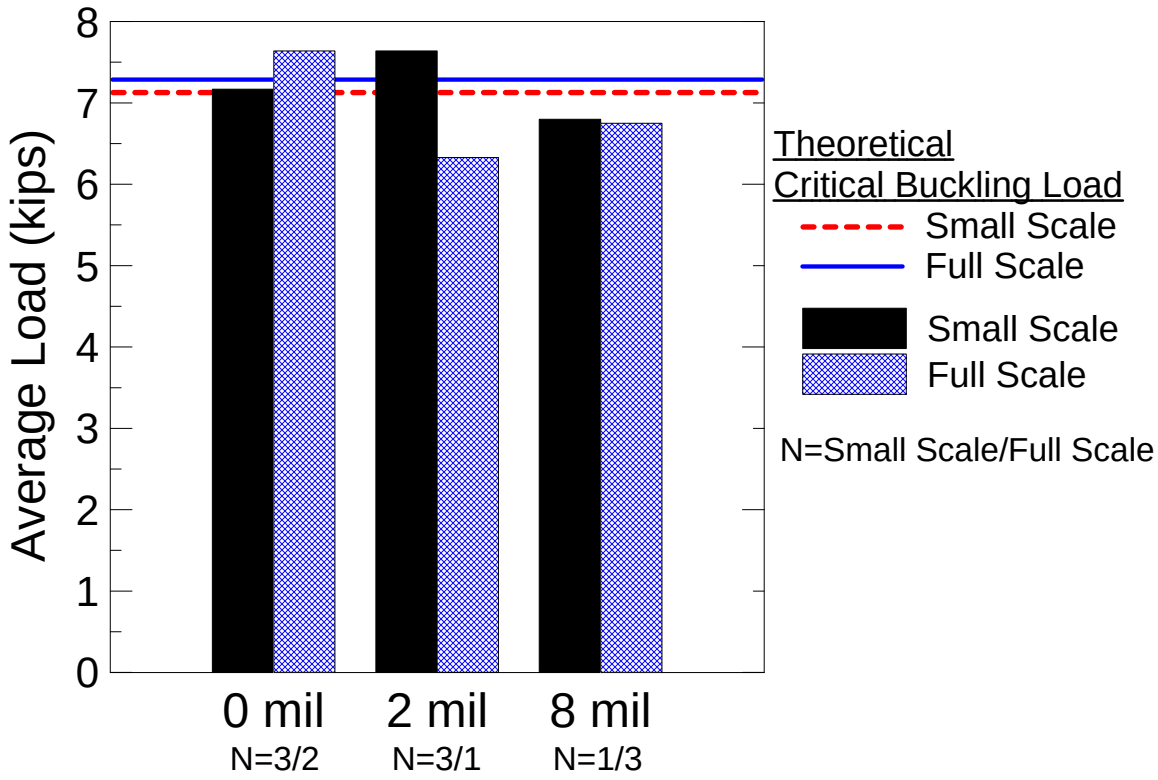

Figure 4.3 Correlation of Load between small scale testing and full scale testing (AR: 1.0 - Monotonic Load)

4.2 Effect of Film and Attachment System

Window film is designed to contain cracked glass in window systems. Because of this, the damage states SDS-2 (Minor Cracking) and UDS-1 (Extensive Cracking) were of particular interest when synthesizing effects of film and attachment system on the system limit states. While the discussion will focus on SDS-2 and UDS-1 damage states, in Figure 4.4 all damage states are shown, for completeness in presentation and use in later discussions.

The average drift ratios in which SDS-2 and UDS-1 occurred for both filmed (unattached) and non filmed specimens from monotonic loading can be found in Figure 4.4. For all damage states (except SDS-1) the filmed window performed better - damage states occurred at a higher drift ratio. SDS-1 (Gasket damage) was not affected by the thickness or application of film because the film (when unattached) does not restrict the movement or rotation of the glass within the mullion. This movement and rotation within the frame is what leads to gasket damage (refer to Section 4.6). For SDS-2, the filmed windows had on average 34% higher drift ratios. For UDS-1, the filmed windows had on average 12% higher drift ratios.

The presence of the wet glazing attachment system increases the secant stiffness, as shown in Figure 4.5. In this case, secant stiffness is calculated as the secant through the origin and the target drift ratio on the x-axis. Note that at each drift ratio, the stiffness of the attached specimen is larger. At 6% drift ratio, the gap between the attached and un-attached specimens is reduced because at this point the attachment system begins to fail in most specimens.

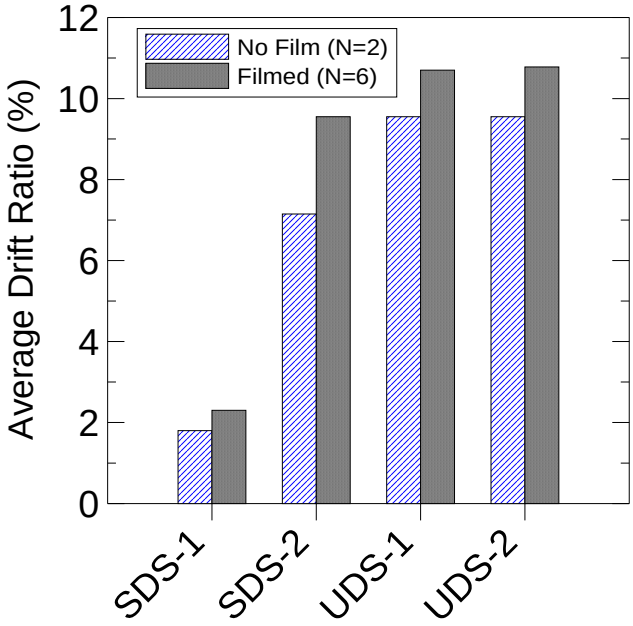

Figure 4.4 Effects of Film on all applicable damage states (all 5'x5' specimens subjected to the Monotonic load protocol)

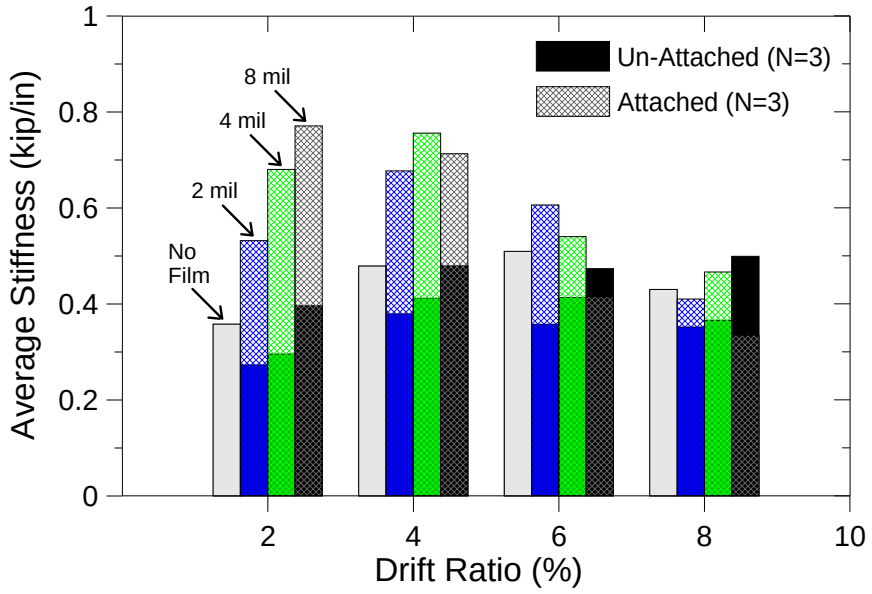

Figure 4.5 Effects of attachment system on the secant stiffness at specified drift ratios (all 5'x5' specimens subjected to the Monotonic load protocol)

The effects of different film thicknesses as well as attachment on all damage states can be found in Figures 4.6 - 4.8. Data shown in these figures are those specimens tested under the FEMA 461 load protocol. There was no discernable trend on the drift ratios associated with the identified damage states with varying the film thickness. However in every case when the attachment system was installed there was a significant drop in drift ratio at which the damage state occurred (except for SDS-1 where the increase is nominal due to specimen to specimen variability). For minor cracking (Figure 4.6b) 2 mil film observed a 33% drop, 4 mil film observed a 49% reduction and 2-ply 8 mil film observed a 14% reduction in drift ratio capacity. For extensive cracking (Figure 4.8a) 2 mil film observed a 32% reduction, 4 mil film observed a 49% reduction and 2-ply 8 mil film observed a 30% reduction in drift ratio. Overall, when the window system was attached, an average reduction in drift capacity associated with minor cracking (SDS-2) of 32% was observed and 37% reduction for extensive cracking (UDS-1). Note that a null value in Figures 4.6 - 4.8 means that the particular damage state was not obtained.

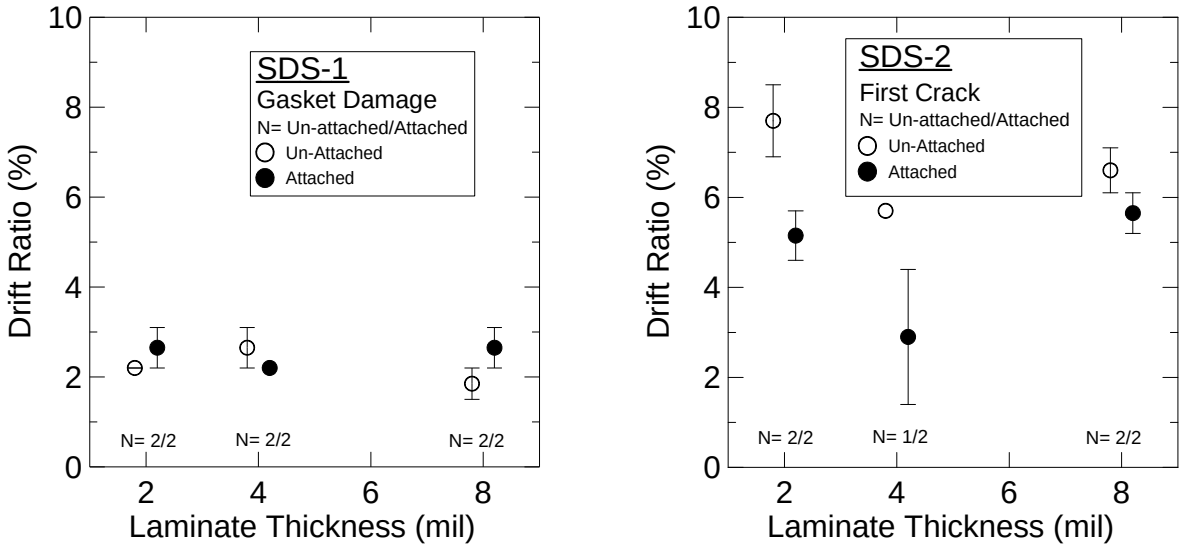

(a) (b)

Figure 4.6 Effects of film and attachment system on serviceability limit states: (a) gasket damage and (b) first crack (AR 1.0 specimens subjected to the FEMA 461 load protocol)

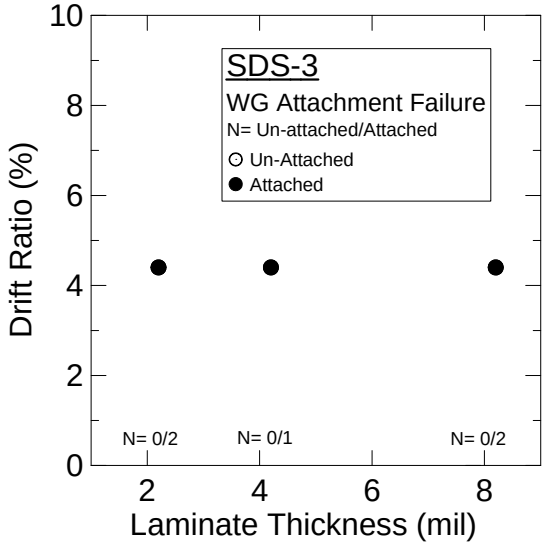

Figure 4.7 Effects of film on attachment system failure (AR 1.0 specimens subjected to the FEMA 461 load protocol)

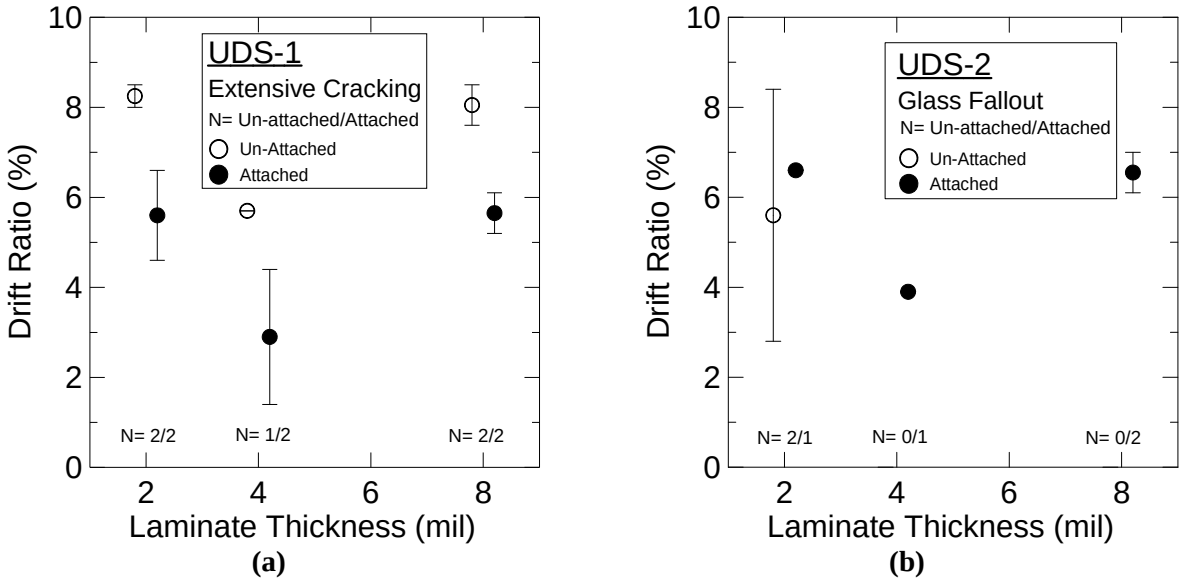

Figure 4.8 Effects of film and attachment system on ultimate damage states: (a) extensive cracking and (b) glass fallout (AR 1.0 specimens subjected to the FEMA 461 load protocol)

The considerable reduction in drift ratio capacity of the windows can be attributed to the increased stiffness the attachment system provides (Figure 4.5). This restricts the movement of the glass within the mullion frame causing stress concentrations along the attached edge, which lead to premature cracking. In Figure 4.9, the specimen was filmed with a 2-ply 8 mil film, which was attached along the top edge. The resulting damage was extensive cracking focused on the top edge around the attachment system. The UDS-1 (extensive cracking) drift ratio for this particular test was 5.6%, where as a similar panel tested without the attachment system had a UDS-1 drift ratio of 8.1%, a 31% decrease in drift ratio capacity.

Figure 4.9 Stress concentrations along the top edge of the glass (5'x5' panel with 2-ply 8mil film and wet glazing attachment system subjected to Monotonic load protocol)

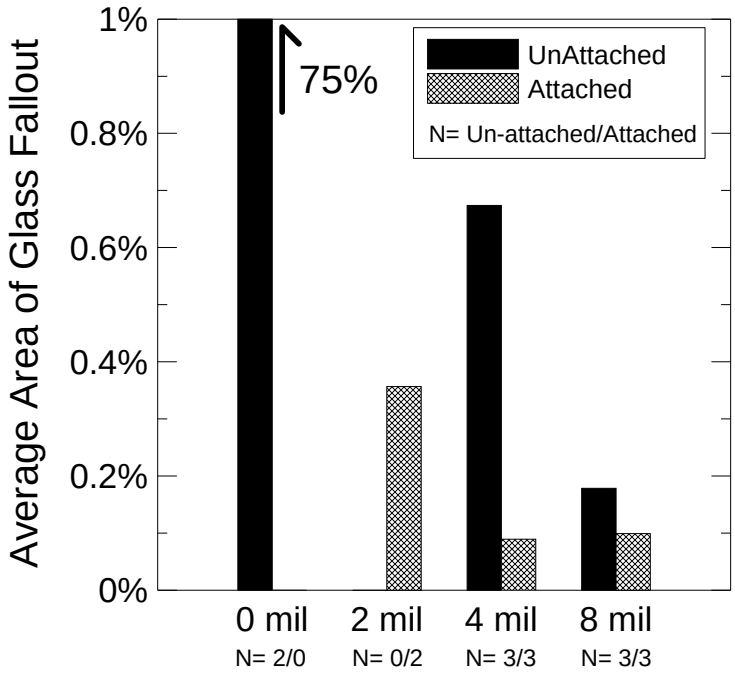

Figure 4.10 Effects of film on percent area of glass fallout (AR 1.0 specimens subjected to the Monotonic load protocol)

Film, in general, when applied, will contain more than 99.0% of the area of an extensively cracked glass panel (Figure 4.10). In comparison with the unfilmed specimens, where of the N = 2 specimens, which reached UDS-2, 75% of the area of glass on average (±20%) fell from the specimen during testing under the Monotonic load protocol. When film is attached using the wet glazing attachment system, it was found that it will contain more than 99.6% of the area of extensively cracked glass. Another pragmatic experimental observation was that when 4 mil or greater film was installed; the glass panels were much more easily and safely removed after they were damaged. The heavy film better secures the large broken shards of glass.

4.3 Effect of Load Protocol

Figures 4.11 - 4.15 present the load versus displacement response for the various load protocols, for the North panel in the two-panel (5'x5') in-series configuration (Figure 2.12) and with 2 mil film applied. While the general shape of the hysteretic response of the various specimens is similar, the point of in which the limit state occurs is different, and is sensitive to the load protocol applied. For example, Figure 4.11, which compares the high cycle count Crescendo load protocol to the relatively low cycle count FEMA 461 load protocol, indicates that the Crescendo load envelopes the hysteresis behavior of the specimen as characterized by the FEMA 461,

however, the damage states are delayed to larger drift ratios for the FEMA 461 specimen. This trend is consistent when comparing the Crescendo with the Mid-rise protocol (Figure 4.15), or when comparing the Mid-rise (20 cycles) and Low-rise (40 cycles) protocols (Figure 4.14). The protocol with a higher cycle count (Low-rise) shows a much lower drift ratio for the SDS and UDS, than the low cycle count (Mid-rise) protocol. Note that rate effects in general seem to have little effect on the damage state or general hysteresis response (Figure 4.13).

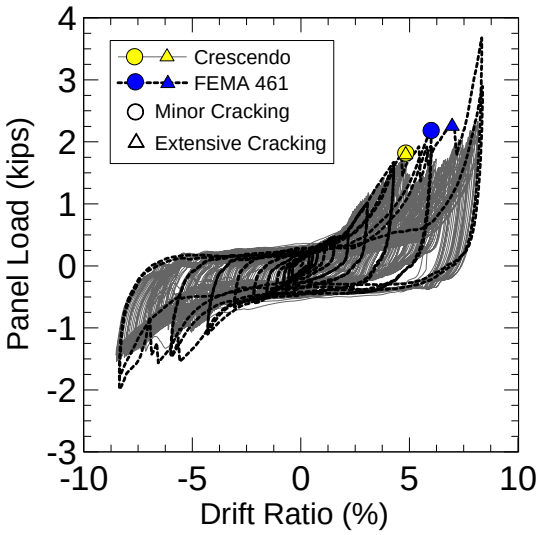

Figure 4.11 Force versus displacement response comparing the Crescendo to the FEMA 461 protocol

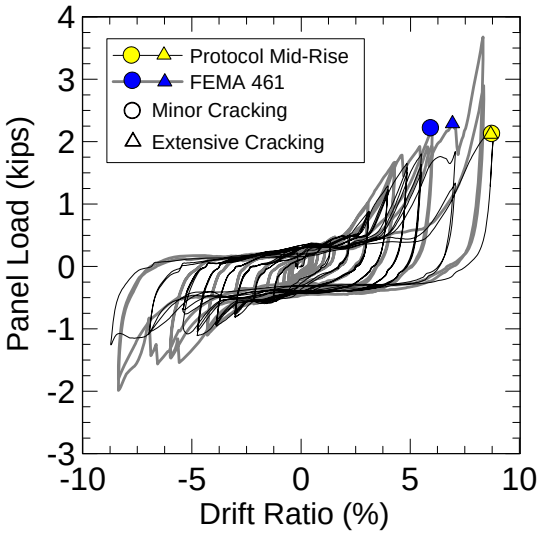

Figure 4.12 Force versus displacement response comparing the Mid-rise to the FEMA 461 Protocol

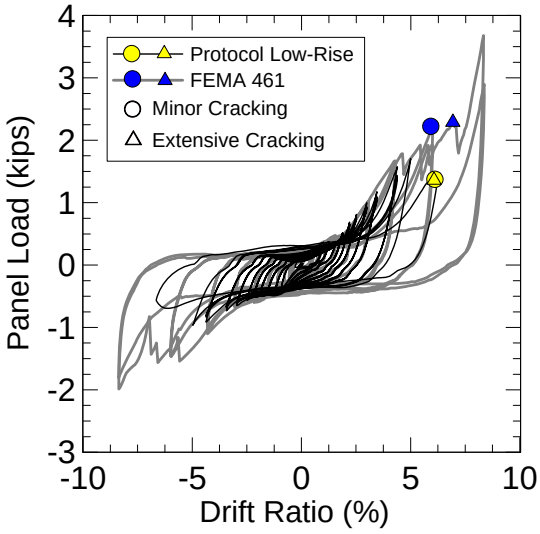

Figure 4.13 Force versus displacement response comparing the Low-rise to the FEMA 461 protocol

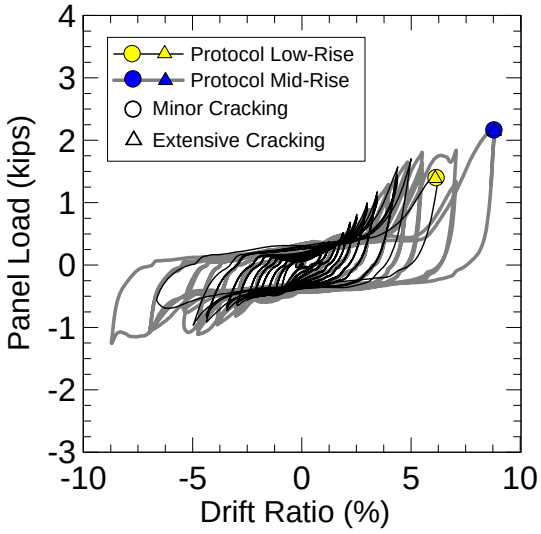

Figure 4.14 Force versus displacement response comparing the Low-rise to the Mid-rise protocol

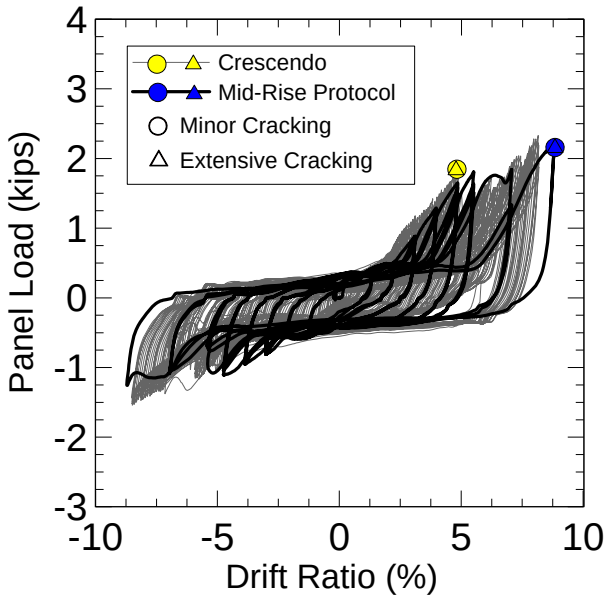

Figure 4.15 Force versus displacement response comparing the Mid-rise to the Crescendo protocol

Table 4.1 summarizes the characteristics of the 5’ x 5’ glazing specimens tested. Of those tested, the series of 2mil unattached filmed specimens (N = 10) are synthesized to evaluate the effects of load protocol variation on damage state drift ratios. Figures 4.16 and 4.17present bar plots to investigate the effect of load protocol on the serviceability and ultimate damage states, respectively. Protocol variation has little effect on the drift ratio at gasket damage (SDS-1). However, when assessing SDS-2 (Minor Glass Cracking), the higher cycle count protocols observe SDS-2 at a lower drift ratio. This trend is also observed considering UDS-1 (extensive glass cracking) (Figure 4.16). When comparing the FEMA 461 (non-dynamic: 20 cycles) and Mid-Rise (dynamic: 20 cycles) protocols the effect of dynamic loading results in higher drift ratios at all damage states. Though the magnitude of the difference is similar to cycle count loading comparisons, more data is needed to fully examine the effects of dynamic loading. The developed load protocols (Mid and Low-Rise), which are designed to replicate, in an aggregate sense, the floor level inter-story drift histories one may anticipate for glass panel systems, result in damage state drift ratios larger than that of the Crescendo protocol and lower than the Monotonic Protocol. Note that for Figures 4.16 and 4.17, a null value for a given protocol indicates that the specific damage state for that load protocol did not occur.

	Count: No attachment (Attached)				
Thickness (mil)	Monotonic	Mid-Rise	FEMA 461	Low-Rise	Crescendo
0	3 (NA)	2 (NA)	0 (NA)	0 (NA)	0 (NA)
2	3 (2)	2 (0)	2 (2)	2 (0)	1 (0)
4	3 (3)	0 (0)	2 (2)	0 (0)	1 (0)
8	3 (3)	0 (0)	2 (2)	0 (0)	0 (0)

Table 4.1 Characteristics of the 5'x5' window specimens tested

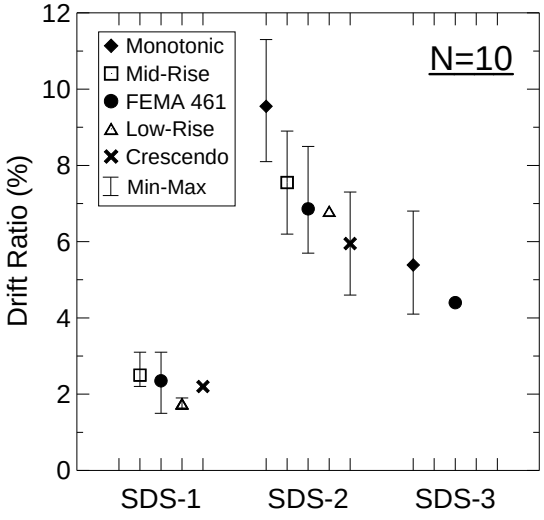

Figure 4.16 Effects of Load protocol on the Serviceability Damage States (5'x5' specimens with 2mil unattached film – 10 specimens total).

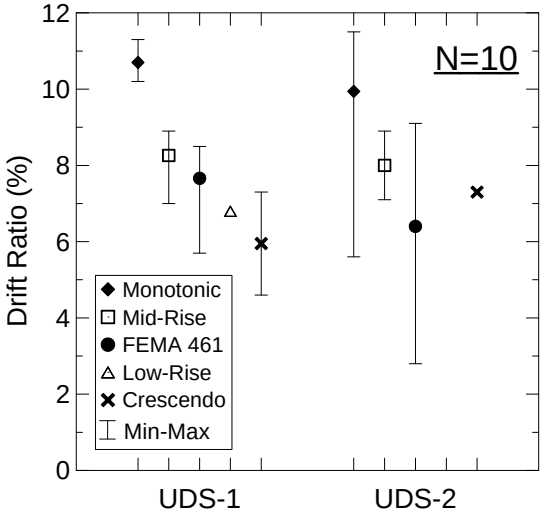

Figure 4.17 Effects of Load protocol on the Ultimate Damage States. (5'x5'specimens with 2mil unattached film – 10 specimens total).

4.4 Effect of Aspect Ratio

To evaluate the effect aspect ratio on the identified damage states, a series of tests were performed on 4'x8' windows (W:H aspect ratio = 0.5), 5'x5' windows (W:H aspect ratio = 1.0) and 6'x4' windows (W:H aspect ratio = 1.5). A total of 3 tests were performed for each aspect ratio using the FEMA 461 load protocol: One window with no film, one with 4 mil and the last with 4 mil film attached with the wet glazing attachment system (Table 2.1). Note that aspect ratio 1.0 tests contained two specimens.

The effect of aspect ratio on serviceability damage states is shown in Figures 4.18 and 4.19. It was observed that the aspect ratio has little to no affect on the drift ratio at which SDS-1 occurred (Figure 4.18). However, the aspect ratio does have a large effect on SDS-2: First crack. For both 0 mil and 4 mil specimens as the aspect ratio increased from 0.5 to 1.5 the drift ratio in which SDS-2 occurred increased. This trend did not hold true though when the wet glazing attachment system was applied. When applied, for aspect ratio 1.0 the drift ratio in which any serviceability damage state occurred was always lower than that of the 0.5 or 1.5 aspect ratios. The trend can be most clearly seen in Figure 4.19 where the effect of aspect ratio on the wet glazing attachment system detachment (SDS-3) is shown. For AR 1.0, SDS-3 was obtained at a relatively low drift ratio of 4.5%, while AR 0.5 and 1.5 reached a high drift ratio and yet still did not obtain this damage state, due to test setup limitations. Note that the test setup maximums are plotted in Figures 4.18 - 4.20 for situations where a damage state was not obtained. It can be concluded from these results that SDS-2: First Crack is the most clear and concise damage state to use as a metric to explore aspect ratio effects.

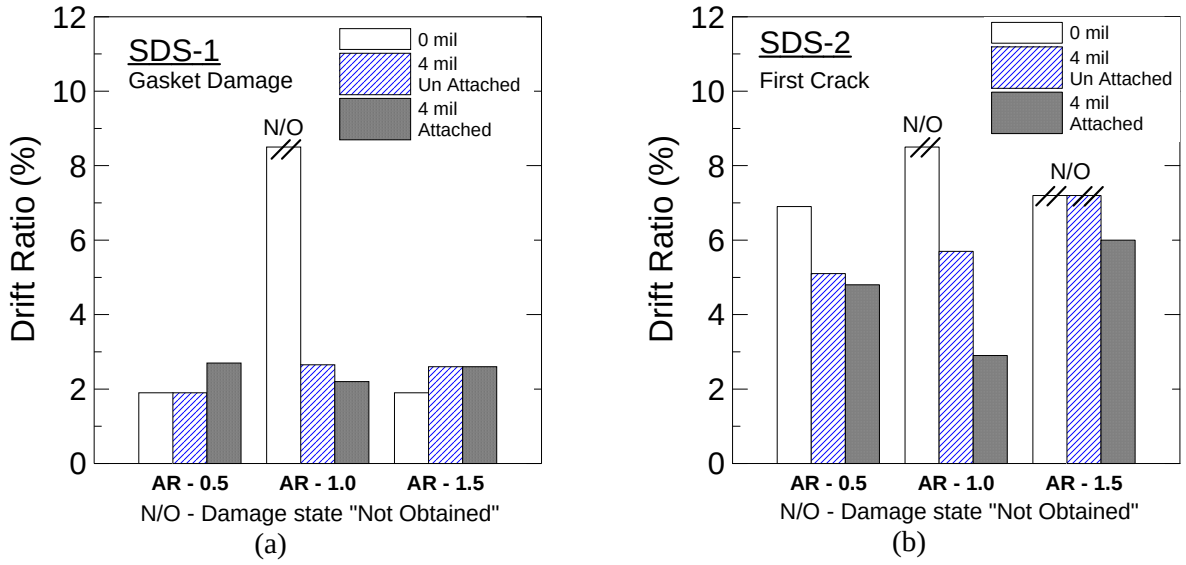

Figure 4.18 Effects of aspect ratio on serviceability damage states: (a) gasket damage and (b) first crack (All specimens tested using FEMA 461 loading protocol)

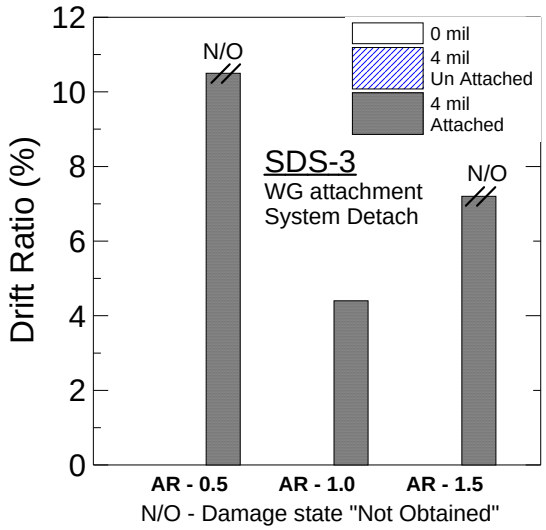

Figure 4.19 Effects of aspect ratio on the serviceability damage state SDS-3: wet glazing attachment system (All specimens tested using FEMA 461 loading protocol)

The effect of aspect ratio on the ultimate damage states is shown in Figure 4.20. Both ultimate damage states show an increase in obtained drift ratio with an increase in aspect ratio for the un-filmed window system. However, a similar trend to serviceability damage states can be observed when the film system is attached. Namely, in each case, the aspect ratio of 1.0 had a much lower drift limit than other aspect ratios.

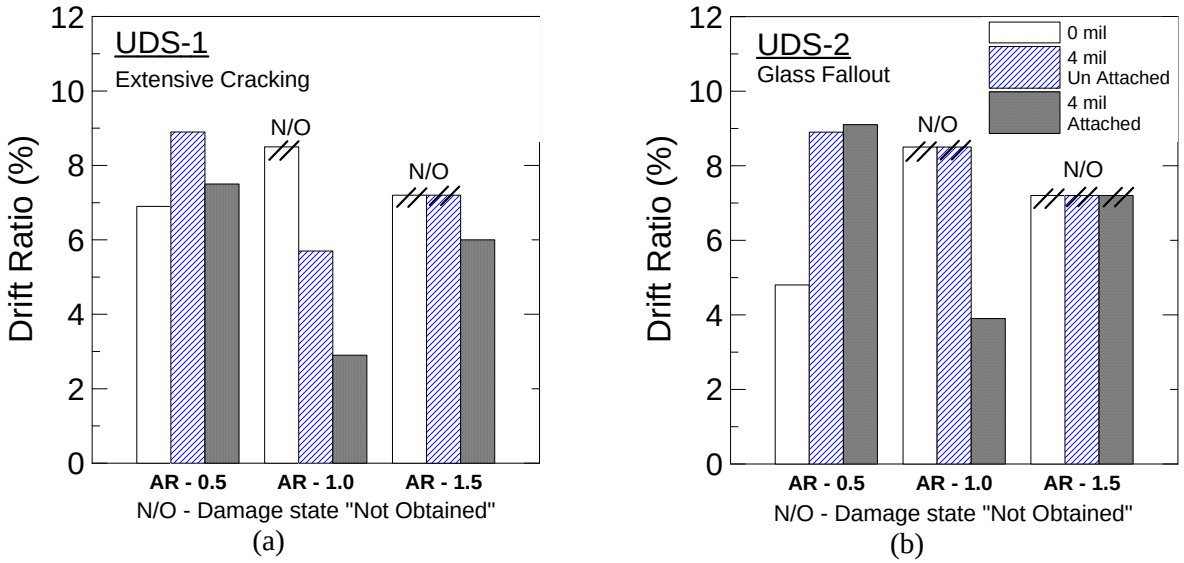

Figure 4.20 Effects of aspect ratio on ultimate damage states: (a) extensive cracking and (b) glass fallout (All specimens tested using FEMA 461 loading protocol)

4.5 Glass Freedom

The glass within the mullion frame is free to translate and rotate, due to the nature of its construction. These particular store-front style window systems are designed to be constructed directly in place. The mullion pieces are cut onsite and installed in place, and then the glazing is slid into the mullion from the bottom. For ease of installation, there is a natural gap between the rubber stoppers and the glazing. This gap increases the drift ratio at which the window systems will observe the various damage states. For the specimens tested in this program, this gap was measured to be on average 0.13 inches. This corresponds to a drift ratio of 0.2% for the 5'x5' specimens. This variability must be considered in the context of the drift limits reported.

Attributed to the construction gaps between the window glass and its surrounding mullion, the window glass rotates within the mullion frame linearly with increased drift ratio until failure. During the experiments, this rotation was measured. It is observed that the amplitude of the rotation changes with aspect ratio and can be seen in Figure 4.21. Aspect ratio 1.0 with a slope of 0.312 degrees per % drift ratio is in between AR 1.5 and 0.5 with slopes of 0.434 and 0.100 (Table 4.2). When the glass is attached using the wet glazing attachment system, the amount of rotation as a function of the drift ratio increases. The severity of increase diminishes as the aspect ratio increases.

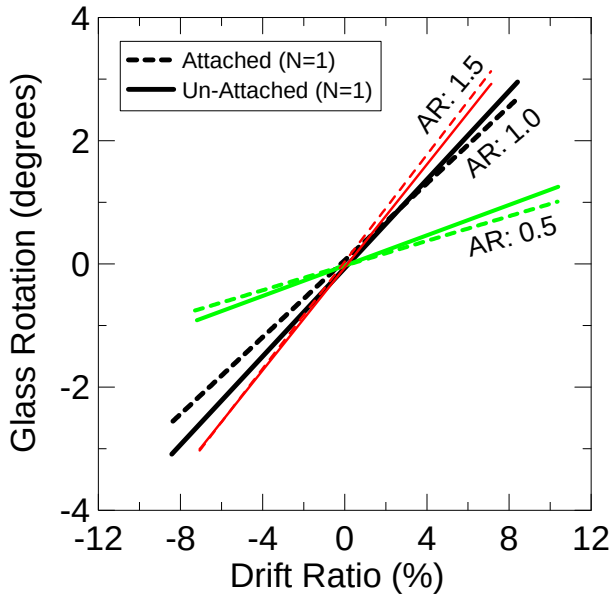

Figure 4.21 Intensity of glass rotation for each tested aspect ratio in attached and un-attached setups (All specimens tested using FEMA 461 loading protocol)

	Slope of Rotation for AR: 0.5 (°/ % Drift ratio)	Slope of Rotation for AR: 1.0 (°/ % Drift ratio)	Slope of Rotation for AR: 1.5 (°/ % Drift ratio)
Un-Attached	0.100	0.312	0.434
Attached	0.123	0.359	0.418
% Change	**23.00**	**15.06**	**-3.69**

Table 4.2 Slope of rotation as aspect ratio changes under FEMA 461 loading protocol

4.6 Comparison to Previous Work

Sucuoglu and Girija-Vallabhan (1997) extended the work of Bouwkamp and Meehen (1960) and developed analytical procedures for calculating the in-plane deformation capacity of window panels subjected to seismic excitations. Sucuoglu et al. concluded that the in-plane deformation capacity of window systems is accommodated by two consecutive mechanisms: rigid body motion (rotation) of the glass within the mullion, and diagonal shortening of the glass under in-plane compressive forces. The authors propose a formula to predict the drift capacity of a single pane, store-front style window system. The first part is the rotational drift capacity (Equation 4.2) where h is the height of the window, b is the width of the window and c is the clearance between the glass and end of the window.

$$\delta_r = 2c\left(1 + \frac{h}{b}\right) \tag{4.2}$$

The second part calculates the diagonal shortening due to buckling failure (Equation 4.3) where d is the diagonal length, σ_{all} is the tensile rupture strength, E is the modulus of elasticity and t is the thickness of the glass.

$$\delta_d = \frac{1}{d}\left(\frac{\sigma_{all} d^2}{\pi E t}\right) \tag{4.3}$$

Equations 4.2 and 4.3 were applied to the baseline window systems in this study using the following values: In equation 4.2 the height (h) and width (b) are 5 feet (60 inches), assuming the rubber stop compresses to half its thickness, a clearance (c) of 1.17 inches (distance from outer edge of mullion to middle of rubber stopper) was chosen. In equation 4.3 the diagonal (d) is calculated from height (h) and width (b), the tensile rupture strength (σ_{all}) is 6000 lbs/in^2, the modulus of elasticity (E) for the glass is 10.6×10^6 lbs/in^2 and the thickness (t) is 0.25 inches. The predicted buckling failure drift ratio is 7.6%. The average peak drift ratio for panels that failed in

buckling tested with the FEMA 461 load protocol (all film thicknesses, un-attached) was 7.7%, which is in good agreement with this theoretical estimate. Aspect ratios 1.5 and 0.5 that reached UDS-1 in this study failed due to modes other than buckling therefore could not be compared to this method of prediction. The results observed in this study confirm the assumptions of Sucuoglu et al. showing large rigid body rotations (up to 3 degrees of rotation at 8.5% drift ratio for aspect ratio 1.0 windows – Figure 4.21) and predict the buckling failure drift ratio of aspect ratio 1.0 windows. Calculations from Sucuoglu et al. (1997) indicate that diagonal shortening accounts for less than one percent of the total drift ratio capacity.

Tables 4.3 and 4.4 summarize the serviceability and ultimate damage state drift limits as observed in this study for full scale tests and compared with studies conducted by others. The monotonic loading column in the present study represents data attained from aspect ratio 1.0 specimens with variable film thicknesses, with wet glazing attachment. The cyclic loading column in the present study summarizes only aspect ratio 1.0 panels tested with the Crescendo protocol and the FEMA 461 load protocol, with variable film thicknesses and without the wet glazing attachment system. The previous work includes data from tests with similar window system properties. Monotonic tests are compared to those conducted by Bouwkamp et al. (1960), which used aluminum frames and attachment top and bottom (Table 1.1). Only serviceability drift limit states were reported in this study. Cyclic test data includes those performed by Behr et al. (1996) using the Crescendo protocol and specimens with annealed monolithic glass of store-front type.

Source	Bouwkamp et al. 1960	Behr et al. 1996	Present study		
Load Protocol	Monotonic (Attached)	Crescendo	Monotonic (Attached)	Crescendo	FEMA 461
Number of Specimens	N=1	N=12	N=7	N=2	N=6
Average	**2.5%**	**4.2%**	**6.7%**	**6.0%**	**6.9%**

Table 4.3 Serviceability limit state drift ratio summary of previous and present study testing

Source	N/A	Behr et al. 1996	Present study		
Load Protocol	Monotonic (Attached)	Crescendo	Monotonic (Attached)	Crescendo	FEMA 461
Number of Specimens	N/A	N=12	N=6	N=2	N=6
Average	**N/A**	**5.9%**	**10.8%**	**6.0%**	**7.7%**

Table 4.4 Ultimate limit state drift ratio summary of previous and present study testing

Differences in serviceability and ultimate drift limits can be attributed primarily to the construction of the window systems. Attributes such as glass to mullion support contacts (structural silicone versus stiff rubber blocks), glass to mullion clearances and specimen to specimen variability affect the drift limits. Stiff rubber blocks provide an increased area of loading on the glass that reduces stress concentration compared with silicone alone. This would effectively increase the obtained serviceability drift ratios yet ultimate damage states would be less affected. An increase in glass clearance or a lighter detailed mullion cross section would increase the damage state drift ratio capacity. It is believed that much larger flexibility is provided at the glass to mullion interface in modern construction, as compared with 50 years ago. Secondary affects can be attributed to the aspect ratio differences (AR 0.83 for previous work and AR 1.0 for present study). From this study larger aspect ratios resulted in larger damage state drift ratios

Chapter 5: Conclusions

5.1 Motivation

Damage to nonstructural components and systems during earthquakes threaten public safety, and are a major source of economic losses and business disruptions. Previous earthquakes have confirmed that despite good overall structural performance of a building, the nonstructural components and systems within it will very likely have sustained heavy damage. Window systems in particular are very susceptible to damage, due to their brittle nature and integration with the building perimeter.

The window system is a highly complex, and variably constructed system, consisting of glass panels, interface material between the mullion and glass, metal, plastic or wood mullions and an attachment mechanism to the building structure. Moreover, the glass may be filmed for safety of thermal purposes, and this film may be mechanically or chemically attached. Each of these elements poses its own risk of failure under seismic loading. Perhaps the most catastrophic, and dangerous situation is the development of cracks in the glass itself. Risk of human danger is increased upon severe cracking or glass fallout. Unfortunately, window systems are traditionally viewed as an architectural component to the overall building envelope, and therefore no attention is provided to them in design. Indirectly, however, one can consider their drift ratio limits and associated damage states as these relate to demands imposed on the building (windows are attached floor-floor).

Experimental investigations of the seismic performance of window systems in the United States date back to the early 1960's. Review of the literature indicates that limited study on the effects of window aspect ratio, loading protocol, and film coating, have been undertaken in the context of seismic performance evaluation. The largest test program to-date, led by UMR and Penn State, adapted use of a single load protocol, termed the *crescendo* protocol, which subjected the window systems to 180+ cycles of reversed cyclic dynamic loading. This high cycle count is noted as excessive when one compares with the actual drift cycles imposed at the elevation of the window system during earthquakes (Hutchinson et al., 2008).

5.2 Scope of Work

A systematic experimental program is undertaken in this work with a focus on evaluating the effects of: (i) load protocol, (ii) film thickness and attachment and (iii) window aspect ratio, on the window system in-plane seismic performance. In total, 12 small scale, and 53 full-scale specimens were tested. Small scale specimens consisted of 12”x12”x1/4” annealed glass panels subjected to monotonic loading. These experiments were conducted primarily to evaluate the validity of video monitoring of the crack development during the large scale tests.

The baseline large-scale window specimens consisted of 5’x5’ window units, constructed of ¼” annealed single pane glass supported by an aluminum frame, with detailing typical of store-front window systems. These specimens were subjected to in-plane seismic racking in a specially designed racking frame mounted on the UCSD Powell Laboratory shake table. The objectives of these tests were to quantify the damage modes and associated drift limits, considering the aforementioned testing variables.

Full-scale testing began with testing baseline 1:1 aspect ratio windows (5’x5’) under monotonic loading. A slow displacement rate of 0.03 in/sec was used to avoid inertial effects, while allowing observation of the progression of damage and a better understanding of failure modes. Each of the different film thickness and attachment system combinations were tested under the monotonic protocol to establish their baseline behavior. The *loading protocol (LP)* series involved testing of like specimens systematically subjected to the (i) Crescendo Load Protocol, (ii) FEMA 461 Load Protocol, (iii) a newly developed Mid-Rise Load Protocol and (iv) and a newly developed Low-Rise Load Protocol. The latter two protocols are described in a companion report by Hutchinson et al. (2008). The effects of each protocol on the specimens’ drift limit capacity were evaluated, and cross-comparison between the various protocols was conducted. The *window film (WF)* series included 5’x5’ specimens with no film, 2 mil, 4 mil, and 2-ply 8 mil film. Each filmed specimen was built unattached and attached. Attachment involved the wet glazing attachment system, which involves placing a bead of caulking at the top edge of the film, adhering the film to the glass panel. The *aspect ratio (AR)* series included 6’x4’ (AR: 1.5), 5’x5’ (AR: 1.0) and 4’x8’ (AR: 0.5) specimens. Each aspect ratio in the series was composed of 3 specimens. The first specimen had no film, the second had 4 mil film and the third specimen had

4 mil film attached with the wet glazing attachment system. Specimens in both the WF and AR series were subjected to the FEMA 461 load protocol.

5.3 Findings

5.3.1 Identified Damage States

Damage to the window units was categorized into two main groups: (i) Serviceability Damage States (SDS) and (ii) Ultimate Damage States (UDS). SDSs are damage modes, which results in the inability to immediately continue normal (service), while UDSs are damage modes, which are not repairable and pose an immediate safety hazard. Upon achieving an UDS, the window system must be completely replaced. Three SDS and two UDS for store-front style window systems were identified in this study. The SDSs identified were: (i) gasket damage, (ii) minor glass cracking, and (iii) wet glazing attachment system detachment. The UDSs identified were: (i) glass fallout and (ii) major glass cracking. The experimentally determined drift ratios, for all window systems tested in this program, considering the aforementioned damage states were as follows:

- SDS-1 (gasket damage): range from 1.9 to 3.1%, with an average of 2.3%
- SDS-2 (minor glass cracking): range from 1.4 to 11.3 %, with an average of 6.6%
- SDS-3 (Attachment system detachment): range from 4.1 to 6.8 %, with an average of 4.9%
- UDS-1 (extensive glass cracking): range from 1.4 to 11.5 %, with an average of 8.0%
- UDS-2 (glass fallout): range from 3.9 to 11.5 %, with an average of 8.3%

5.3.2 Load Protocol Effects

The effects of load protocol are detailed in a companion report by Hutchinson et al. (2008) and therefore only abbreviated in bullet form herein. Table 5.2 summarizes the minimum, average, and maximum drift ratio associated with the various damage states. Additional findings regarding load protocol include the following:

- Load protocol has an effect on the drift ratio associated with the identified damage states. Specifically, it was observed that the crescendo protocol caused specimens to acquire

damage at an earlier drift ratio than any other load protocol. The cause for the low drift ratio is associated with cycle count.

- From the limited study the loading rate has minimal effect on the drift limits associated with both the serviceability and ultimate damage states. The FEMA 461 protocol (20 cycles – static) had slightly smaller drift ratio values compared with the Mid-rise protocol (20 cycles – dynamic).
- To characterize the serviceability damage state, minor cracking was identified as a good metric for loading protocol comparison. Using the FEMA 461 load protocol as a base (20 cycles), the Monotonic load protocol resulted in a 39% increase in drift ratio capacity, the Mid-Rise protocol (20 cycles) showed a 10% increase in drift ratio capacity, the Low-Rise protocol (40 cycles) showed a 1% decrease in drift ratio capacity and the Crescendo load protocol (+180 cycles) showed a 13% decrease in drift ratio. The ultimate damage state extensive cracking showed the same trend when comparing the FEMA 461 load protocol to the others: 39% increase for Monotonic load protocol, 8% increase for Mid-Rise load protocol, 11% decrease for Low-rise load protocol and 22% decrease with Crescendo load protocol.

	(min / average / max) %				
	Monotonic	Crescendo	FEMA 461	Mid-rise	Low-Rise
SDS-1:	N/O	2.2 / 2.2 / 2.2	1.5 / 2.2 / 3.1	2.2 / 2.4 / 3.1	1.6 / 1.8 / 1.9
SDS-2:	2.3 / 7.8 / 11.3	4.6 / 6.0 / 7.3	4.4 / 6.8 / 8.5	6.2 / 7.55 / 8.9	6.8 / 6.8 / 6.8
SDS-3:	4.1 / 5.4 / 6.8	N/A	4.4 / 4.4 / 4.4	N/A	N/A
UDS-1:	5.6 / 8.6 / 11.5	4.6 / 6.0 / 7.3	4.4 / 6.5 / 8.5	7.0 / 8.0 / 8.9	6.8 / 6.8 / 6.8
UDS-2:	5.6 / 8.6 / 11.5	7.3 / 7.3 / 7.3	3.9 / 6.5 / 8.9	7.1 / 8.0 / 8.9	N/A

Table 5.1 Summary of load protocol effects

5.3.3 Film and Attachment System Effects

The most notable observation regarding the window system seismic performance when the unit is filmed is related to the securing capacity of the film, post-damage. Even a moderate amount of film (2 mil) suppresses damage to the window system, and greatly assists with retaining the glass itself, thereby reducing the potential for the safety hazard of glass fallout. Table 5.2 summarizes

the minimum, average, and maximum drift ratio associated with the various damage states. Additional findings regarding film include the following:

- When there is no film applied to the glass, the effects of extensive cracking cause on average 74% of the glass to fallout (range of 20%). With only minimal film application (2 mil), less than 1% of glass is observed to fall from the specimen. Increased film thickness (4 and 2-ply 8 mil) increases the level of containment further to less than 0.75% glass fallout.
- For the serviceability damage states there was an average increase of 34% in drift ratio capacity from no film to filmed specimens. For the ultimate damage state the increase in drift ratio capacity from no film to filmed specimens was 12%.
- Increasing the film thickness had no discernable trend in terms of its effects on drift ratio capacity at any damage state when unattached. The minimal amount of film considered in this study (2 mil), would suffice in terms of increasing the drift ratio capacity associated with the identified damage states.
- When the window film is attached using the wet glazing attachment system, the drift ratio values for all damage states was reduced. The attachment system increases the system stiffness, which in-turn creates local stress concentrations along the attached edge of the glass. For like specimens, on average, the serviceability damage state drift ratio was reduced by 32% for specimens attached with the wet glazing attachment system. The ultimate damage state drift ratio was reduced by 37% for like specimens that were attached with the wet glazing attachment system.
- The safety aspects of window film were very evident during the testing. Thicker films (4 and 2-ply 8 mil) reduced replacement time and increased safety by containing the glass in one manageable sheet. The attachment system, when it did not fail, held the shattered panel in place after testing, which provided ample time to setup for safe removal of the specimen.

	(min / average / max) %		
	no film	Filmed	
		Un-attached	Attached
SDS-1 (gasket damage):	2.2 / 2.7 / 3.1	1.5 / 3.1 / 2.2	2.2 / 4.7 / 8.3
SDS-2 (minor glass cracking):	6.8 / 7.8 / 8.9	1.5 / 11.3 / 6.9	1.4 / 4.7 / 8.3
SDS-3 (attach. system detachment)	N/A	N/A	4.1 / 5.0 / 6.8
UDS-1 (extensive glass cracking)	7.6 / 9.2 / 11.5	4.6 / 9.0 / 11.3	1.4 / 6.7 / 10.9
UDS-2 (glass fallout)	7.6 / 9.2 / 11.5	7.3 / 9.1 / 11.3	3.9 / 7.6 / 10.8

Table 5.2 Summary of film and attachment drift ratios

5.3.4 Aspect Ratio effects

The most notable conclusion observed from the experimental program, as related to aspect ratio was that as the aspect ratio increases the obtained drift ratio values for the serviceability damage states increases. For the serviceability damage state minor cracking AR 0.5 had a range of 4.8% to 6.9% and an average 11% drop in drift ratio capacity compared to AR 1.0. SDS-2 (minor cracking) was not attained for AR 1.5 however the drift ratio achieved before system limitations were reached was 7.2%, a 26% increase in drift ratio capacity compared to AR1.0. This observation was consistent only for window systems without film or with film unattached. Stress localization associated with the film attachment increases the variability of the drift ratio capacity. Ultimate damage states showed no discernable trend which could be attributed to limitations of the loading system (the ultimate damage state was not attained for taller specimens), as well as specimen to specimen variability.

5.4 Future Work

This study demonstrated that window film application can beneficially suppress the damage to window systems associated with seismic loading. Most notably, the drift ratios associated with key serviceability and ultimate damage states were increased and glass fallout was largely mitigated. However, the experiments also demonstrated the unfortunate attributes, namely development of local stress concentrations, when the film was attached to the glass unit. These findings were limited to the type of window system considered, namely, store-front type

construction. To broaden the application of these findings, future studies should consider the following:

- Additional window system types
- Varying film attachment systems
- Varying glass type and thickness
- Varying sash and mullion details
- Less likely geometries (highly squat or tall slender window systems)

References

AAMA. (2001). *AAMA 501.6-01 – Recommended dynamic test method for determining the seismic drift causing glass fallout from a wall system.* American Architectural Manufacturers Association. Schaummberg, Ill.

ATC (1992). *Guidelines for Cyclic Testing of Components of Steel Structures.* Applied Technology Council (ATC). Report ATC-24. Redwood City, California.

Ayres, J., and Sun T., (1973). *Nonstructural damage, the San Fernando earthquake of Feb 9, 1971*, US Department of Commerce, National Oceanic and Atmospheric Administration.

Behr, R., (1998). Seismic performance of architectural glass in mid-rise curtain wall, *Journal of Architectural Engineering ASCE* **4**, 94-98.

Behr, R., and Belarbi, A., (1996). Seismic test methods for architectural glazing systems, *Earthquake Spectra* **12**, 129-143.

Behr, R., and Warner, S., (2003). Earthquake-resistant architectural glass new design provisions and test methods, *The Construction Specifier*, (May), 29-33.

Behr, R., Belarbi, A., Culp, J., (1995a). Dynamic racking tests of curtain wall glass elements with in-plane and out-of-plane motions, *Earthquake Engineering and Structural Dynamics* **24**, 1-14.

Behr, R., Belarbi, A., Brown, A., (1995b). Seismic performance of architectural glass in a store-front wall system, *Earthquake Spectra* **11**, 367-391.

Bouwkamp, J., (1960). Behavior of window panels under in-plane forces, *Institute of Engineering Research Report*, University of California, Berkeley, CA.

Bouwkamp, J., and Meehan. J., (1960). Drift limitations imposed by glass, in *Proc. of the Second World Conference on Earthquake Engineering (2WCEE)*, Tokyo, Japan, 1763-1778.

Brueggeman, J., Behr, R., Wulfert, H., Memari, A., and Kremer, P., (2000). Dynamic racking performance of an earthquake-isolated curtain wall system, *Earthquake Spectra* **16**, 735-756.

Dinehart, D., and Shenton, H., (1998). Comparison of Static and Dynamic Response of Timber Shear Walls, *Journal of Structural Engineering, Inc. 686-695.*

Earthquake Engineering Research Institute (EERI) (1990). Loma Prieta earthquake reconnaissance report, *Earthquake Spectra* **6** (S1), 1-448.

Earthquake Engineering Research Institute (EERI) (1995a). Northridge earthquake reconnaissance report, *Earthquake Spectra* **11** (S2), 1-514.

Earthquake Engineering Research Institute (EERI) (1995b). The Hyogo-ken Nanbu Earthquake January 17, 1995: Preliminary Reconnaissance Report, *EERI Rep. No. 95-04.*

Earthquake Engineering Research Institute (EERI) (2001). The Nisqually, Washington, Earthquake February 28, 2001: Preliminary Reconnaissance Report, *EERI Rep. No.2001-01*.

Evans, D., and Ramirez, F., (1989). Glass damage in the 19 September 1985 Mexico City earthquake, In *Lessons Learned from the 1985 Mexico City Earthquake*, V. Bertero (Editor), Earthquake Engineering Research Institute (EERI), Oakland, CA.

FHWA (2004). *Recommendations for Seismic Performance Testing of Bridge Piers*. Report by the U.S. Department of Transportation Federal Highway Administration. June.

Ficcadenti, S., Steiner, M., Pardoen, G., and Kazanjy, R., (1998). Cyclic load testing of wood-framed, plywood sheathed shear walls using ASTM E564 and three loading sequences, *Proceedings of 6th US National Conference on Earthquake Engineering (6NCEE)*, Seattle, WA, May 31 - June 4.

Federal Emergency Management Agency (FEMA) (2006). *Interim protocols for determining seismic performance characteristics of structural and non-structural components through laboratory testing*, FEMA 461 (draft), Washington, DC.

Gatto, K., and Uang, C., (2003), Effects of Loading Protocol on the Cyclic Response of Woodframe Shearwalls, *Journal of Structural Engineering, Inc. 1384-1393.*

Hoehler, M., Panagiotou, M.m Restrepo, J., Silva, J., Floriani, L., Bourgund, U., and Gassner, H., (2009) "Performance of Suspended Pipes and their Anchorages during Shake Table Testing of a 7-story Building." Earthquake Spectra, EERI, 25(1): pp 71-91

Hutchinson, T., Zhang, J., Eva C., (2008) Development of a Load Protocol for Glass Panel System Racking Experiments Considering a Damage Index Concept, *University of California, Structural Systems Research Project report No. 08-08.*

Krawinkler, H. (1996). Cyclic loading histories for seismic experimentation on structural components, *Earthquake Spectra* **12**, 1-12.

Krawinkler, H., Gupta, A., Medina, R., and Luco, N., (2000). Loading histories for seismic performance testing of SMRF components and assemblies, *SAC/BD-00/10 Report*, SAC Joint Venture, Sacramento, CA.

Logario, H., (1990). Earthquakes: An architect's guide to non-structural seismic hazards, Wiley, New York.

Malhotra, P., Senseny, P., Braga, A., and Allard, R., (2003). Testing sprinkler-pipe seismic-brace components, *Earthquake Spectra* **19**, 87-109.

Memari, A., Behr, R., and Kremer, P., (2000). Toward development of a predictive model for drift limits in architectural glass under seismic loadings, *Proceedings of 12th World Conference on Earthquake Engineering (12WCEE)*, 3317-3321, Auckland, New Zealand, January 31-February 4.

Memari, A., Behr, R., and Kremer, P., (2003). Seismic behavior of curtain walls containing insulating glass units, *Journal of Architectural Engineering ASCE* ***9***, 70-85.

Memari, A., Behr, R., and Kremer, P., (2004). Dynamic racking crescendo tests on architectural glass fitted with anchored pet film, *Journal of Architectural Engineering ASCE* **10**, 5-14.

Memari, A., Chen, X., Kremer, P., and Behr, R., (2006a). Seismic performance of two-side structural silicone glazing systems, *Journal of ASTM International* **3**, 1-6.

Memari, A., Kremer, P., and Behr, R., (2006b). Architectural glass panels with rounded corners to mitigate earthquake damage, *Earthquake Spectra* 22, 129-150.

Memari, A., Shirazi, A., and Kremer, P., (2007). Static finite element analysis of architectural glass curtain walls under in-plane loads and corresponding full-scale test, *Structural Engineering and Mechanics* **25**, 365-382.

Sakamato, I., Itoh, H., and Ohashi, Y., (1984). Proposals for a seismic design method on nonstructural elements, *Proceedings of 8th World Conference on Earthquake Engineering (8WCEE)*, Vol. 5, 1093-1100.

Shepherd, R. (1996). Standardized experimental testing procedures for low-rise structures, *Earthquake Spectra* **12**, 111-127.

Sucuoglu, H., and Girija-Vallabhan, C., (1997). Behavior of window glass panels during earthquakes, *Engineering Structures* **19**, 685-694.

Thurston, S., and King, A., (1992). Two-directional cyclic racking of corner curtain wall glazing, *Building Research Association of New Zealand (BRANZ) Study Report No. 44*.

Uniform Building Code (UBC) (1994). *Structural engineering design provisions*, International Conference of Building Officials.

Appendices

Appendix A: Construction Drawings

Appendix B: Load-Deflection Response Curves

Appendix C: Summary of Previous Experiments

Appendix D: Glass Specifications

Appendix E: Calculations

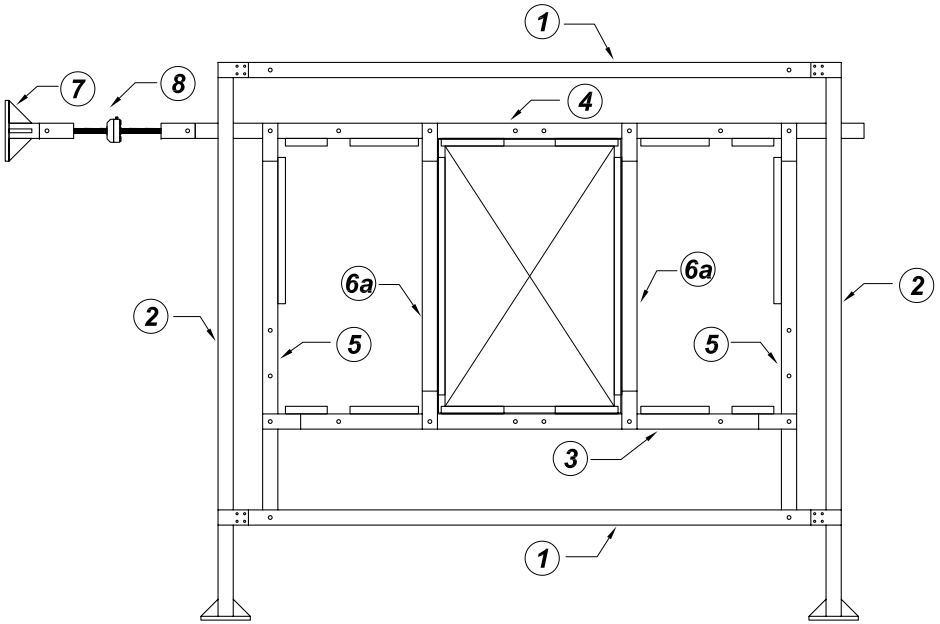

FRONT VIEW with 6' x 4' Panel Configuration

	PART NAME	Detail Page	Qty.
1	Horizontal Perimeter Beams	S3	2
2	Vertical Perimeter Columns	S4 & S5	2
3	Interior Bottom Horizontal Beam	S6	1
4	Interior Top Horizontal Beam	S7	1
5	Interior Vertical Columns	S8	2
6a	Interior Support Column - Type A	S9	2
7	Strong Wall Attachment Fixture	S12	1
8	Link Fixture	S13	1

Dept. of Structural Engineering, UC San Diego

Glass Panel Frame

Dr. by: Christopher Latham based on drawings by Francisco Nguyen & Corina De Pablo	AIMCAL PROJECT	
	2007	PAGE S1 of 16

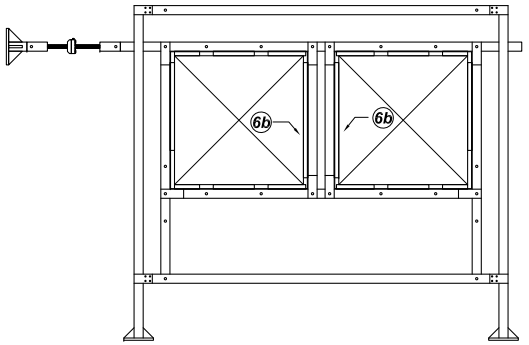

FRONT VIEW with Dual 5' x 5' Panel Configuration

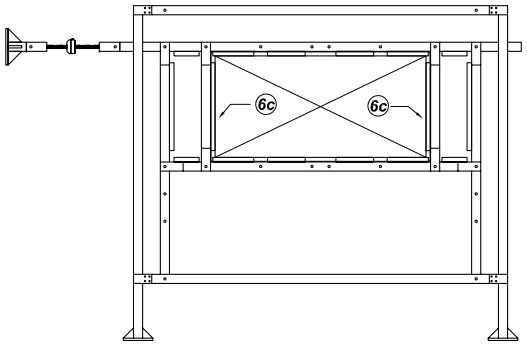

FRONT VIEW with 4' x 8' Panel Configuration

Note: Refer to S1 for most part names.
This drawing shows the repositioning of the interior beams and columns to hold the 4"x8" panels and dual 5"x5" panels.

	PART NAME	Detail Page	Qty.
6b	Interior Support Column - Type B	S10	2
6c	Interior Support Column - Type C	S11	2

Dept. of Structural Engineering, UC San Diego

Glass Panel Frame

Dr. by: Christopher Latham based on drawings by Francisco Nguyen & Corina De Pablo	AIMCAL PROJECT	
	2007	PAGE S2 of 16

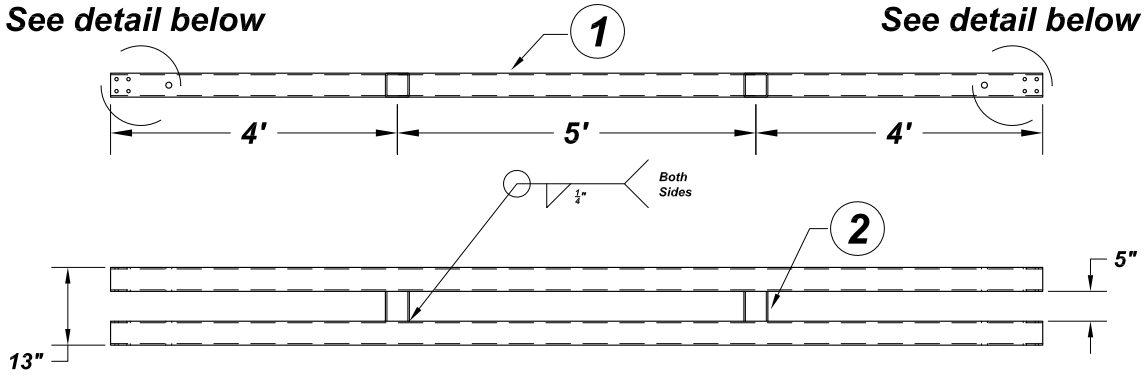

Horizontal Perimeter Beams

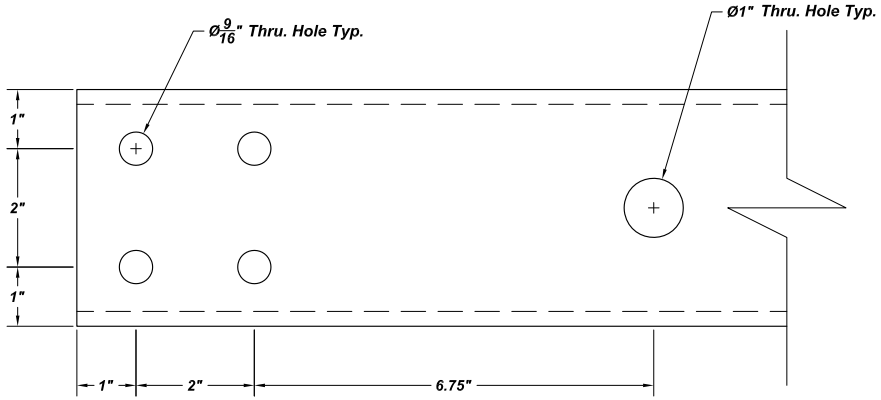

Details of Holes in Horizontal Perimeter Beams

	PART NAME	Material	Qty.
1	Horizontal Perimeter Beam Main Tube 4" x 4" x 1/4" x 13' long	A46-Steel	4
2	Horizontal Perimeter Beam Cross Tube 4" x 4" x 1/4" x 5" long	A46-Steel	4

Dept. of Structural Engineering, UC San Diego

Glass Panel Frame

Dr. by: Christopher Latham based on drawings by Francisco Nguyen & Corina De Pablo

AIMCAL PROJECT

2007

PAGE S3 of 16

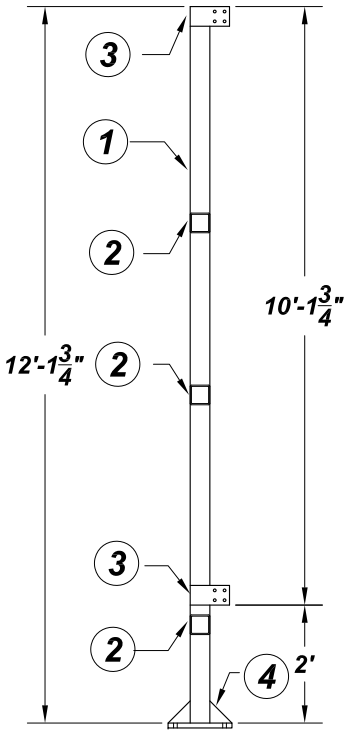

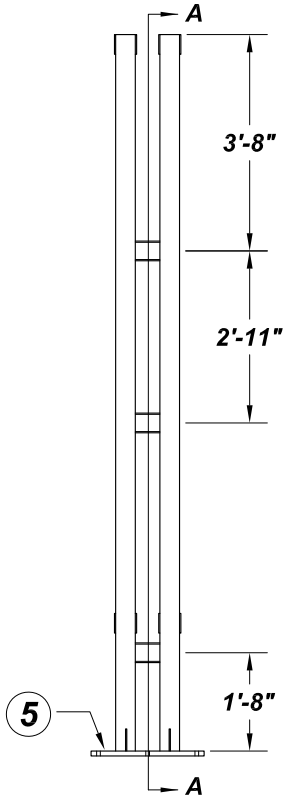

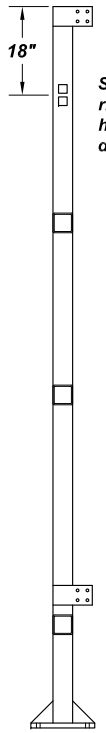

See to right for hole details

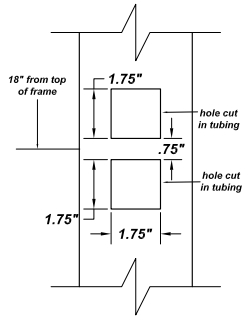

Vertical Perimeter Column Inside Hole Detail

Vertical Perimeter Columns

Note: Refer to S5 for part details.

	PART NAME	Material	Qty.
1	Vertical Perimeter Column Main Tube 4" x 4" x $\frac{1}{4}$" x 12' - 1$\frac{3}{4}$" long	A46-Steel	4
2	Vertical Perimeter Column Cross Tube 4" x 4" x $\frac{1}{4}$" x 5" long	A46-Steel	6
3	Vertical Perimeter Column Moment Connecting Plate 4" x 8" x $\frac{1}{4}$" thick	A36-Steel	16
4	Vertical Perimeter Column Base Plate Stiffener 4.5" x 4.5" x $\frac{1}{4}$" thick	A36-Steel	8
5	Vertical Perimeter Column Base Plate 23" x 13" x 1" thick	A36-Steel	2

Dept. of Structural Engineering, UC San Diego

Glass Panel Frame

Dr. by: Christopher Latham based on drawings by Francisco Nguyen & Corina De Pablo

AIMCAL PROJECT

2007

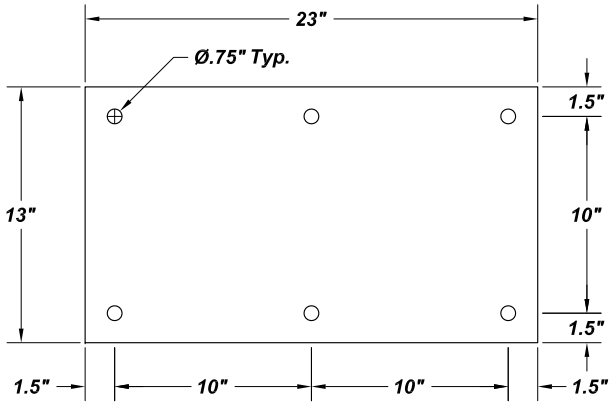

Perimeter Column Base Plate Dimensions

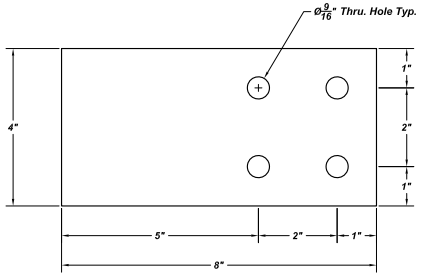

Perimeter Column Moment Connecting Plate Dimensions

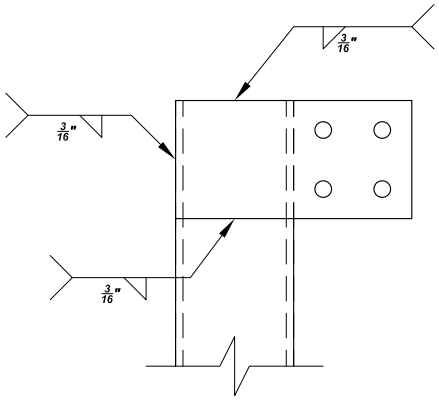

Perimeter Column Moment Connecting Plate Weld Details

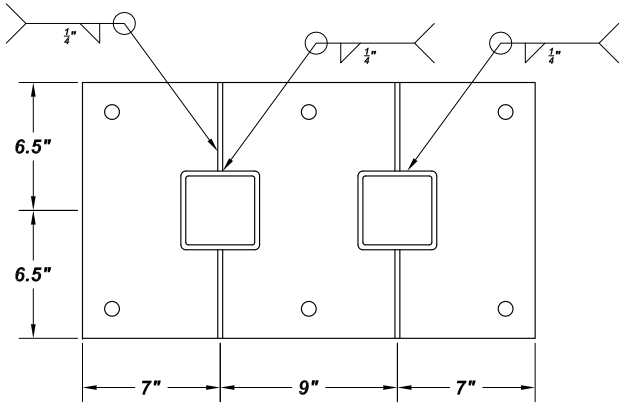

Perimeter Column Base Plate Welding

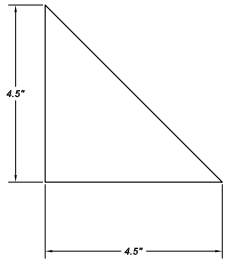

Perimeter Column Base Plate Stiffener Dimensions

Dept. of Structural Engineering, UC San Diego		
Glass Panel Frame		
Dr. by: Christopher Latham based on drawings by Francisco Nguyen & Corina De Pablo	AIMCAL PROJECT	
	2007	PAGE S5 of 16

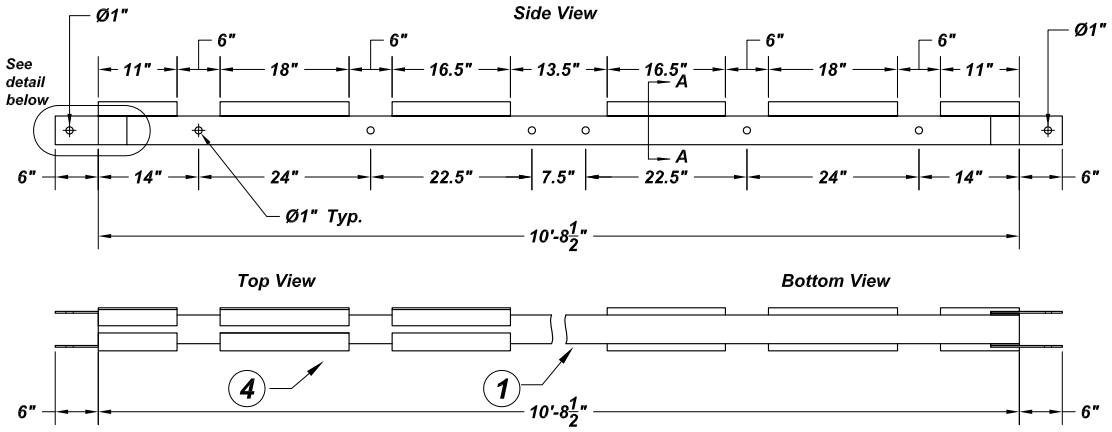

Interior Bottom Horizontal Beam

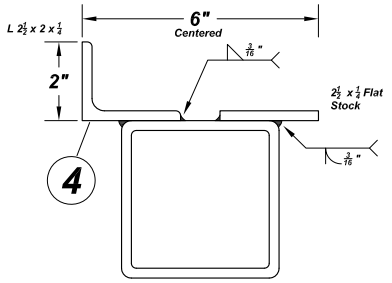

Section A-A

	PART NAME	Material	Qty.
1	Interior Bottom Horizontal Beam Main Tube 4" x 4" x 1/4" x 10' - 8 1/2" long	A46-Steel	1
2	Interior Bottom Horizontal Beam Hinge Plate - 10" x 4" x 1/4" thick	A36-Steel	4
3	Interior Bottom Horizontal Beam Spacer Plate - 4" x 4" x 1/4" thick	A36-Steel	4
4	Interior Bottom Horizontal Beam Window Support Channels - L 2 1/2 x 2 x 1/4 and 2 1/2 x 1/4 flat stock Various lengthes	A36-Steel	6 each

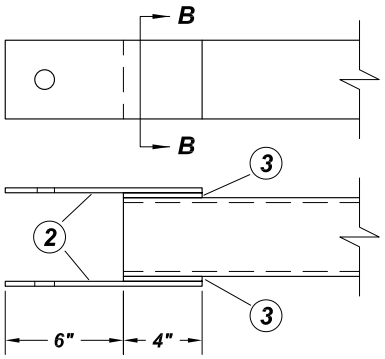

Interior Bottom Horizontal Beam End Details

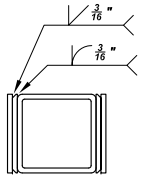

Section B-B

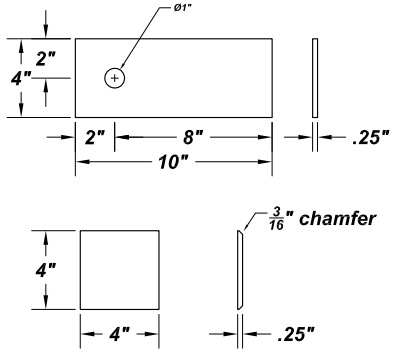

Interior Bottom Horizontal Beam Hinge & Spacer Plates

Dept. of Structural Engineering, UC San Diego

Glass Panel Frame

Dr. by: Christopher Latham based on drawings by Francisco Nguyen & Corina De Pablo

AIMCAL PROJECT

2007

PAGE S6 of 16

Side View

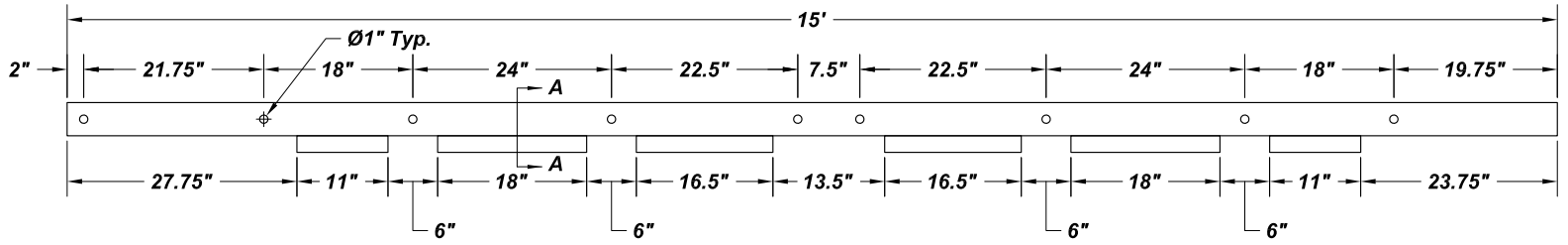

Top View

Bottom View

Interior Top Horizontal Beam

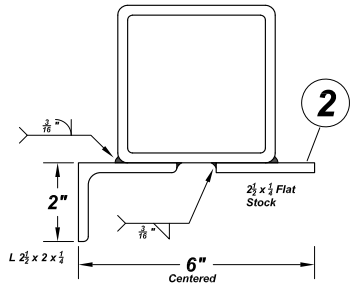

Section A-A

	PART NAME	Material	Qty.
1	Interior Top Horizontal Beam Main Tube 4" x 4" x ¼" x 15' long	A46-Steel	1
2	Interior Top Horizontal Beam Window Support Channels - L 2½ x 2 x ¼ and 2½ x ¼ flat stock Various lengthes	A36-Steel	6 each

Dept. of Structural Engineering, UC San Diego

Glass Panel Frame

Dr. by: Christopher Latham based on drawings by Francisco Nguyen & Corina De Pablo	AIMCAL PROJECT
	2007 PAGE S7 of 16

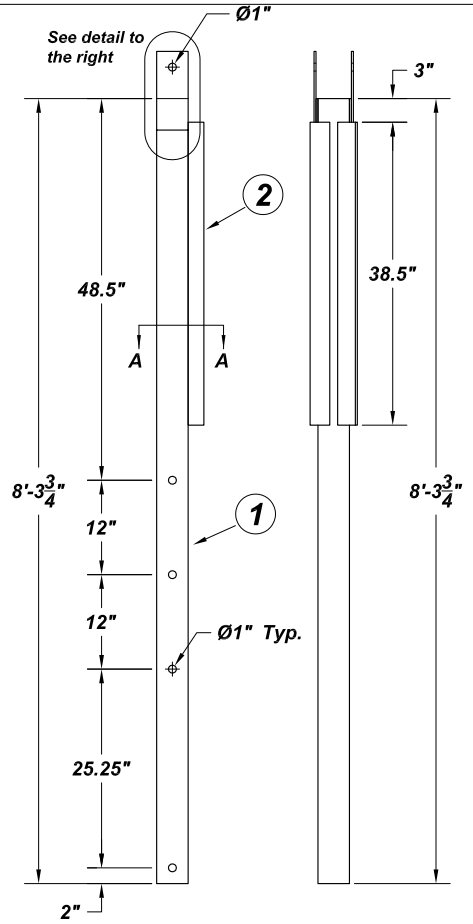

Interior Vertical Columns

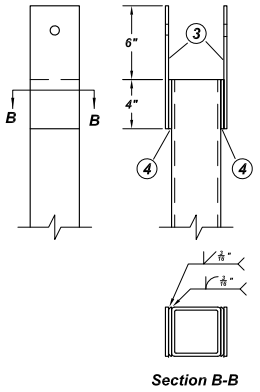

Interior Vertical Columns
End Details

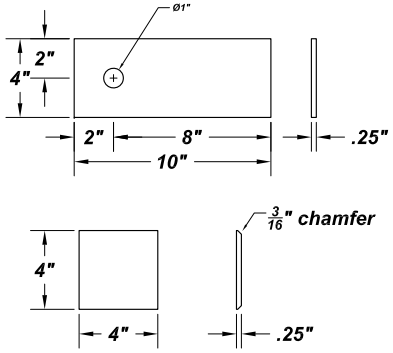

Interior Vertical Columns
Hinge & Spacer Plates

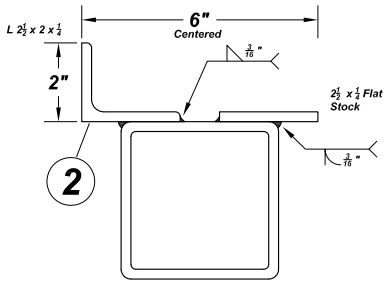

Section A-A

	PART NAME	Material	Qty.
1	Interior Vertical Columns Main Tube 4" x 4" x 1/4" x 8' - 3 3/4" long	A46-Steel	2
2	Interior Vertical Columns Window Support Channels - L 2 1/2 x 2 x 1/4 and 2 1/2 x 1/4 flat stock - 38.5" long	A36-Steel	2 each
3	Interior Vertical Columns Hinge Plate - 10" x 4" x 1/4" thick	A36-Steel	4
4	Interior Vertical Columns Spacer Plate - 4" x 4" x 1/4" thick	A36-Steel	4

Dept. of Structural Engineering, UC San Diego

Glass Panel Frame

Dr. by: Christopher Latham based on drawings by Francisco Nguyen & Corina De Pablo

AIMCAL PROJECT

2007

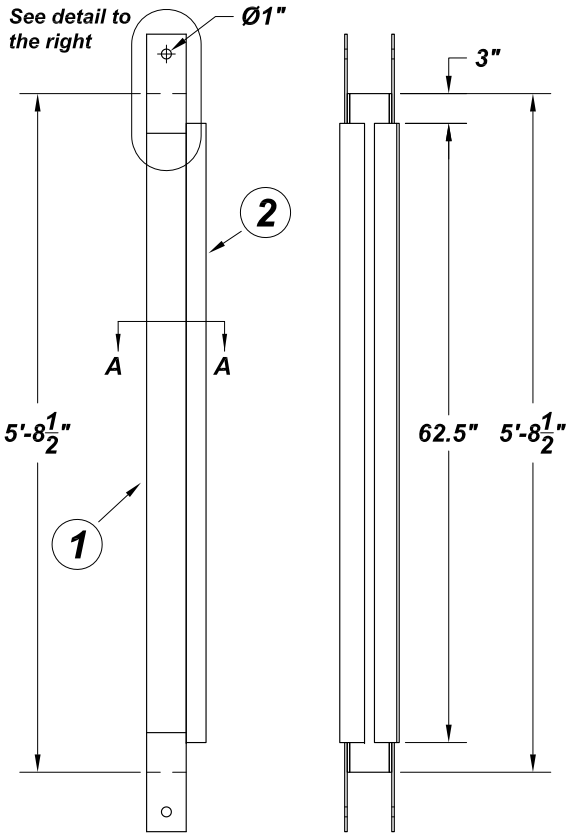

Interior Support Columns Type A

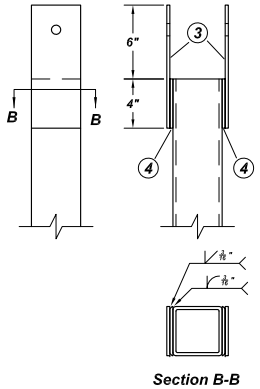

Section B-B

Interior Support Columns Type A End Details

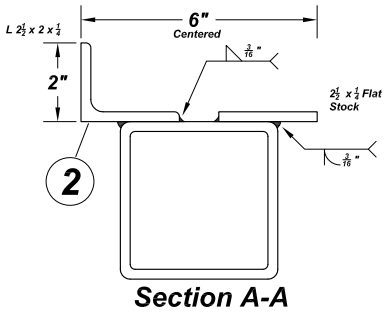

Section A-A

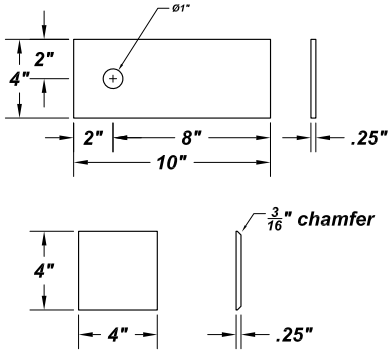

Interior Support Columns Type A Hinge & Spacer Plates

	PART NAME	Material	Qty.
1	Interior Support Columns Type A Main Tube 4" x 4" x 1/4" x 5' - 8 1/2" long	A46-Steel	2
2	Interior Support Columns Type A Window Support Channels - L 2 1/2 x 2 x 1/4 and 2 1/2 x 1/2 flat stock - 62.5" long	A36-Steel	2 each
3	Interior Support Columns Type A Hinge Plate - 10" x 4" x 1/4" thick	A36-Steel	8
4	Interior Support Columns Type A Spacer Plate - 4" x 4" x 1/4" thick	A36-Steel	8

Dept. of Structural Engineering, UC San Diego

Glass Panel Frame

Dr. by: Christopher Latham based on drawings by Francisco Nguyen & Corina De Pablo

AIMCAL PROJECT

2007

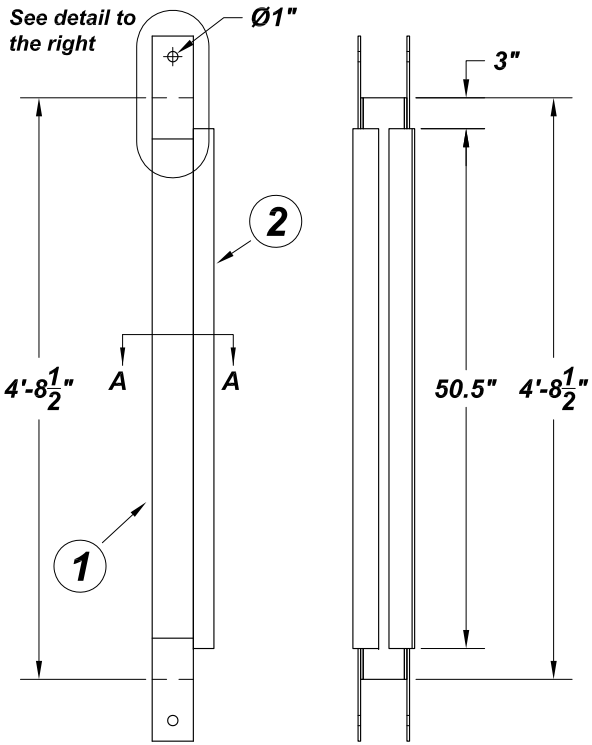

Interior Support Columns Type B

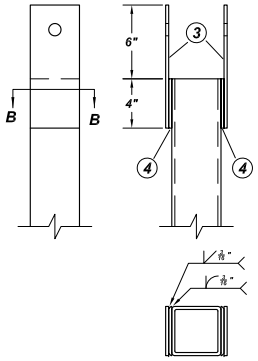

Interior Support Columns Type B End Details

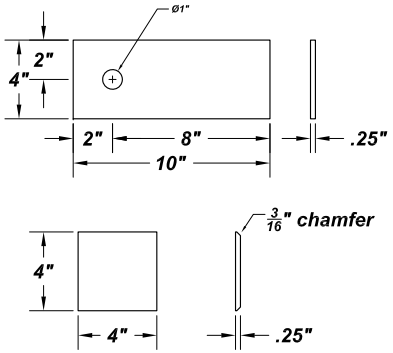

Interior Support Columns Type B Hinge & Spacer Plates

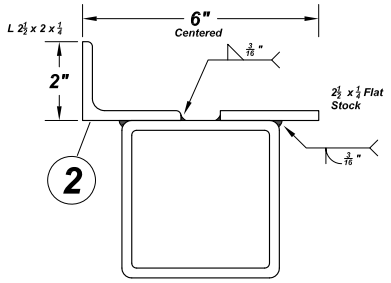

Section A-A

	PART NAME	Material	Qty.
1	Interior Support Columns Type B Main Tube 4" x 4" x 1/4" x 4' - 8 1/2" long	A46-Steel	2
2	Interior Support Columns Type B Window Support Channels - L 2 1/2 x 2 x 1/4 and 2 1/2 x 1/4 flat stock - 50.5" long	A36-Steel	2 each
3	Interior Support Columns Type B Hinge Plate - 10" x 4" x 1/4" thick	A36-Steel	8
4	Interior Support Columns Type B Spacer Plate - 4" x 4" x 1/4" thick	A36-Steel	8

Dept. of Structural Engineering, UC San Diego

Glass Panel Frame

Dr. by: Christopher Latham based on drawings by Francisco Nguyen & Corina De Pablo

AIMCAL PROJECT

2007

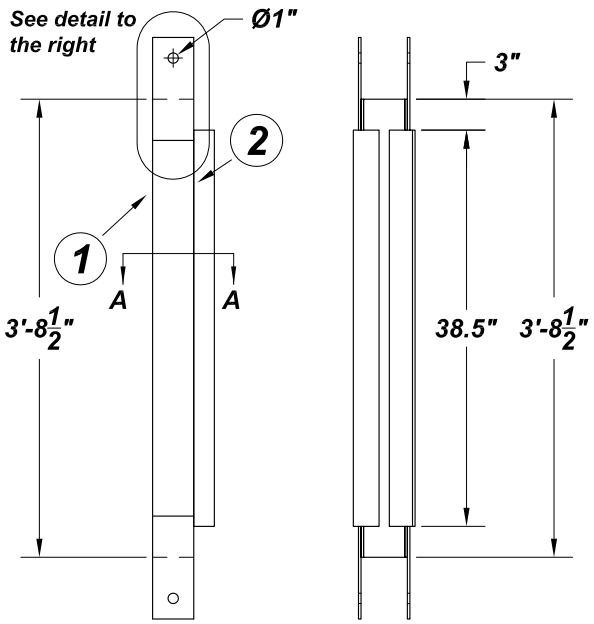

Interior Support Columns Type C

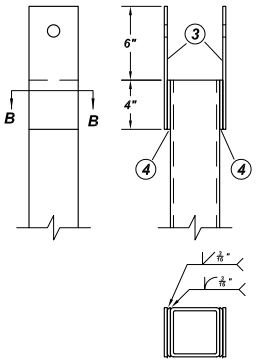

Section B-B

Interior Support Columns Type C End Details

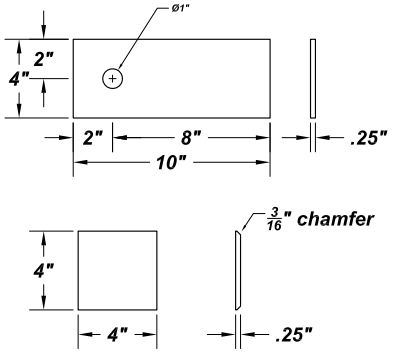

Interior Support Columns Type C Hinge & Spacer Plates

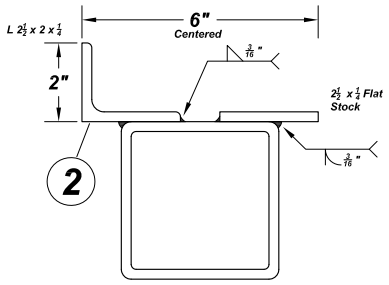

Section A-A

	PART NAME	Material	Qty.
1	Interior Support Columns Type C Main Tube 4" x 4" x 1/4" x 3' - 8 1/2" long	A46-Steel	2
2	Interior Support Columns Type C Window Support Channels - L 2 1/2 x 2 x 1/4 and 2 1/2 x 1/4 flat stock - 38.5" long	A36-Steel	2 each
3	Interior Support Columns Type C Hinge Plate - 10" x 4" x 1/4" thick	A36-Steel	8
4	Interior Support Columns Type C Spacer Plate - 4" x 4" x 1/4" thick	A36-Steel	8

Dept. of Structural Engineering, UC San Diego

Glass Panel Frame

Dr. by: Christopher Latham based on drawings by Francisco Nguyen & Corina De Pablo

AIMCAL PROJECT

2007

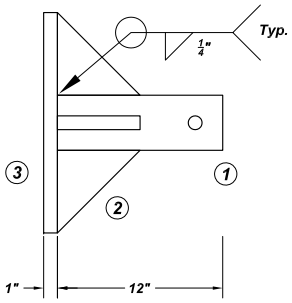

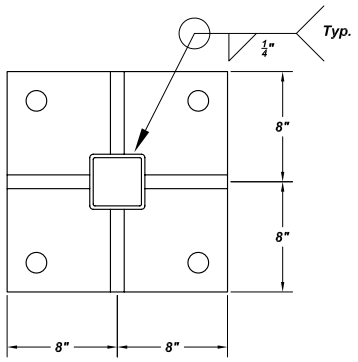

Strong Wall Attachment Fixture

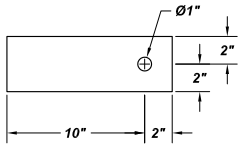

Strong Wall Attachment Fixture Main Tube

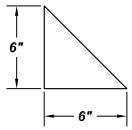

Strong Wall Attachment Fixture Stiffener Plate

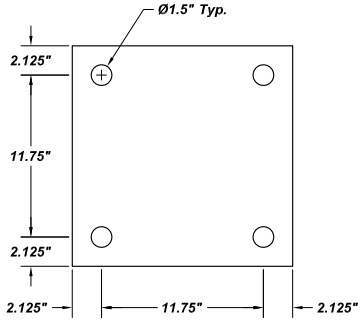

Strong Wall Attachment Fixture Base Plate

	PART NAME	Material	Qty.
1	Strong Wall Attachment Fixture Main Tube 4" x 4" x $\frac{1}{4}$" x 12" long	A46-Steel	1
2	Strong Wall Attachment Fixture Stiffener 6" x 6" x 1" thick triangular plate	A36-Steel	4
3	Strong Wall Attachment Fixture Base Plate 16" x 16" x 1" thick plate	A36-Steel	1

Dept. of Structural Engineering, UC San Diego

Glass Panel Frame

Dr. by: Christopher Latham based on drawings by Francisco Nguyen & Corina De Pablo

AIMCAL PROJECT

2007

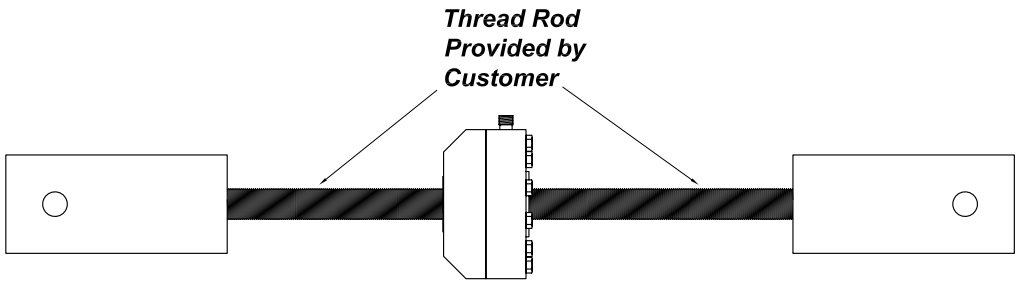

Load Cell Provided by Customer

Link Fixture

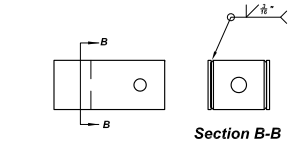

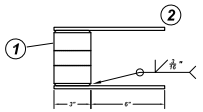

Link Fixture
Hinge Block

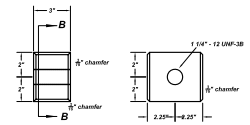

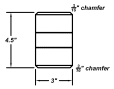

Link Fixture
Main Block

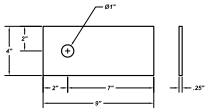

Link Fixture
Hinge Plate

	PART NAME	Material	Qty.
1	Link Fixture Main Main Block 4" x $4\frac{1}{2}$" x 3"	A36-Steel	2
2	Link Fixture Hinge Plate 9" x 4" x $\frac{1}{4}$ " thick plate	A36-Steel	4

Dept. of Structural Engineering, UC San Diego		
Glass Panel Frame		
Dr. by: Christopher Latham based on drawings by Francisco Nguyen & Corina De Pablo	AIMCAL PROJECT	
	2007	PAGE S13 of 16

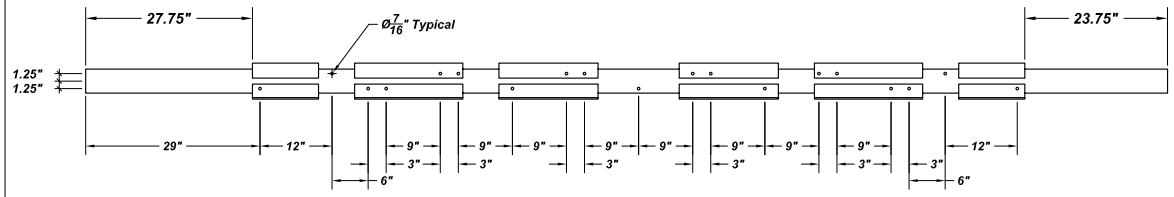

Interior Top Horizontal Beam See S7 for most fabrication details

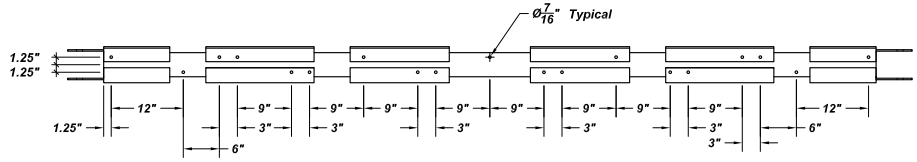

Interior Bottom Horizontal Beam See S6 for most fabrication details

Note: Holes completely through tube

Dept. of Structural Engineering, UC San Diego

Glass Panel Frame

Dr. by: Christopher Latham based on drawings by Francisco Nguyen & Corina De Pablo	*AIMCAL PROJECT*	
	2007	*PAGE S14 of 16*

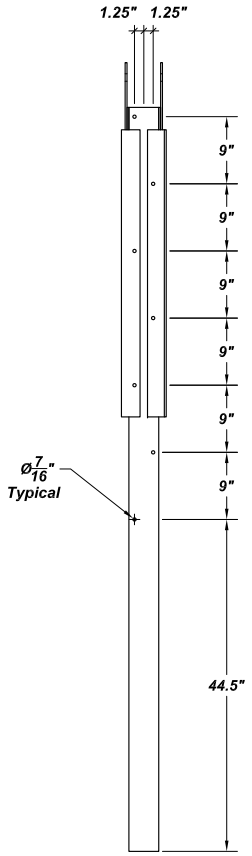

Interior Vertical Columns See S8 for most fabrication details

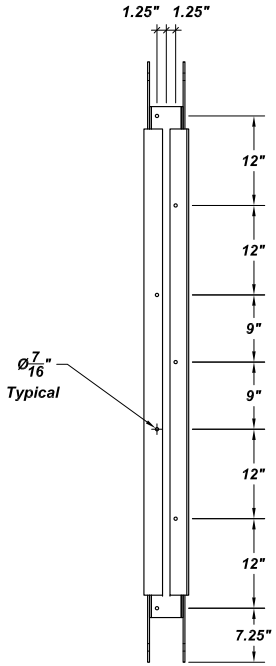

Interior Support Columns Type A See S9 for most fabrication details

Note: Holes completely through tube

Dept. of Structural Engineering, UC San Diego	
Glass Panel Frame	
Dr. by: Christopher Latham based on drawings by Francisco Nguyen & Corina De Pablo	AIMCAL PROJECT
	2007 PAGE S15 of 16

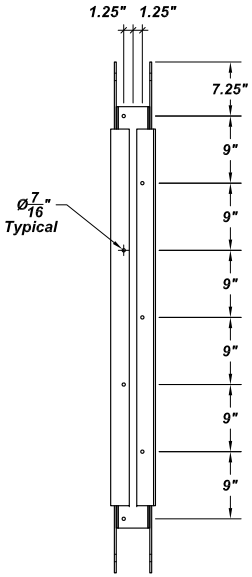

Interior Support Columns Type B
See S10 for most fabrication details

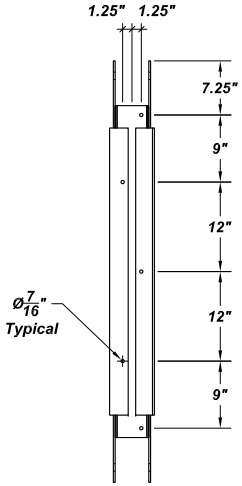

Interior Support Columns Type C
See S11 for most fabrication details

Note: Holes completely through tube

Dept. of Structural Engineering, UC San Diego		
Glass Panel Frame		
Dr. by: Christopher Latham based on drawings by Francisco Nguyen & Corina De Pablo	AIMCAL PROJECT	
	2007	PAGE S15 of 16

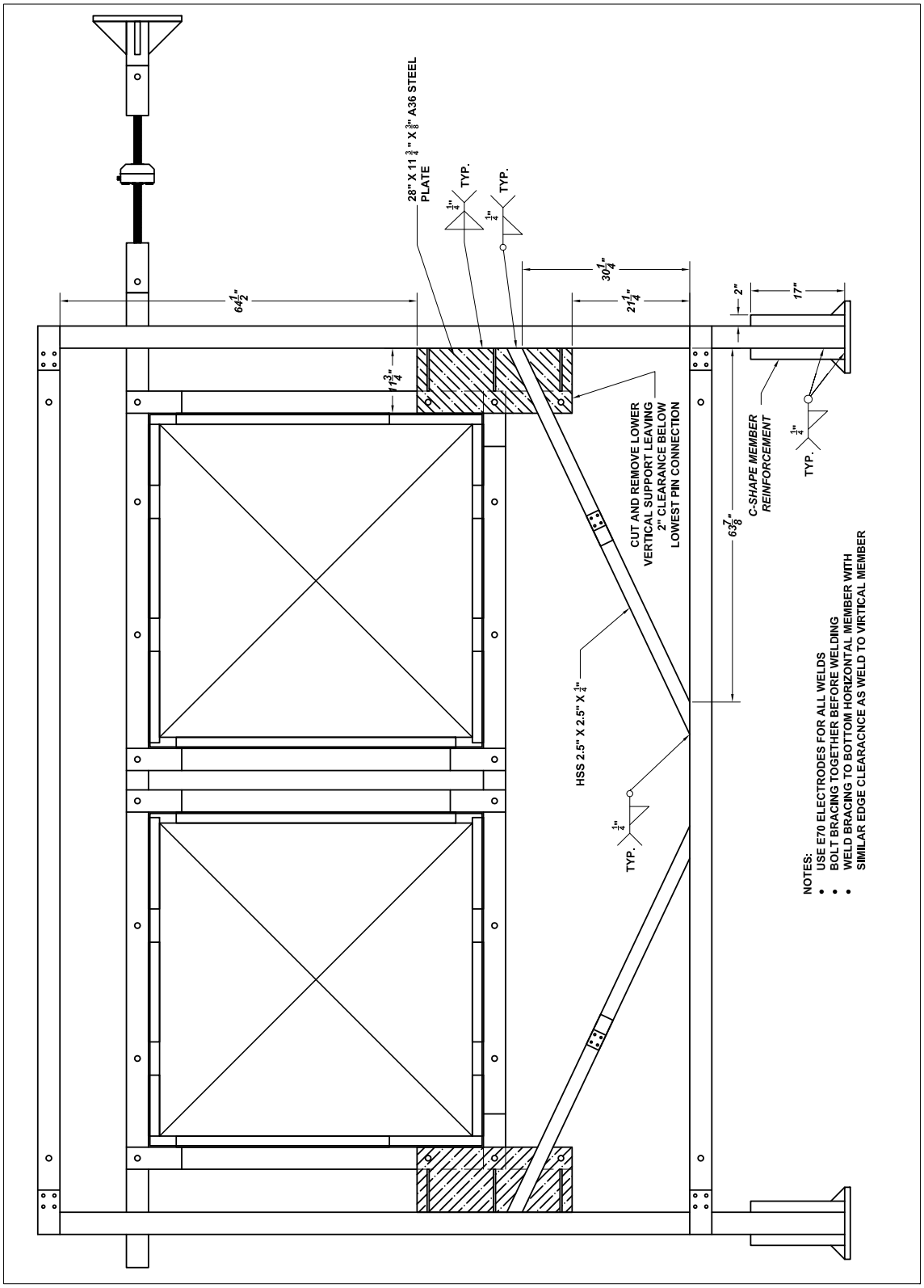
28" X 11 3/4" X 3/8" A36 STEEL PLATE
TYP.
TYP.
TYP.
TYP.
TYP.
64 1/2"
30 1/4"
21 1/4"
2"
17"
1 3/4"
CUT AND REMOVE LOWER VERTICAL SUPPORT LEAVING 2" CLEARANCE BELOW LOWEST PIN CONNECTION
C-SHAPE MEMBER REINFORCEMENT
63 7/8"
HSS 2.5" X 2.5" X 1/4"
NOTES:
• USE E70 ELECTRODES FOR ALL WELDS
• BOLT BRACING TOGETHER BEFORE WELDING
• WELD BRACING TO BOTTOM HORIZONTAL MEMBER WITH SIMILAR EDGE CLEARACNCE AS WELD TO VIRTICAL MEMBER

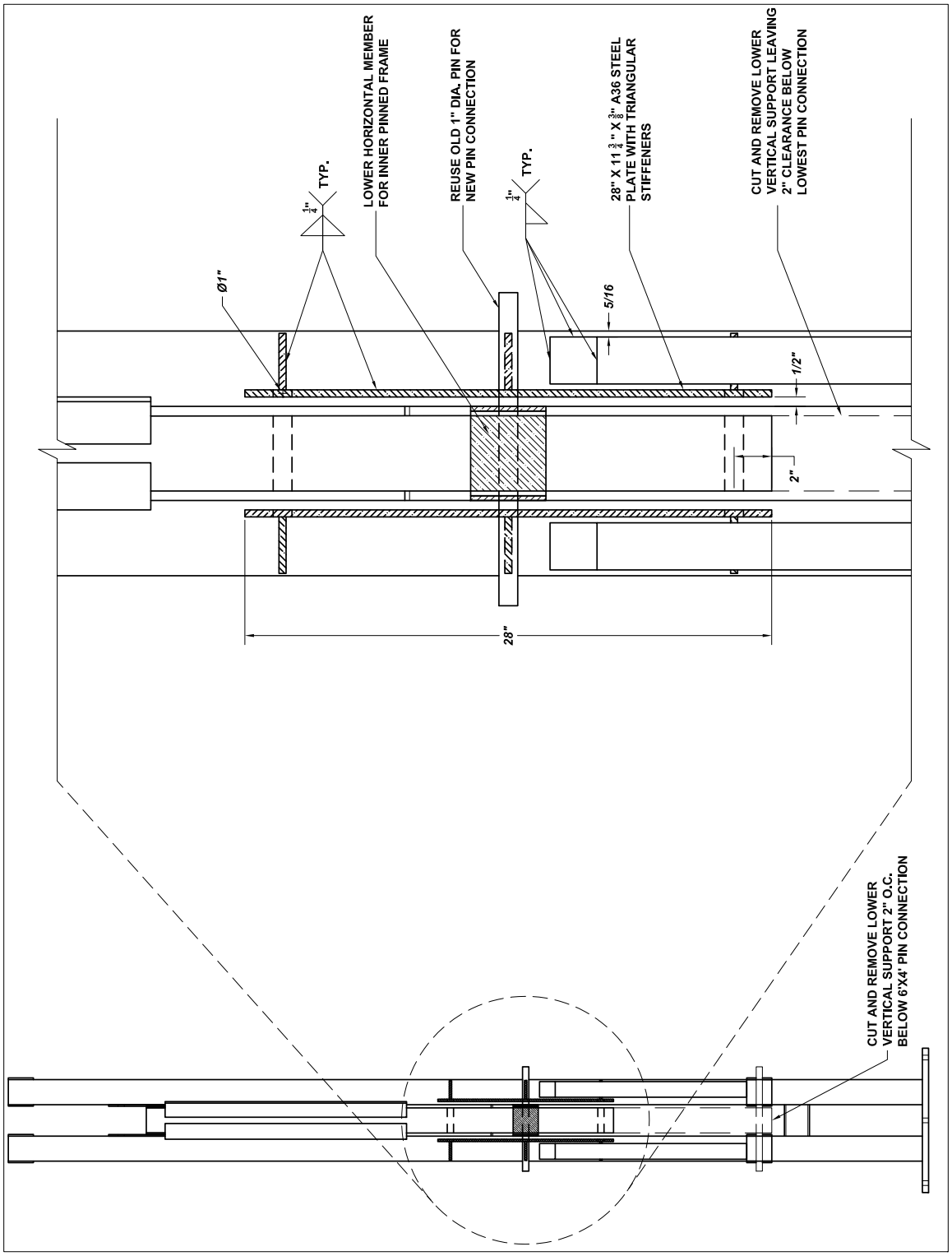
LOWER HORIZONTAL MEMBER FOR INNER PINNED FRAME
REUSE OLD 1" DIA. PIN FOR NEW PIN CONNECTION
28" X 11 3/4" X 3/8" A36 STEEL PLATE WITH TRIANGULAR STIFFENERS
CUT AND REMOVE LOWER VERTICAL SUPPORT LEAVING 2" CLEARANCE BELOW LOWEST PIN CONNECTION
1/4" TYP.
1/4" TYP.
Ø1"
5/16
1/2"
2"
28"
CUT AND REMOVE LOWER VERTICAL SUPPORT 2" O.C. BELOW 6'X4' PIN CONNECTION

SUPPORT PLATE
QUANTITY: 4

$\frac{3}{8}$" THICK A36 STEEL PLATE WITH $\frac{3}{8}$" THICK TRIANGULAR STIFFENERS

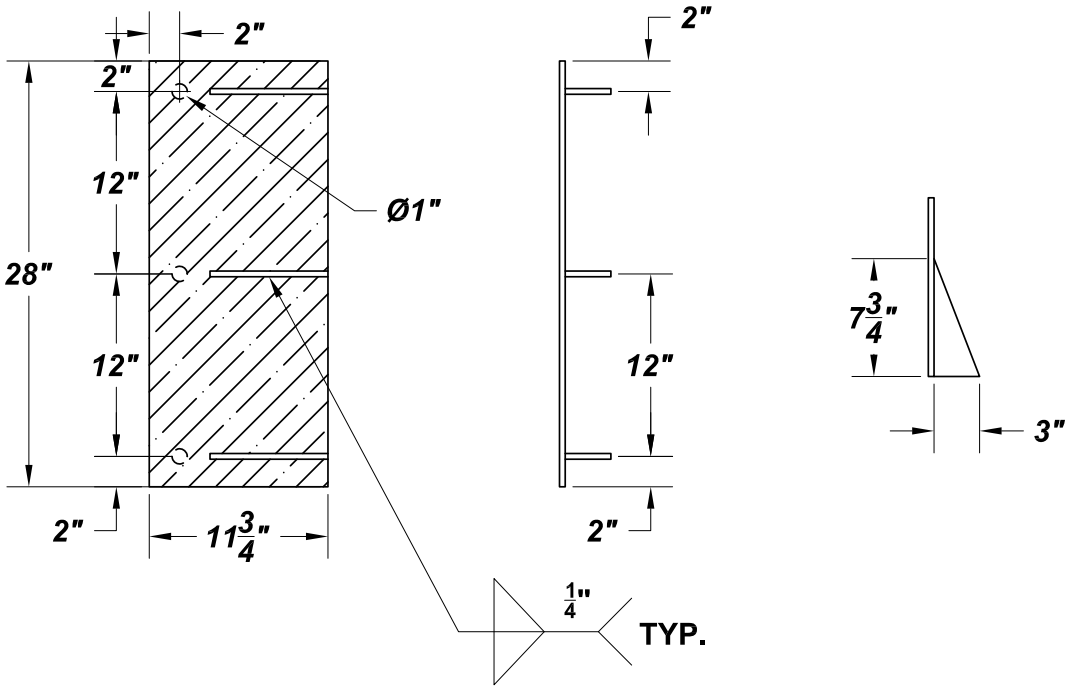

NOTES:
USE E70 ELECTRODES FOR ALL WELDS

C-SHAPE MEMBER REINFORCEMENT
QUANTITY: 8
$\frac{1}{4}$" A36 STEEL PLATE

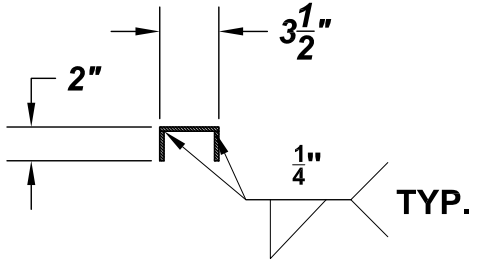

PLACEMENT DETAIL:
NORTH FOOTING

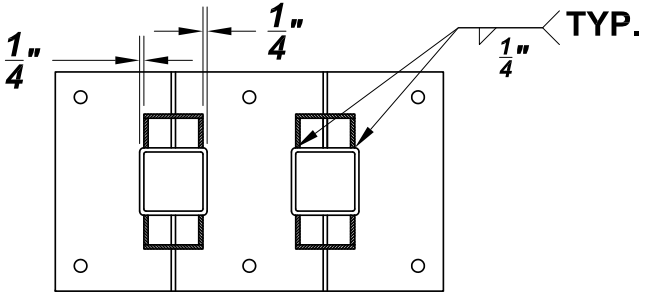

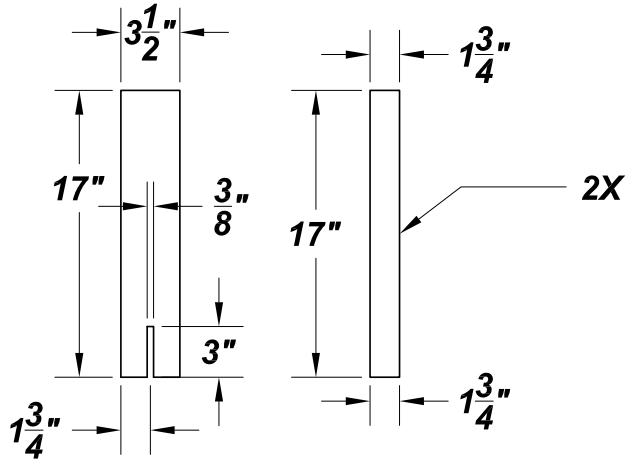

NOTES:
USE E70 ELECTRODES FOR ALL WELDS

MOMENT FRAME BRACING
QUANTITY: 4

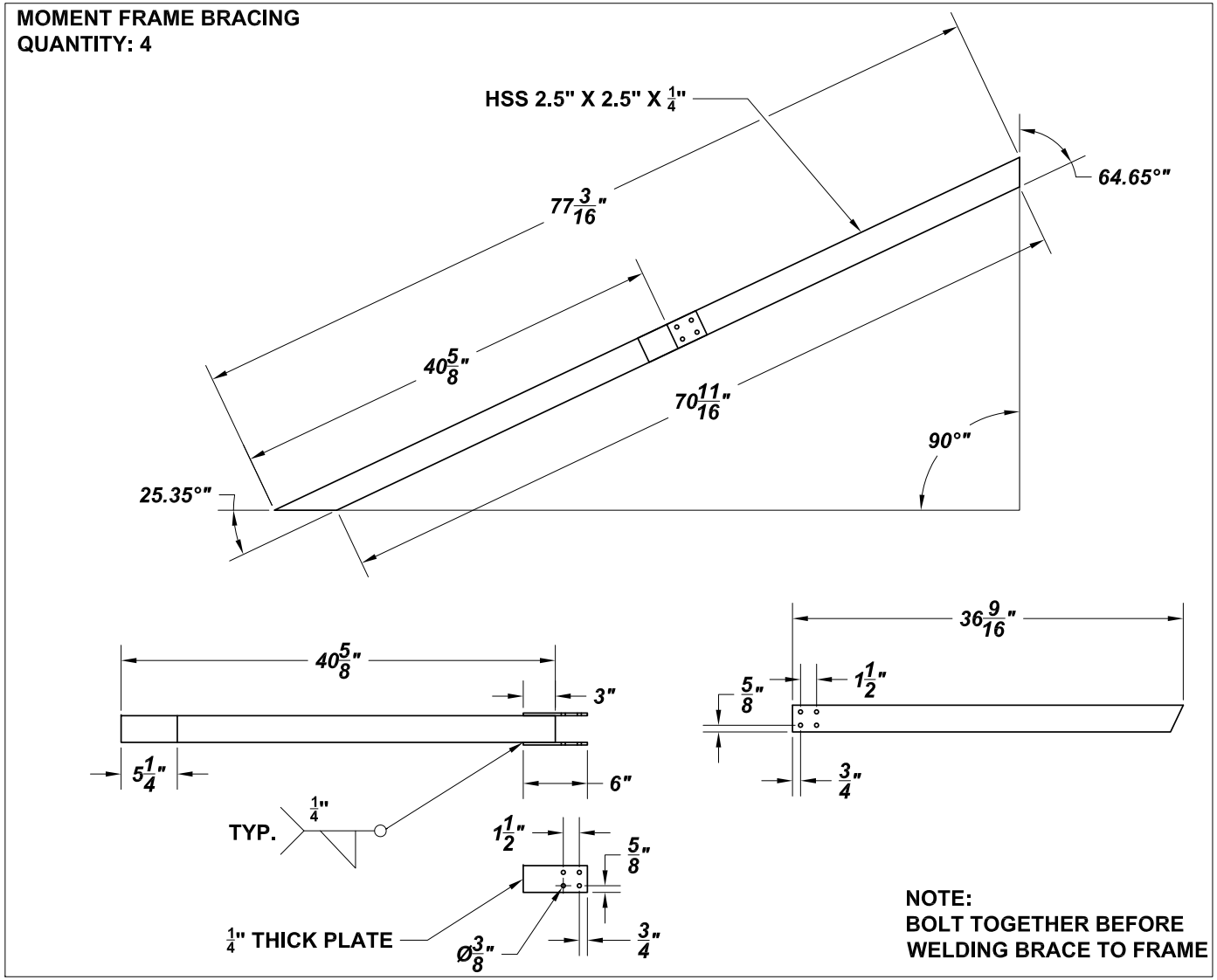

NOTE:
BOLT TOGETHER BEFORE WELDING BRACE TO FRAME

Charge: SSRTH15
Name: Charles Eva
Email: ceva@ucsd.edu
Phone:
Quantity: 2

TOP

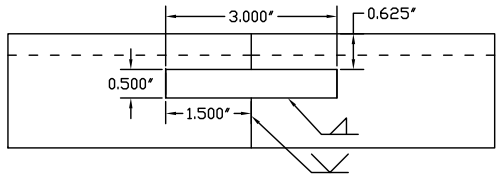

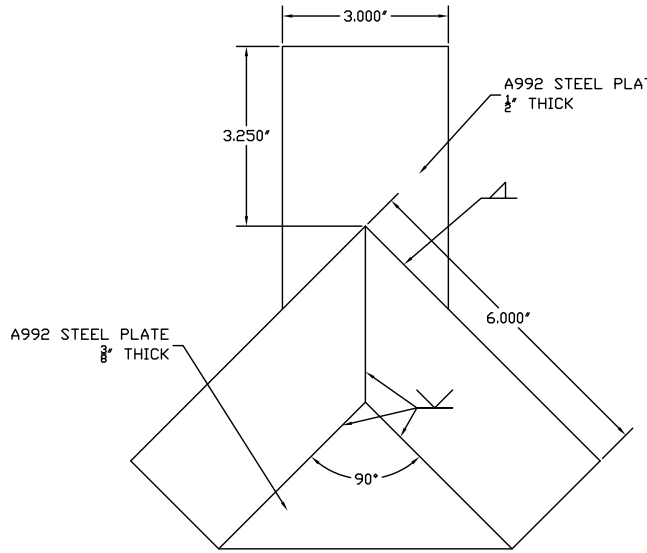

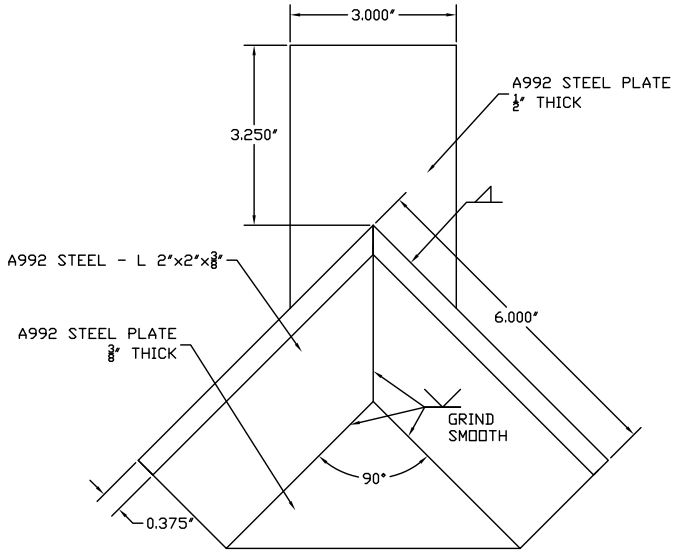

PARTS

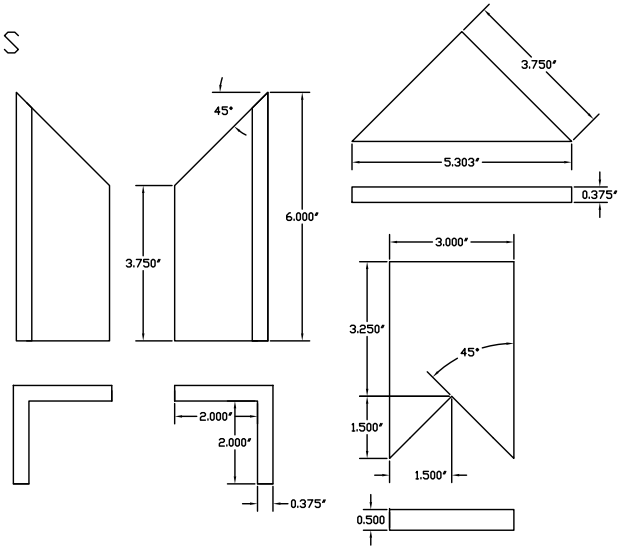

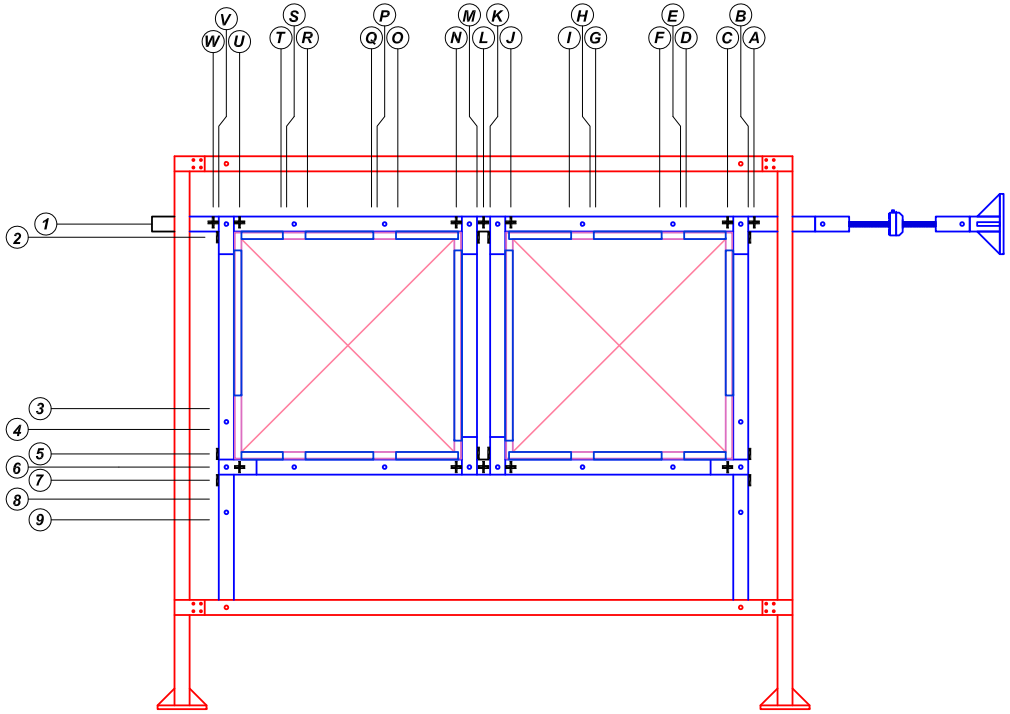

NOTES:

- L - STRAIN GAUGE PLACED LONGITUDINAL ALONG MEMBER
- T - STRAIN GAUGE PLACED TRANSVERSE ALONG MEMBER
- PLACE STRAIN GAUGE ON OPPOSITE FACE FROM WINDOW
- OFFSET STRAIN GAUGE 3.5 INCHES FROM NEAREST BOLT

FRONT VIEW with 5' x 5' Panel Configuration

STRAIN GAUGE TABLE		
Location	***Label***	***Orientation***
A1	***SG01***	***L***
	SG02	***T***
B2	***SG03***	***L***
C1	***SG04***	***L***
	SG05	***T***
J1	***SG06***	***L***
	SG07	***T***
K2	***SG08***	***L***
L1	***SG09***	***L***
	SG10	***T***
M2	***SG11***	***L***
N1	***SG12***	***L***
	SG13	***T***
U1	***SG14***	***L***
	SG15	***T***
V2	***SG16***	***L***
W1	***SG17***	***L***
	SG18	***T***
B5	***SG19***	***L***
B7	***SG20***	***L***
C6	***SG21***	***L***
	SG22	***T***
J6	***SG23***	***L***
	SG24	***T***
K5	***SG25***	***L***
L6	***SG26***	***L***
	SG27	***T***
M5	***SG28***	***L***
N6	***SG29***	***L***
	SG30	***T***
U6	***SG31***	***L***
	SG32	***T***
V5	***SG33***	***L***
V7	***SG34***	***L***

STRAIN GAUGE LAYOUT

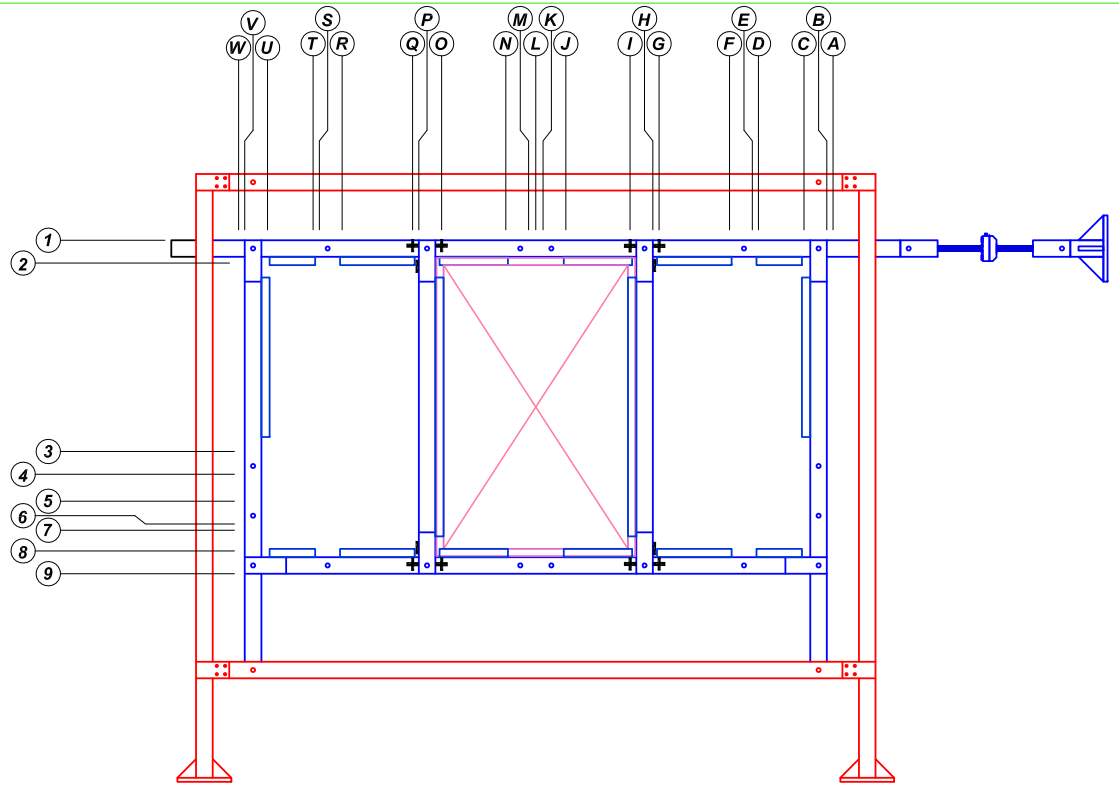

NOTES:

- L - STRAIN GAUGE PLACED LONGITUDINAL ALONG MEMBER
- T - STRAIN GAUGE PLACED TRANSVERSE ALONG MEMBER
- PLACE STRAIN GAUGE ON OPPOSITE FACE FROM WINDOW
- OFFSET STRAIN GAUGE 3.5 INCHES FROM NEAREST BOLT

FRONT VIEW with Dual 6' x 4' Panel Configuration

STRAIN GAUGE TABLE

Location	Label	Orientation
G1	SG35	L
	SG36	T
H2	SG37	L
I1	SG38	L
	SG39	T
O1	SG40	L
	SG41	T
P2	SG42	L
Q1	SG43	L
	SG44	T
G9	SG45	L
	SG46	T
H8	SG47	L
I9	SG48	L
	SG49	T
O9	SG50	L
	SG51	T
P8	SG52	L
Q9	SG53	L
	SG54	T

STRAIN GAUGE LAYOUT

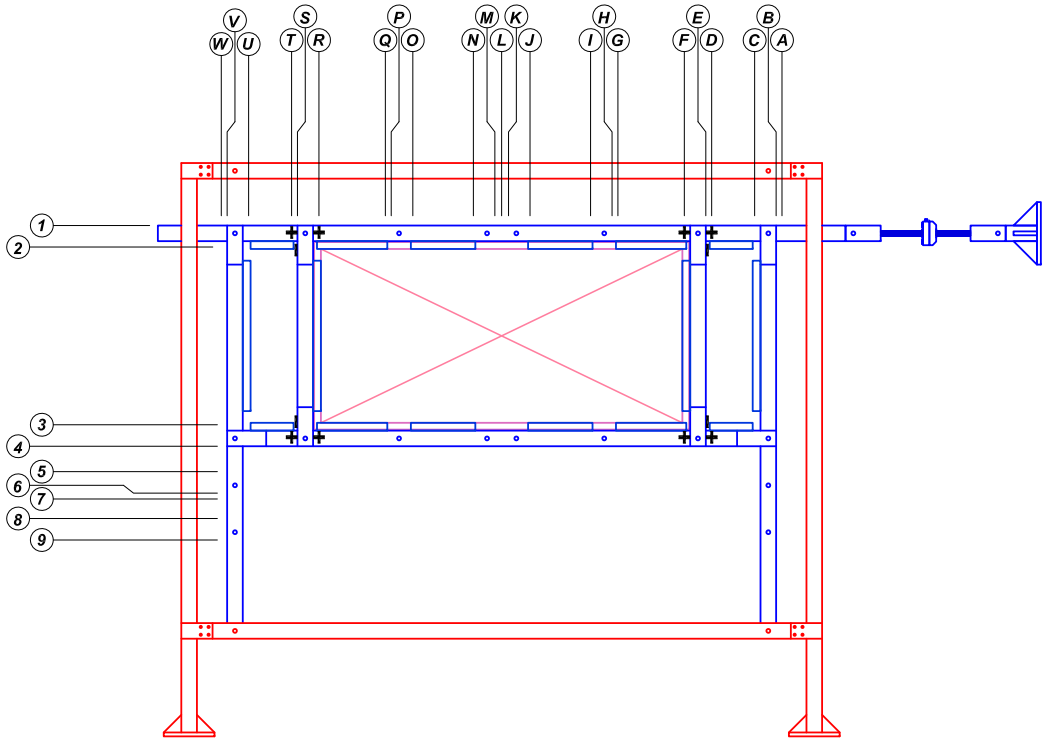

NOTES:

- L - STRAIN GAUGE PLACED LONGITUDINAL ALONG MEMBER
- T - STRAIN GAUGE PLACED TRANSVERSE ALONG MEMBER
- PLACE STRAIN GAUGE ON OPPOSITE FACE FROM WINDOW
- OFFSET STRAIN GAUGE 3.5 INCHES FROM NEAREST BOLT

FRONT VIEW with 4' x 8' Panel Configuration

SG LOCATION TABLE		
Location	***Label***	***Orientation***
D1	***SG55***	***L***
	SG56	***T***
E2	***SG57***	***L***
F1	***SG58***	***L***
	SG59	***T***
R1	***SG60***	***L***
	SG61	***T***
S2	***SG62***	***L***
T1	***SG63***	***L***
	SG64	***T***
D4	***SG65***	***L***
	SG66	***T***
E3	***SG67***	***L***
F4	***SG68***	***L***
	SG69	***T***
R4	***SG70***	***L***
	SG71	***T***
S3	***SG72***	***L***
T4	***SG73***	***L***
	SG74	***T***

STRAIN GAUGE LAYOUT

Appendix B:

Load-Deflection Response Curves

Monotonic Load Protocol Curves

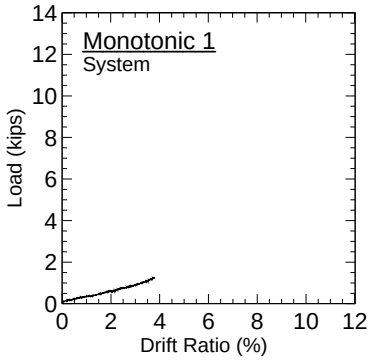

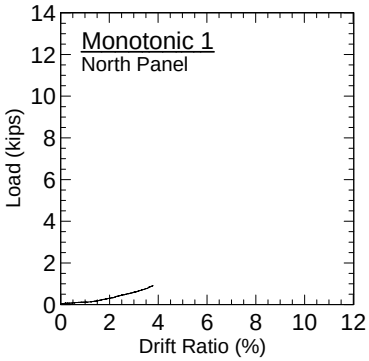

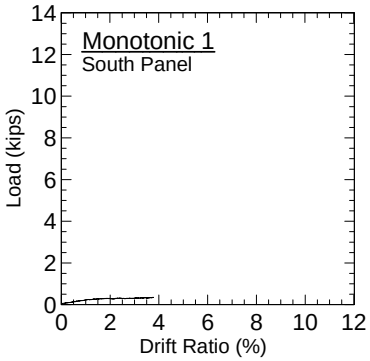

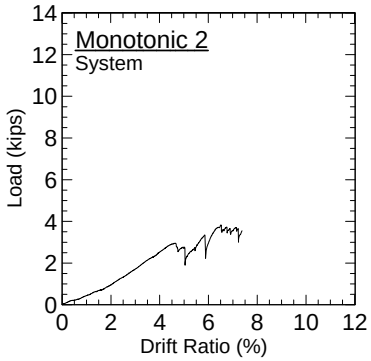

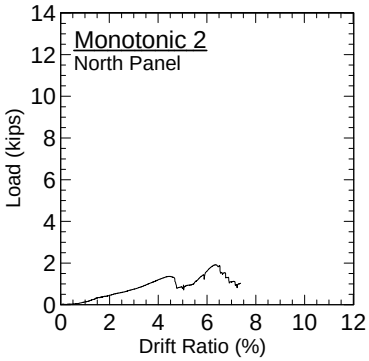

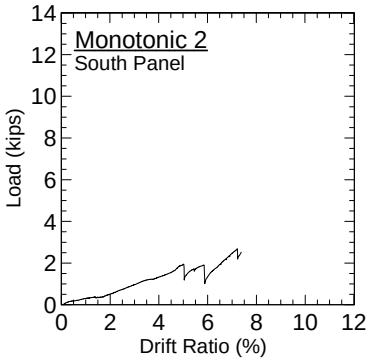

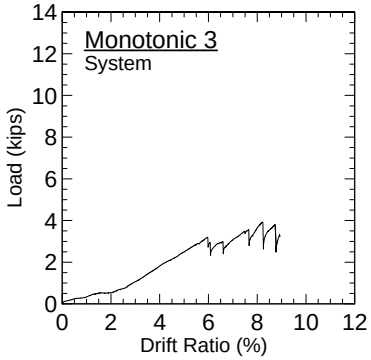

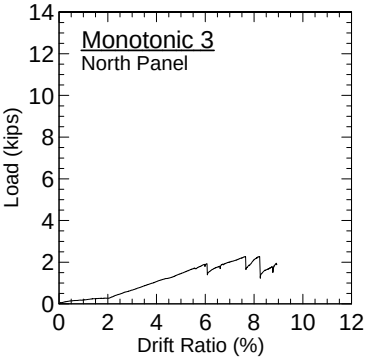

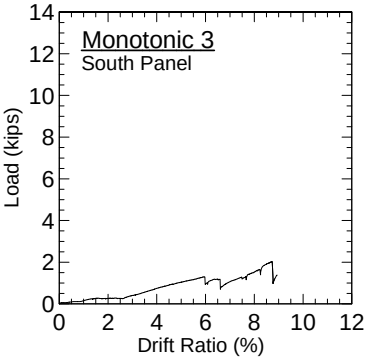

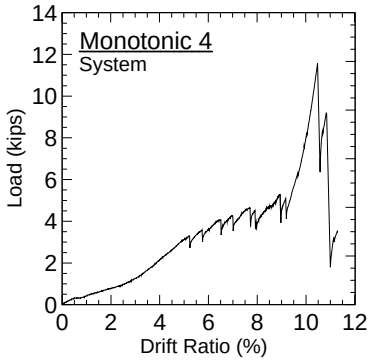
Monotonic 4
System
Load (kips)
Drift Ratio (%)

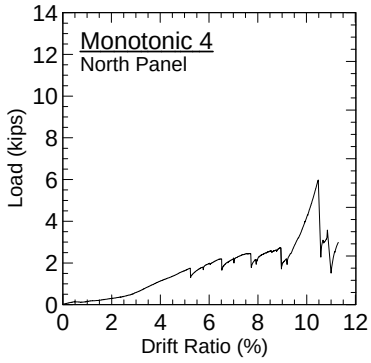
Monotonic 4
North Panel
Load (kips)
Drift Ratio (%)

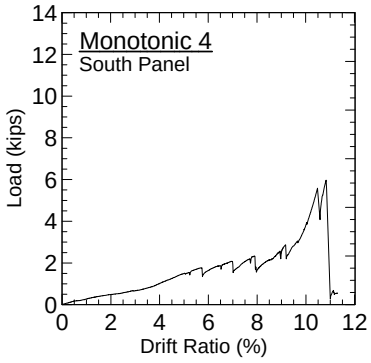
Monotonic 4
South Panel
Load (kips)
Drift Ratio (%)

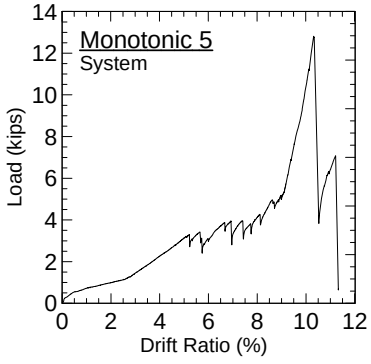
Monotonic 5
System
Load (kips)
Drift Ratio (%)

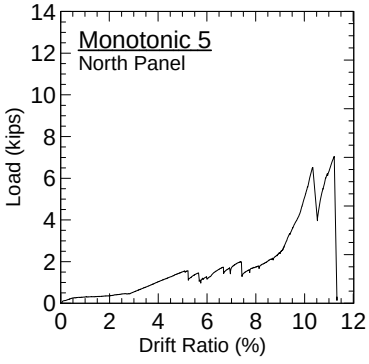
Monotonic 5
North Panel
Load (kips)
Drift Ratio (%)

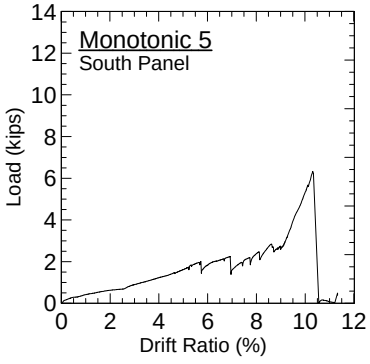
Monotonic 5
South Panel
Load (kips)
Drift Ratio (%)

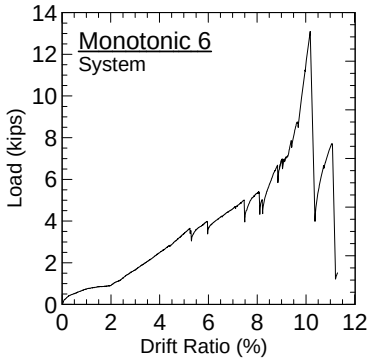
Monotonic 6
System
Load (kips)
Drift Ratio (%)

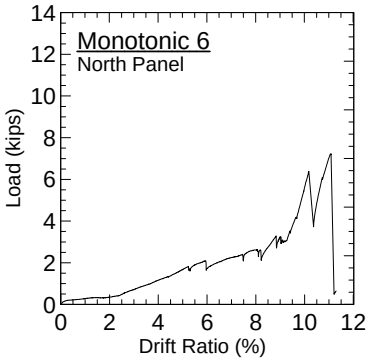
Monotonic 6
North Panel
Load (kips)
Drift Ratio (%)

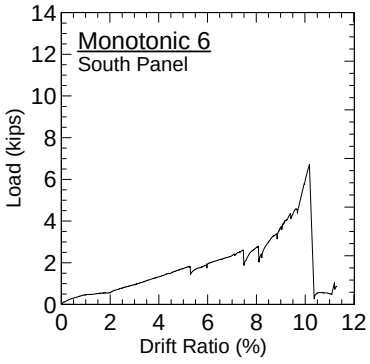
Monotonic 6
South Panel
Load (kips)
Drift Ratio (%)

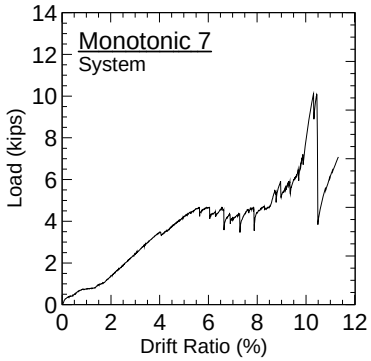
Monotonic 7
System
Load (kips)
Drift Ratio (%)

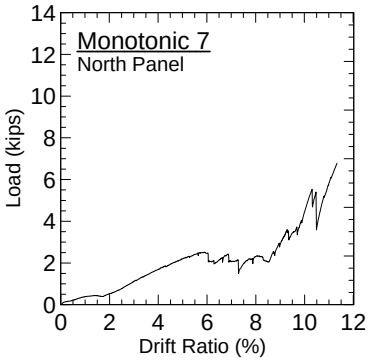
Monotonic 7
North Panel
Load (kips)
Drift Ratio (%)

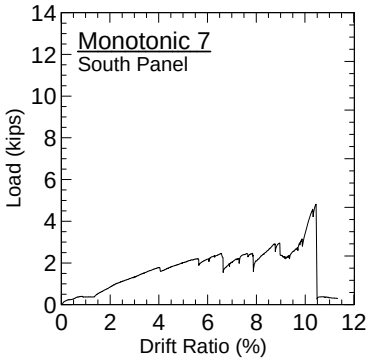
Monotonic 7
South Panel
Load (kips)
Drift Ratio (%)

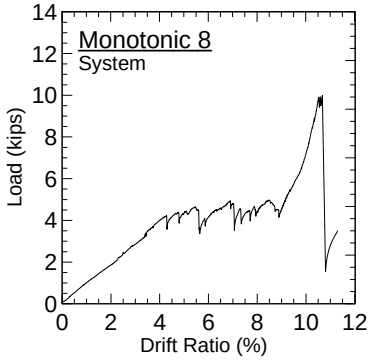
Monotonic 8
System
Load (kips)
Drift Ratio (%)

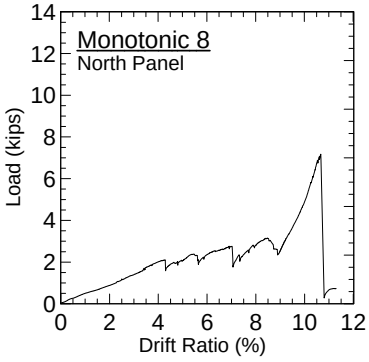
Monotonic 8
North Panel
Load (kips)
Drift Ratio (%)

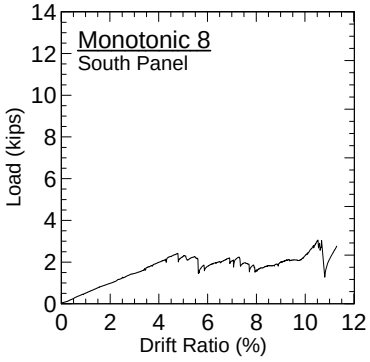
Monotonic 8
South Panel
Load (kips)
Drift Ratio (%)

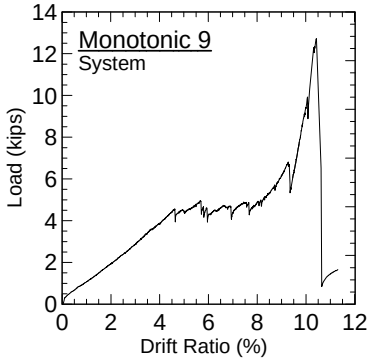
Monotonic 9
System
Load (kips)
Drift Ratio (%)

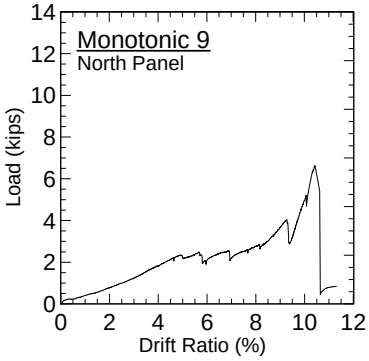
Monotonic 9
North Panel
Load (kips)
Drift Ratio (%)

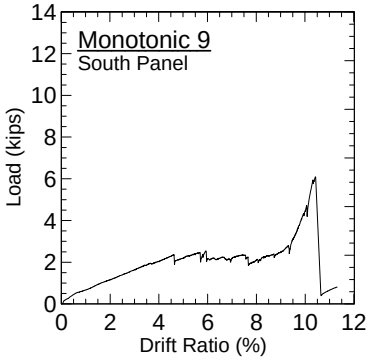
Monotonic 9
South Panel
Load (kips)
Drift Ratio (%)

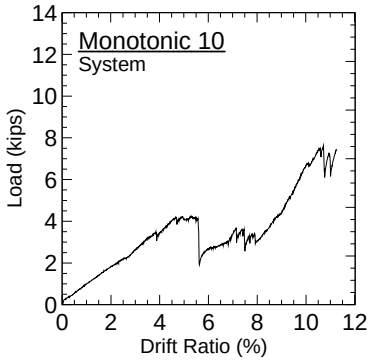

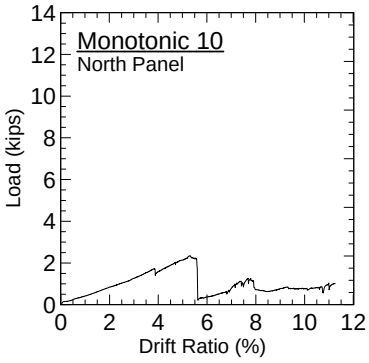

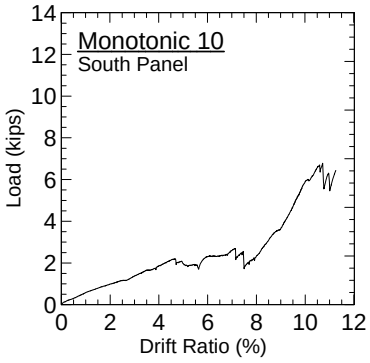

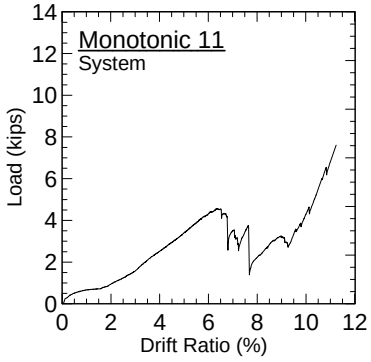

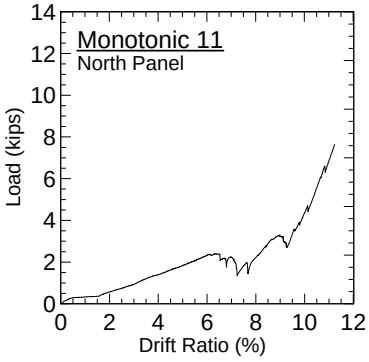

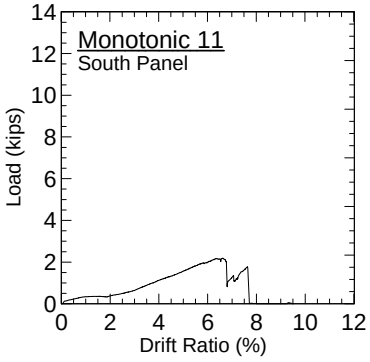

Crescendo Load Protocol Curves

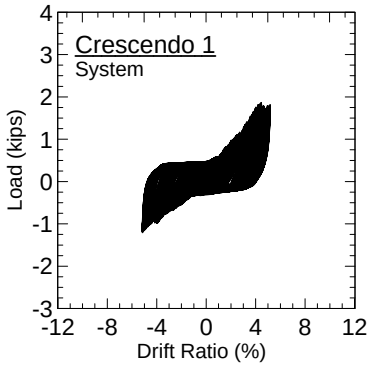

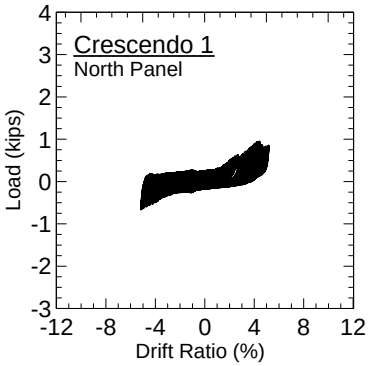

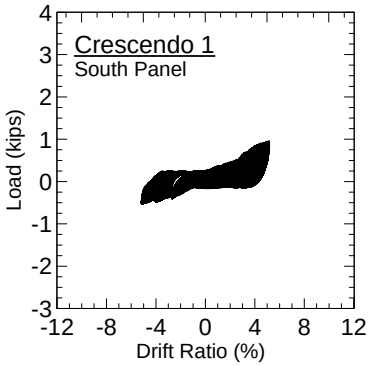

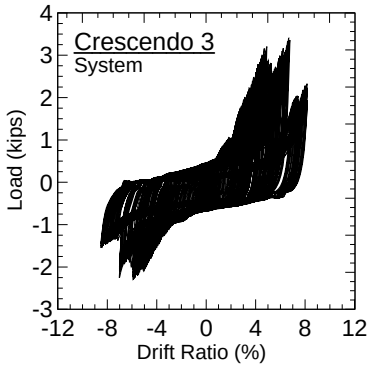

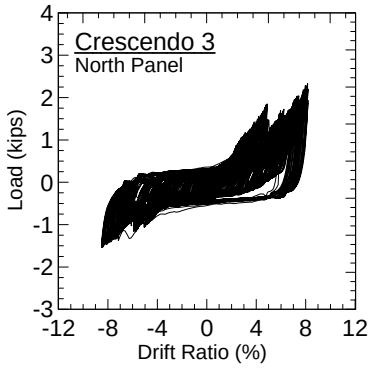

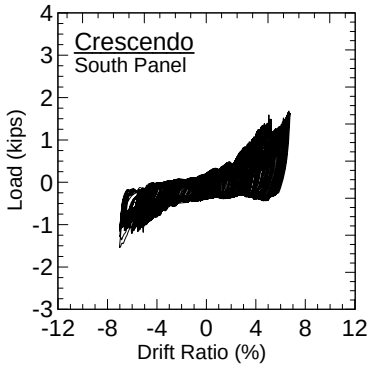

FEMA 461 Load Protocol Curves

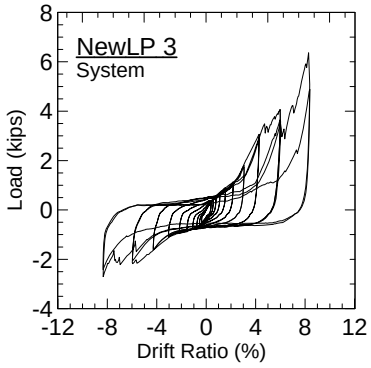

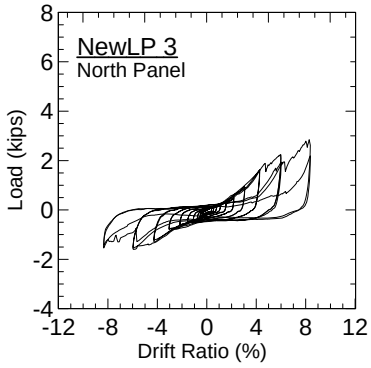

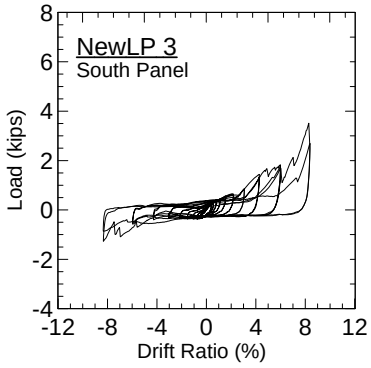

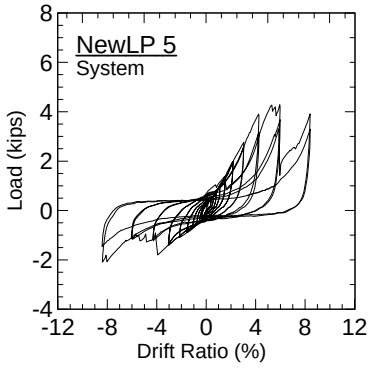

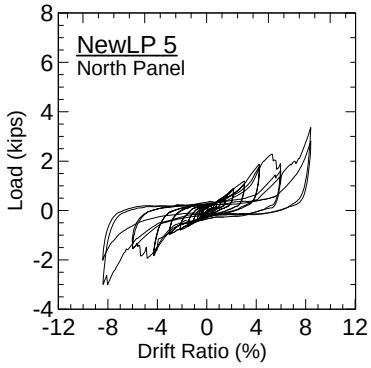

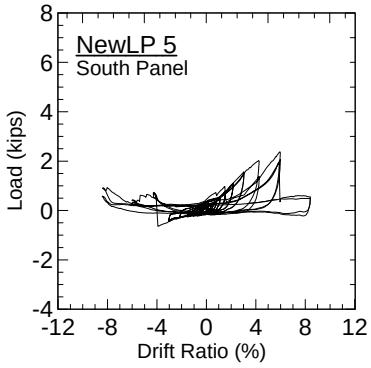

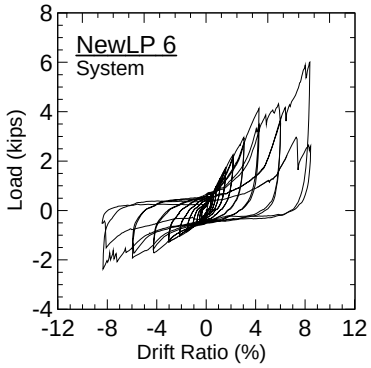

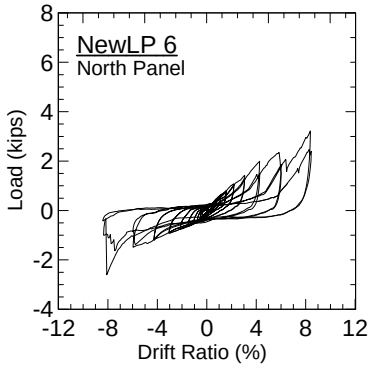

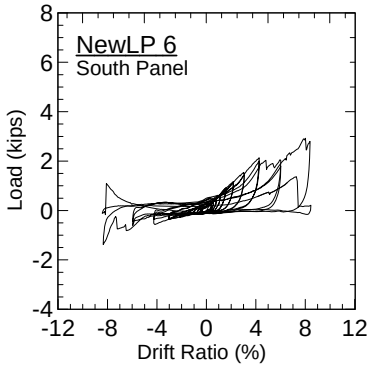

Aspect Ratio Curves

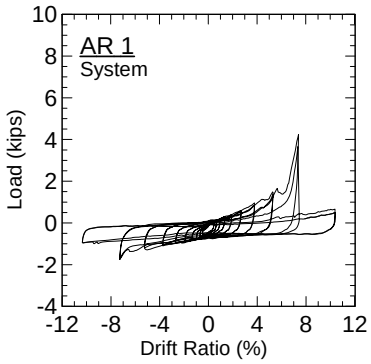

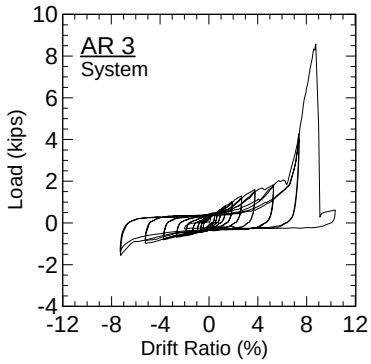

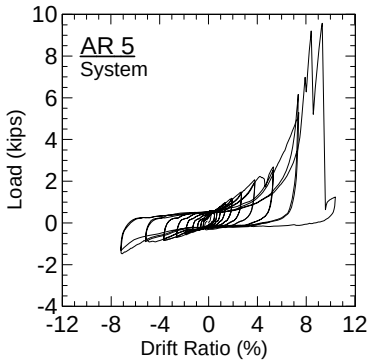

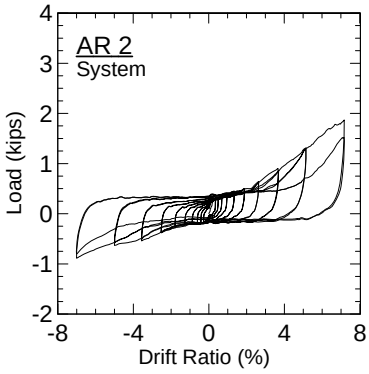

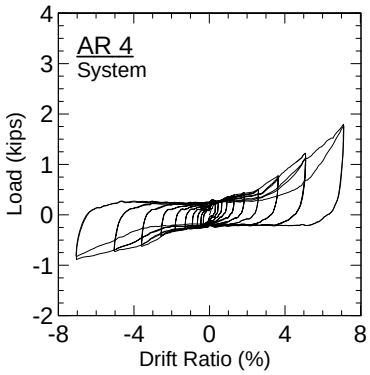

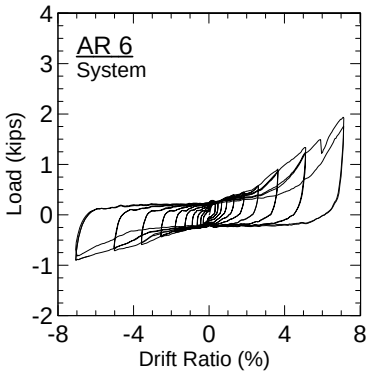

Mid-Rise Load Protocol Curves

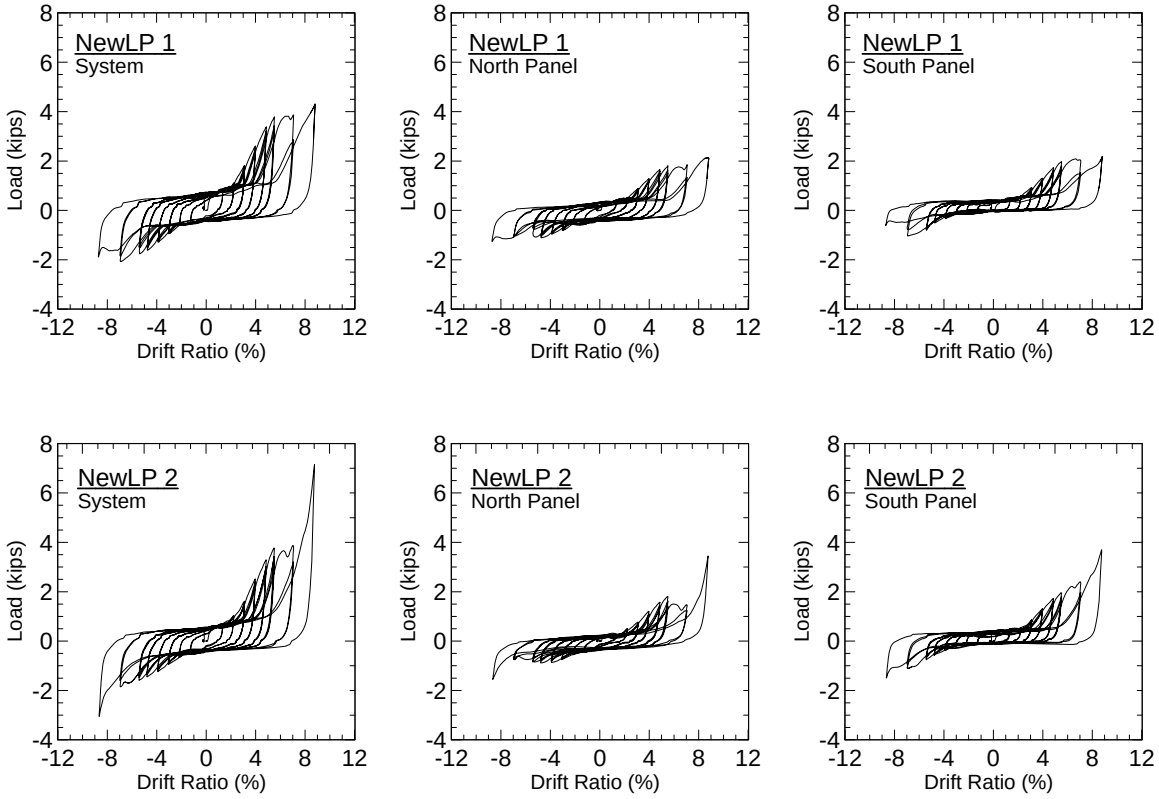

Low-Rise Load Protocol Curves

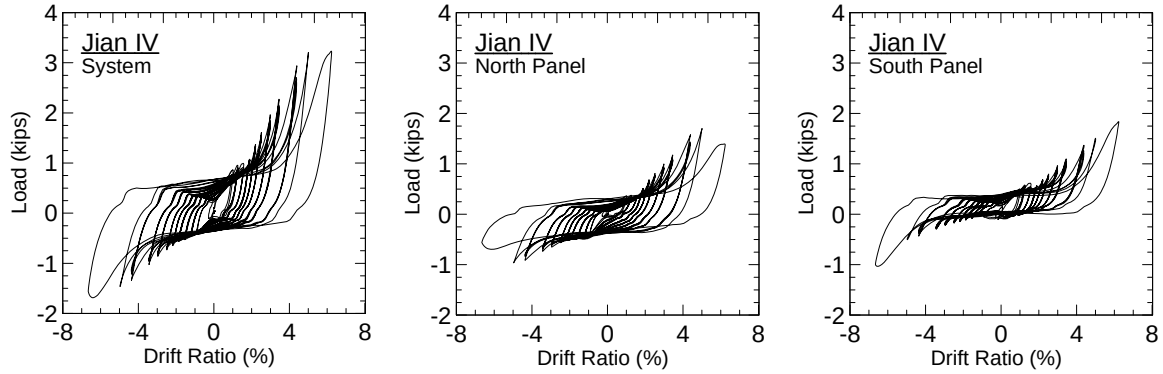

Appendix C:

Summary of Previous Experiments

Experiment condition					Experiment results			
					Glass cracking		(Glass fallout)	
Glass size (ft)	Glass thick (inch)	Glass type	Load type	Specimen number	Drift (inch)	Drift ratio	Drift (inch)	Drift ratio
Memari et al (2003) - Test Objectives: All insulating glass unit (IGU) were manufactured with an annealed monolithic pane and a laminated pane with an argon fill and an anodized aluminum spacer between the panes. The annealed inside pane were constant. The laminated pane parameters are varied.								
5X6	1.013	IGU, 1/4in AN* inner pane; 0.5in space; laminated glass outer pane (1/8in AN, 0.03in PVB interlayer, 1/8in AN)	crescendo	6	2.88	3.66%	5.16	6.55%
5X6	1.043	IGU, 1/4in AN inner pane; 0.5in space; laminated glass outer pane (1/8in AN, 0.06in PVB interlayer, 1/8in AN)	crescendo	6	2.96	3.76%	4.74	6.02%
5X6	1.197	IGU, 1/4in AN inner pane; 0.5in space; laminated glass outer pane (1/4in AN, 0.03in PVB interlayer, 1/4in AN)	crescendo	6	3.04	3.86%	5.45	6.92%
5X6	1.038	IGU, 1/4in AN inner pane AN; 0.5in space; laminated glass outer pane (1/8in HS, 0.06in PVB interlayer, 1/8in HS)	crescendo	6	3.1	3.94%	5.71	7.25%
5X6	1.253	IGU, 1/4in AN inner pane; 0.5in space; laminated glass outer pane (1/4in HS, 0.06in PVB interlayer, 1/4in HS)	crescendo	5	2.85	3.62%	5.75	7.30%
5X6	1.238	IGU, 1/4in AN inner pane; 0.5in space; laminated glass outer pane (1/4in FT, 0.06in PVB interlayer, 1/4in FT)	crescendo	6	3.29	4.18%	5.51	7.00%
5X6	0.275	laminated glass unit, 1/8in AN, 0.03in PVB interlayer, 1/8in AN	crescendo	6	N/A		3.22	4.09%
Memari et al (2004) - Test Objectives: To study the glass fitted with anchored pet film								
5X6	0.25	clear annealed monolithic glass, with film (edge grip)	crescendo	2	2.6	3.30%	4.7	5.97%
5X6	0.25	clear annealed monolithic glass, with film (side anchor)	crescendo	2	1.4	1.78%	3.9	4.95%
5X6	0.25	clear annealed monolithic glass, with film (top anchor)	crescendo	2	1.8	2.29%	3.1	3.94%
Memari et al (2006) - Test Objectives: To study glass panels with different rounded corners								
5X6	0.25	AN with 0 in radius corner, cut edge finish, cut corner finish	crescendo	6	1.54	1.92%	1.75	2.18%
5X6	0.25	AN with 1/2 in radius corner, cut edge finish, ground corner finish	crescendo	4	2.19	2.73%	2.31	2.88%
5X6	0.25	AN with 3/4 in radius corner, cut edge finish, ground corner finish	crescendo	3	2	2.49%	2.17	2.70%
5X6	0.25	AN with 1 in radius corner, cut edge finish, ground corner finish	crescendo	2	1.88	2.34%	2	2.49%
5X6	0.25	AN with 3 in radius corner, cut edge finish, ground corner finish	crescendo	1	1.75	2.18%	2	2.49%
5X6	0.25	AN with 1 in radius corner, seamed edge finish, ground corner finish	crescendo	3	2.92	3.64%	3.08	3.83%
5X6	0.25	AN with 3/4 in radius corner, flat polish edge and corner finish	crescendo	1	1.75	2.18%	2.5	3.11%
5X6	0.25	AN with 1 in radius corner, flat polish edge and corner finish	crescendo	1	2	2.49%	2.5	3.11%
5X6	0.25	HS with 0 in radius corner, seamed edge and corner finish	crescendo	8	2.44	3.04%	2.53	3.15%
5X6	0.25	HS with 3/4 in radius corner, flat polish edge and corner finish	crescendo	2	3.63	4.52%	3.63	4.52%
5X6	0.25	FT with 0 in radius corner, seamed edge and corner finish	crescendo	7	2.88	3.59%	2.88	3.59%
5X6	0.25	FT with 1 in radius corner, seamed edge finish, rough ground corner finish	crescendo	4	1.81	2.25%	1.81	2.25%
5X6	0.25	FT with 0 in radius corner, flat polish edge and corner finish	crescendo	3	3.25	4.05%	3.25	4.05%
5X6	0.25	FT with 1 in radius corner, flat polish edge and corner finish	crescendo	2	4.33	5.39%	4.33	5.39%

Experiment condition					Experiment results			
					Glass cracking		(Glass fallout)	
Glass size (ft)	Glass thick (inch)	Glass type	Load type	Specimen number	Drift (inch)	Drift ratio	Drift (inch)	Drift ratio
Memari et al (2007) - Test Objectives: To study structural silicone glazed mockups made up of three side-by-side glass panels								
5X6	0.25	AN monolithic (panel 1)	crescendo	2	2.63	3.27%	2.88	3.59%
5X6	0.25	AN monolithic (panel 2)	crescendo	2	3	3.74%	3.25	4.05%
5X6	0.25	AN monolithic (panel 3)	crescendo	2	2.88	3.59%	2.88	3.59%
5X6	0.25	FT monolithic (panel 1)	crescendo	2	4.5	5.60%	4.5	5.60%
5X6	0.25	FT monolithic (panel 2)	crescendo	2	4.5	5.60%	4.5	5.60%
5X6	0.25	FT monolithic (panel 3)	crescendo	2	3.75	4.67%	3.75	4.67%
5X6	0.125	AN laminate (panel 1)	crescendo	2	3.38	4.21%	4.13	5.14%
5X6	0.125	AN laminate (panel 2)	crescendo	2	3.88	4.83%	4.25	5.29%
5X6	0.125	AN laminate (panel 3)	crescendo	2	3.5	4.36%	4.25	5.29%
5X6	0.25	AN IGU (panel 1)	crescendo	2	5	6.23%	5.25	6.54%
5X6	0.25	AN IGU (panel 2)	crescendo	2	5	6.23%	5.25	6.54%
5X6	0.25	AN IGU (panel 3)	crescendo	2	5	6.23%	5.25	6.54%
Behr et al (1996) - Test Objectives: To test architectural glass								
5X6	0.25	Annealed monolithic (store front)	crescendo	12	3.02	4.23%	4.21	5.90%
5X6	0.25	Fully tempered monolithic	crescendo	16	3.98	5.57%	3.98	5.57%
5X6	0.25	Annealed Laminate	crescendo	12	5.71	8.00%	5.71	8.00%
5X6	1	Annealed insulating glass units	crescendo	12	4.6	6.44%	5.44	7.62%
5X6	1	Fully tempered insulating glass units	crescendo	12	5.01	7.02%	5.01	7.02%
Behr et al (1998) - Test Objectives: To test architectural glass								
5X6	0.25	Annealed monolithic (Cladding)	crescendo	6	1.97	2.80%	2.17	3.08%
5X6	0.25	Heat-strengthened monolithic	crescendo	5	3.39	4.82%	3.39	4.82%
5X6	0.25	Fully tempered monolithic	crescendo	5	2.95	4.19%	2.95	4.19%
5X6	0.25	Annealed laminated	crescendo	6	1.81	2.58%	5.59	7.95%
5X6	0.25	Annealed monolithic with 0.1mm PET film	crescendo	6	1.97	2.80%	3.98	5.66%
5X6	0.25	Heat-strengthened monolithic spandrel	crescendo	6	2.40	3.42%	2.48	3.53%
5X6	0.25	Heat-strengthened laminated	crescendo	6	2.13	3.02%	5.12	7.28%
5X6	1	Annealed insulating glass unit	crescendo	6	2.68	3.81%	3.07	4.37%
5X6	1	Heat-strengthened insulating glass units	crescendo	6	2.76	3.92%	2.76	3.92%
Bouwkamp (1960) - Test Objectives: Study the effect of sash material and panel attachment								
4X2	0.125	double-strength glass, aluminum sash, all around attachment of the sash to the boards, 1/4 clearance, soft putty	static	1	0.85	3.54%		
4X2	0.125	double-strength glass, aluminum sash, head-and-sill attachment of the sash to the boards, 1/4 clearance, soft putty	static	1	0.82	3.42%		
4X8	0.25	plate glass, aluminum sash, all around attachment of the sash to the boards, 1/4 clearance, soft putty	static	1	1.46	1.52%		

Experiment condition					Experiment results			
					Glass cracking		(Glass fallout)	
Glass size (ft)	Glass thick (inch)	Glass type	Load type	Specimen number	Drift (inch)	Drift ratio	Drift (inch)	Drift ratio
4X8	0.25	plate glass, aluminum sash, head-and-sill attachment of the sash to the boards, 1/4 clearance, soft putty	static	1	2.36	2.46%		
4X2	0.125	double-strength glass, steel sash, all around attachment of the sash to the boards, 3/8 clearance, soft putty	static	1	1.19	4.96%		
4X2	0.125	double-strength glass, steel sash, head-and-sill attachment of the sash to the boards, 3/8 clearance, soft putty	static	1	1.19	4.96%		
4X8	0.25	plate glass, steel sash, all around attachment of the sash to the boards, 3/8 clearance, soft putty	static	1	2.26	2.35%		
4X8	0.25	plate glass, steel sash, head-and-sill attachment of the sash to the boards, 3/8 clearance, soft putty	static	1	1.84	1.92%		
4X2	0.125	double-strength glass, wood sash, all around attachment of the sash to the boards, 1/4 clearance, soft putty	static	1	1.41	5.88%		
4X2	0.125	double-strength glass, wood sash, head-and-sill attachment of the sash to the boards, 1/4 clearance, soft putty	static	1	2	8.33%		
4X8	0.25	plate glass, wood sash, all around attachment of the sash to the boards, 1/4 clearance, soft putty	static	1	3.52	3.67%		
4X8	0.25	plate glass, wood sash, all around attachment of the sash to the boards, 1/4 clearance, soft putty	static	1	3.83	3.99%		
Bouwkamp (1960) - Test Objectives: Study of the effect of panel size, glass clearance and hardness of putty								
4X2	0.125	double-strength glass, aluminum sash, all around attachment of the sash to the boards, 1/4 clearance, soft putty	static	1	0.81	3.38%		
4X2	0.125	double-strength glass, aluminum sash, all around attachment of the sash to the boards, 1/2 clearance, soft putty	static	1	1.36	5.67%		
4X4	0.188	crystal glass, aluminum sash, all around attachment of the sash to the boards, 1/4 clearance, soft putty	static	1	1.09	2.27%		
4X4	0.188	crystal glass, aluminum sash, all around attachment of the sash to the boards, 1/2 clearance, soft putty	static	1	1.88	3.92%		
4X8	0.25	plate glass, aluminum sash, all around attachment of the sash to the boards, 1/4 clearance, soft putty	static	1	2.06	2.15%		
4X8	0.25	plate glass, aluminum sash, all around attachment of the sash to the boards, 1/2 clearance, soft putty	static	1	2.8	2.92%		
4X2	0.125	double-strength glass, aluminum sash, all around attachment of the sash to the boards, 1/4 clearance, hard putty	static	1	0.16	0.67%		
4X2	0.125	double-strength glass, aluminum sash, all around attachment of the sash to the boards, 1/2 clearance, hard putty	static	1	0.27	1.13%		

Experiment condition					Experiment results			
					Glass cracking		(Glass fallout)	
Glass size (ft)	Glass thick (inch)	Glass type	Load type	Specimen number	Drift (inch)	Drift ratio	Drift (inch)	Drift ratio
4X4	0.188	crystal glass, aluminum sash, all around attachment of the sash to the boards, 1/4 clearance, hard putty	static	1	0.48	1.00%		
4X4	0.188	crystal glass, aluminum sash, all around attachment of the sash to the boards, 1/2 clearance, hard putty	static	1	0.67	1.40%		
4X8	0.25	plate glass, aluminum sash, all around attachment of the sash to the boards, 1/4 clearance, hard putty	static	1	1.01	1.05%		
4X8	0.25	plate glass, aluminum sash, all around attachment of the sash to the boards, 1/2 clearance, hard putty	static	1	2.2	2.29%		
Bouwkamp (1960) - Test Objectives: Study the effect of subdivided window panels								
4X4	0.188	crystal glass, aluminum sash, panel subdivided horizontally, all around attachment of the sash to the boards, 1/4 clearance, hard putty	static	1	1.82	3.79%		
4X4	0.188	crystal glass, aluminum sash, panel subdivided horizontally, all around attachment of the sash to the boards, 1/2 clearance, soft putty	static	1	3.02	6.29%		
4X8	0.25	plate glass, aluminum sash, panel subdivided horizontally, all around attachment of the sash to the boards, 1/4 clearance, soft putty	static	1	4.31	4.49%		
4X8	0.25	aluminum sash, panel subdivided horizontally, all around attachment of the sash to the boards, 1/2 clearance, soft putty	static	1	6.06	6.31%		
4X4	0.188	crystal glass, aluminum sash, panel subdivided vertically, all around attachment of the sash to the boards, 1/4 clearance, soft putty	static	1	1.6	3.33%		
4X4	0.188	crystal glass, aluminum sash, panel subdivided vertically, all around attachment of the sash to the boards, 1/2 clearance, soft putty	static	1	2.76	5.75%		
4X8	0.25	plate glass, aluminum sash, panel subdivided vertically, all around attachment of the sash to the boards, 1/4 clearance, soft putty	static	1	2.49	2.59%		
4X8	0.25	plate glass, aluminum sash, panel subdivided vertically, all around attachment of the sash to the boards, 1/2 clearance, soft putty	static	1	5.41	5.64%		
Bouwkamp (1960) - Test Objectives: Study the effect of the repeated load								
4X2ft	0.125	double-strength glass, aluminum sash, all around attachment of the sash to the boards, 1/4 clearance, fuller steel DAP 1012 putty	repeated load	1	0.8	3.33%		
4X2ft	0.125	double-strength glass, aluminum sash, all around attachment of the sash to the boards, 1/2 clearance, fuller steel DAP 1012 putty	repeated load	1	1.3	5.42%		

Experiment condition					Experiment results			
					Glass cracking		(Glass fallout)	
Glass size (ft)	Glass thick (inch)	Glass type	Load type	Specimen number	Drift (inch)	Drift ratio	Drift (inch)	Drift ratio
Bouwkamp (1960) - Test Objectives: Study the effect of the impact load								
4X4	0.188	crystal glass, aluminum sash, all around attachment of the sash to the boards, 1/4 clearance, soft putty	impact load	1	No failure. The energy of impact was about twice the maximum energy required to produce failure under static loads. This indicated that a panel under an impact load can stand a higher load before failure occurs than a corresponding panel under a static load.			
4X4	0.188	crystal glass, aluminum sash, all around attachment of the sash to the boards, 1/2 clearance, soft putty	impact load	1				
4X4	0.188	crystal glass, aluminum sash, all around attachment of the sash to the boards, 1/2 clearance, hard putty	impact load	1				
Sakamoto et al (1984) - Test Objectives: Glass with adhesive film in an full scale building model test					1.26	1.67%		

*AN= Annealed
FT= Fully Tempered
HS= Heat Strengthened
IGU= Insulating Glass Unit

Appendix D:

Specifications

Product Description

CLEAR GLASS is a transparent float glass which has a true flat parallel plane surface of subtle brilliance and reflectivity. Transparency, clarity, flatness and longevity are only a few of its distinguishing characteristics.

[illegible] Information

ASTM Specification C1036.

For additional technical information contact: Flat Glass Technical Services, Phone (412) 434-2858.

[illegible] Physical** Properties

Hardness

a. Moh's scale (scratch hardness): diamond, 10; sapphire, 9; etc. float glass approximately 6

b. Knoop Hardness Number (indentation hardness) indenter load – 500 grams 470

Poisson's Ratio 0.22

Density .....156 lb/ft³ .....2.5 g/cm³

Modulus of Elasticity (Young's).....10,600,000 psi .....73.1 GPa

Tensile Strength (determined as Modulus of Rupture, ultimate) .....6,000 lbs/sq. in .....41.4 M Pa

Specific Gravity at 70°F (21°C) 2.5

Approximate Weight.....

Per sq. foot	Per sq. meter
3/32 in = 1.2 lbs.	2.5mm = 6.3 kg.
1/8 in = 1.6 lbs.	3.3mm = 8.3 kg.
5/32 in = 2.0 lbs.	4mm = 10.0 kg.
3/16 in = 2.4 lbs.	5mm = 12.5 kg.
1/4 in = 3.3 lbs.	6mm = 15.0 kg.
5/16 in = 4.1 lbs.	8mm = 20.0 kg.
3/8 in = 4.9 lbs.	10mm = 25.0 kg.
1/2 in = 6.4 lbs.	12mm = 30.0 kg.

[illegible] Physical** Properties

Hemispherical Emissivity at 0°-150°F (–18°-66°C) 0.84

Expansion Coefficient, linear in the range 25°C to 300°C (per degree C) .....8.6x10⁻⁶ (per degree F).....4.8x10⁻⁶

Specific heat at 32°-212°F (0°-100°C) 0.205

Thermal Conductivity (k) at 120°F (49°C) measured for a thickness of one inch. Btu per hour per square foot per °F .....6.5 Watt per square meter per °K 36.9

Softening point.....1333°F (723°C)

Annealing point .....1011°F (544°C)

Strain point .....939°F (504°C)

[illegible] Availability Table And Performance Values**

Glass Thickness		Transmittance²				Reflectance²		U-Value³ (BTU/hr/sq. ft./°F)		R-Value³ (Watts/sq. meter • °K)		Shading Coefficient⁴	Solar Heat Gain Coefficient⁵
Inches	mm	Ultraviolet %	Visible %	Infrared %	Total Solar Energy %	Visible %	Total Solar Energy %	Winter	Summer	Winter	Summer		
3/32	2.5	82	90	82	87	7	8	1.13	1.16	6.42	6.59	1.01	0.87
1/8	3.0	80	90	79	85	7	8	1.12	1.15	6.36	6.53	1.00	0.86
5/32	4.0	79	90	79	84	7	8	1.11	1.14	6.30	6.47	0.99	0.85
3/16	5.0	76	89	73	81	7	8	1.11	1.14	6.30	6.47	0.97	0.83
1/4	6.0	74	88	72	79	8	7	1.10	1.13	6.25	6.42	0.96	0.83
5/16	8.0	71	88	63	75	8	7	1.09	1.12	6.19	6.36	0.94	0.81
3/8	10.0+	69	88	58	72	8	7	1.08	1.11	6.13	6.30	0.91	0.78
1/2	12.0+	66	86	50	67	8	7	1.06	1.09	6.02	6.19	0.87	0.75

+ indicates thickness with limited availability. Contact nearest PPG Zone Office for specific details.

Availability and Performance Footnotes

1. Figures may vary due to manufacturing tolerances.
2. Transmittance and reflectance values based on spectrophotometric measurements and energy distribution of solar radiation.
3. U-Value (k-Value) is the overall coefficient of heat transmission or heat flow measured in BTU/Hour/Square Foot/°F (watts/meter²•°K). Lower U-Values indicate better insulating performance. Winter nighttime U-Values are calculated using an outdoor air temperature of 0°F (-17.8°C), indoor air temperature of 70°F (21°C), outdoor air velocity of 15 mph (24 km/h), indoor air velocity of 0 mph (0 km/h) and a solar intensity of 0 BTU/Hour/Square Foot (0 w/m²). Summer daytime U-Values are calculated using an outdoor air temperature of 89°F (32°C), indoor air temperature of 75°F (24°C), outdoor air velocity 7.5 mph (12 kph), indoor air velocity of 0 mph (0 kph), and a solar intensity of 248 BTU/Hour/Square Foot (790 w/m²).
4. Shading coefficient is the ratio of the total amount of solar energy that passes through a glass relative to ⅛" (3.0mm) thick clear glass under the same design conditions. It includes both solar energy transmitted directly plus any absorbed solar energy re-radiated or convected. Lower shading coefficient values indicate better performance in reducing summer heat gain.

   Shading coefficients at 89°F (32°C), outdoor air velocity of 7.5 mph (12 km/h), indoor air temperature of 75°F (24°C), indoor air velocity of 0 mph (0 km/h) and solar intensity of 248 BTU/Hour/Square Foot (790 w/m²).
5. Solar heat gain coefficient represents the solar heat gain through the glass relative to the incident solar radiation. It is equal to 86% of the shading coefficient.
6. Standard maximum size for ¾ in. (2.5mm) glass is 72" x 130" (1828mm x 3302mm). Standard maximum size for ⅛ in. (3.3mm) glass is 96" x 130" (2438mm x 3302mm). Standard maximum size for all other thicknesses is 130" x 204" (3302mm x 5182mm). For sizes over standard maximum and minimum sizes, contact nearest PPG Zone Office for specific details.

Appendix E:

Calculations

Source Data

Input Filtered Data

$Fdata_a := READPRN("NewLP 5 - WF6a_WF6b_Filtered_Data_a.prn")$

$Fdata_b := READPRN("NewLP 5 - WF6a_WF6b_Filtered_Data_b.prn")$

$file := augment(Fdata_a, Fdata_b)$ Combine file into original Configuration

Check Number of Rows and Columns

$cfile := cols(file)$ Number of Columns within "file" $cfile = 75$

$rfile := rows(file)$ Number of Rows within "file" $rfile = 5.548 \times 10^3$

Define Channels

Create time index - seconds + miliseconds

$t := (file^{\langle 0 \rangle})$ $millisecond := \frac{file^{\langle 1 \rangle}}{1000}$ $t := (t - t_{0,0}) + millisecond$ $time := t$

Define and zero Table Acceleration

$tableaccel := file^{\langle xx \rangle}$ $unfilttableaccel := tableaccel$ $tableaccel := tableaccel - tableaccel_{0,0}$

Define and zero Table displacement

$tabledisp := file^{\langle 74 \rangle}$ $unfilttabledisp := tabledisp$ $tabledisp := tabledisp - tabledisp_{0,0}$

Define Acceleration Channels

$AC1 := file^{\langle 3 \rangle}$ $AC5 := file^{\langle 7 \rangle}$

$AC2 := file^{\langle 4 \rangle}$ $AC6 := file^{\langle 8 \rangle}$

$AC3 := file^{\langle 5 \rangle}$ $AC7 := file^{\langle 9 \rangle}$

$AC4 := file^{\langle 6 \rangle}$ $AC8 := file^{\langle 10 \rangle}$

Define Displacement Channels

$D02 := file^{\langle 11 \rangle}$ $D11 := file^{\langle 18 \rangle}$

$D03 := file^{\langle 12 \rangle}$ $D12 := file^{\langle 19 \rangle}$

$D04 := file^{\langle 13 \rangle}$ $D13 := file^{\langle 20 \rangle}$

$D05 := file^{\langle 14 \rangle}$ $D15 := file^{\langle 21 \rangle}$

$D06 := file^{\langle 15 \rangle}$ $D16 := file^{\langle 22 \rangle}$

$D09 := file^{\langle 16 \rangle}$ $D17 := file^{\langle 23 \rangle}$

$D10 := file^{\langle 17 \rangle}$ $D18 := file^{\langle 24 \rangle}$

Define Rotational Channels

IN1 := file⟨25⟩

IN2 := file⟨26⟩

Define Load Cell Channels

load := file⟨27⟩·kip

Define Strain Gauge Channels

SG01 := file⟨28⟩

SG02 := file⟨29⟩

SG03 := file⟨30⟩

SG04 := file⟨33⟩

SG04A := file⟨32⟩

SG05 := file⟨31⟩

SG05A := file⟨34⟩

SG06 := file⟨36⟩

SG07 := file⟨35⟩

SG08 := file⟨37⟩

SG09 := file⟨38⟩

SG09A := file⟨39⟩

SG10 := file⟨40⟩

SG10A := file⟨41⟩

SG11 := file⟨42⟩

SG12 := file⟨43⟩

SG13 := file⟨44⟩

SG14 := file⟨45⟩

SG14A := file⟨46⟩

SG15 := file⟨47⟩

SG15A := file⟨48⟩

SG16 := file⟨49⟩

SG17 := file⟨50⟩

SG18 := file⟨51⟩

SG19 := file⟨52⟩

SG20 := file⟨53⟩

SG21 := file⟨54⟩

SG22 := file⟨55⟩

SG23 := file⟨56⟩

SG23A := file⟨57⟩

SG24 := file⟨58⟩

SG24A := file⟨59⟩

SG25 := file⟨60⟩

SG26A := file⟨61⟩

SG27 := file⟨62⟩

SG27A := file⟨63⟩

SG28 := file⟨64⟩

SG29 := file⟨65⟩

SG29A := file⟨66⟩

SG30 := file⟨67⟩

SG30A := file⟨68⟩

SG31 := file⟨69⟩

SG32 := file⟨70⟩

SG33 := file⟨71⟩

SG34 := file⟨72⟩

SG35 := file⟨73⟩

SG36 := file⟨74⟩

SG37 := file⟨▮⟩

SG38 := file⟨75⟩

SG39 := file⟨76⟩

SG40 := file⟨77⟩

SG41 := file⟨78⟩

SG42 := file⟨▮⟩

SG43 := file⟨79⟩

SG44 := file⟨80⟩

SG45 := file⟨81⟩

SG46 := file⟨82⟩

SG47 := file⟨▮⟩

SG48 := file⟨83⟩

SG49 := file⟨84⟩

SG50 := file⟨85⟩

SG51 := file⟨86⟩

Define Strain Gauge Channels continued

SG52 := file⟨⟩
SG53 := file⟨87⟩
SG54 := file⟨88⟩
SG55 := file⟨89⟩
SG56 := file⟨90⟩
SG57 := file⟨⟩
SG58 := file⟨91⟩
SG59 := file⟨92⟩
SG60 := file⟨93⟩
SG61 := file⟨94⟩
SG62 := file⟨⟩
SG63 := file⟨95⟩

SG64 := file⟨96⟩
SG65 := file⟨97⟩
SG66 := file⟨98⟩
SG67 := file⟨⟩
SG68 := file⟨99⟩
SG69 := file⟨100⟩
SG70 := file⟨101⟩
SG71 := file⟨102⟩
SG72 := file⟨⟩
SG73 := file⟨103⟩
SG74 := file⟨104⟩

NOTE:

$SG03 := -1 \cdot SG19$ SG03 is bad... therefore SG03 = -SG19

Convert Strain to Forces

FOR SGs measuring axial plus moment (mounted TOP and/or BOTTOM)

$E := 29000\ ksi$ Modulus of Elasticity for steel

$A := (0.25 \cdot 4) \cdot in^2$ Area of steel for Location A

$$F\_SG06 := \frac{SG06 \cdot E \cdot A}{10^6} \qquad F\_SG29 := \frac{SG29 \cdot E \cdot A}{10^6}$$

$$F\_SG09 := \frac{SG09 \cdot E \cdot A}{10^6} \qquad F\_SG23 := \frac{SG23 \cdot E \cdot A}{10^6}$$

FOR SGs measuring axial (not at lap joints) or in very low moment locations - close to pins

$E := 29000 \cdot ksi$ Modulus of Elasticity for steel

$A := 3.37 \cdot in^2$ Area of steel for Location A

$$F\_SG09A := \frac{SG09A \cdot E \cdot A}{10^6} \qquad F\_SG33 := \frac{SG33 \cdot E \cdot A}{10^6} \qquad F\_SG01 := \frac{SG01 \cdot E \cdot A}{10^6}$$

$$F\_SG29A := \frac{SG29A \cdot E \cdot A}{10^6} \qquad F\_SG34 := \frac{SG34 \cdot E \cdot A}{10^6} \qquad F\_SG04 := \frac{SG04 \cdot E \cdot A}{10^6}$$

$$F\_SG26A := \frac{SG26A \cdot E \cdot A}{10^6} \qquad F\_SG19 := \frac{SG19 \cdot E \cdot A}{10^6} \qquad F\_SG12 := \frac{SG12 \cdot E \cdot A}{10^6}$$

$$F\_SG23A := \frac{SG23A \cdot E \cdot A}{10^6} \qquad F\_SG20 := \frac{SG20 \cdot E \cdot A}{10^6} \qquad F\_SG14A := \frac{SG14A \cdot E \cdot A}{10^6}$$

$$F\_SG14 := \frac{SG14 \cdot E \cdot A}{10^6} \qquad F\_SG17 := \frac{SG17 \cdot E \cdot A}{10^6}$$

FOR SGs measuring axial (at lap joints) or in very low moment locations - close to pins

$E := 29000 \cdot ksi$ Modulus of Elasticity for steel

$A := [3.37 + (0.25 \cdot 4) \cdot 2]in^2$ Area of steel for Location A

$$F\_SG16 := \frac{SG16 \cdot E \cdot A}{10^6} \qquad F\_SG21 := \frac{SG21 \cdot E \cdot A}{10^6}$$

$$F\_SG11 := \frac{SG11 \cdot E \cdot A}{10^6} \qquad F\_SG31 := \frac{SG31 \cdot E \cdot A}{10^6}$$

$$F\_SG08 := \frac{SG08 \cdot E \cdot A}{10^6} \qquad F\_SG28 := \frac{SG28 \cdot E \cdot A}{10^6}$$

$$F\_SG03 := \frac{SG03 \cdot E \cdot A}{10^6} \qquad F\_SG25 := \frac{SG25 \cdot E \cdot A}{10^6}$$

FOR SGs measuring axial (transverse direction) or in very low moment locations - close to pins

$E := 29000 \cdot ksi$ Modulus of Elasticity for steel

$A := .25 \cdot 4 \cdot 2 \cdot in^2$ Area of steel for Location A

$$F\_SG02 := \frac{SG02 \cdot E \cdot A}{10^6} \qquad F\_SG18 := \frac{SG18 \cdot E \cdot A}{10^6} \qquad F\_SG10A := \frac{SG10A \cdot E \cdot A}{10^6}$$

$$F\_SG05 := \frac{SG09 \cdot E \cdot A}{10^6} \qquad F\_SG30 := \frac{SG30 \cdot E \cdot A}{10^6} \qquad F\_SG30A := \frac{SG30A \cdot E \cdot A}{10^6}$$

$$F\_SG07 := \frac{SG09 \cdot E \cdot A}{10^6} \qquad F\_SG27 := \frac{SG27 \cdot E \cdot A}{10^6} \qquad F\_SG27A := \frac{SG27A \cdot E \cdot A}{10^6}$$

$$F\_SG10 := \frac{SG10 \cdot E \cdot A}{10^6} \qquad F\_SG24 := \frac{SG24 \cdot E \cdot A}{10^6} \qquad F\_SG24A := \frac{SG24A \cdot E \cdot A}{10^6}$$

$$F\_SG13 := \frac{SG13 \cdot E \cdot A}{10^6} \qquad F\_SG32 := \frac{SG32 \cdot E \cdot A}{10^6}$$

$$F\_SG15 := \frac{SG15 \cdot E \cdot A}{10^6} \qquad F\_SG22 := \frac{SG22 \cdot E \cdot A}{10^6}$$

Compute Force Per Panel

$D_{avg} := \left(\frac{D17 \cdot in + D18 \cdot in}{2} \right)$ Average the displacement gauges at bottom of beam

$E := 29000 \cdot ksi$ Modulus of Elasticity for Steel

$L := 136.5 \cdot in$ Length of beam member

Compute Weighted Moment of Inertia

$I_A := 16.26 \cdot in^4$ Section A-A Moment of Inertia

$L_A := 91 \cdot in$ Section A-A Total Length

$I_B := 7.80 \cdot in^4$ Section B-B Moment of Inertia

$L_B := 45.5 \cdot in$ Section B-B Total Length

$I_{wa} := \frac{I_A \cdot L_A + I_B \cdot L_B}{L}$ Weighted Average Moment of inertia $I_{wa} = 13.44\ in^4$

Load Distribution on North Panel per timestep

$$F_{north} := \left| \begin{array}{l} \text{for } i \in 0 .. rows(D_{avg}) - 1 \\ \quad F_{north_{i,0}} \leftarrow \left(load_{i,0} - \frac{D_{avg_{i,0}} \cdot 48 \cdot E \cdot 2 \cdot I_{wa}}{L^3} \right) \cdot \frac{1}{2} \\ F_{north} \end{array} \right.$$

Force on north panel equals one half the total load minus the load required to bend the member to recorded dispacement

Load Distribution on South Panel per timestep

$F_{south} + F_{north} := load$ Therefore $F_{south} := load - F_{north}$

Percent Load Distribution Panels per timestep

$$\%North := \frac{F_{north}}{load + .0000000000000001 kip}$$

$$\%South := \frac{F_{south}}{load + .00000000000001 kip}$$

Output Files for Plotting in Grapher

Output Force Per Panel Information

PCTNorth := augment(%Drift, %North)

PCTSouth := augment(%Drift, %South)

$$FNorth := augment\left(\%Drift, F_{north} \cdot \frac{1}{kip}\right)$$

$$FSouth := augment\left(\%Drift, F_{south} \cdot \frac{1}{kip}\right)$$

Convert F_{north} and F_{south} to unitless for augmentation

export := WRITEPRN("FNorth" , FNorth)

export := WRITEPRN("FSouth" , FSouth)

export := WRITEPRN("PCTNorth" , PCTNorth)

export := WRITEPRN("PCTSouth" , PCTSouth)

Output Glass Rotation Information

Glassrotation := augment(%Drift, IN1·−1)

export := WRITEPRN("Glass rotation" , Glassrotation)

NewLP 5 - WF06a_WF06b

System Load (kips) vs. System Drift (%)

(Load from load cell)

$$\text{Window\_Deflection} := D03 \cdot in \qquad \%Drift := \frac{\text{Window\_Deflection}}{64.5 \cdot in} \cdot 100$$

$$\text{System\_Load} := load$$

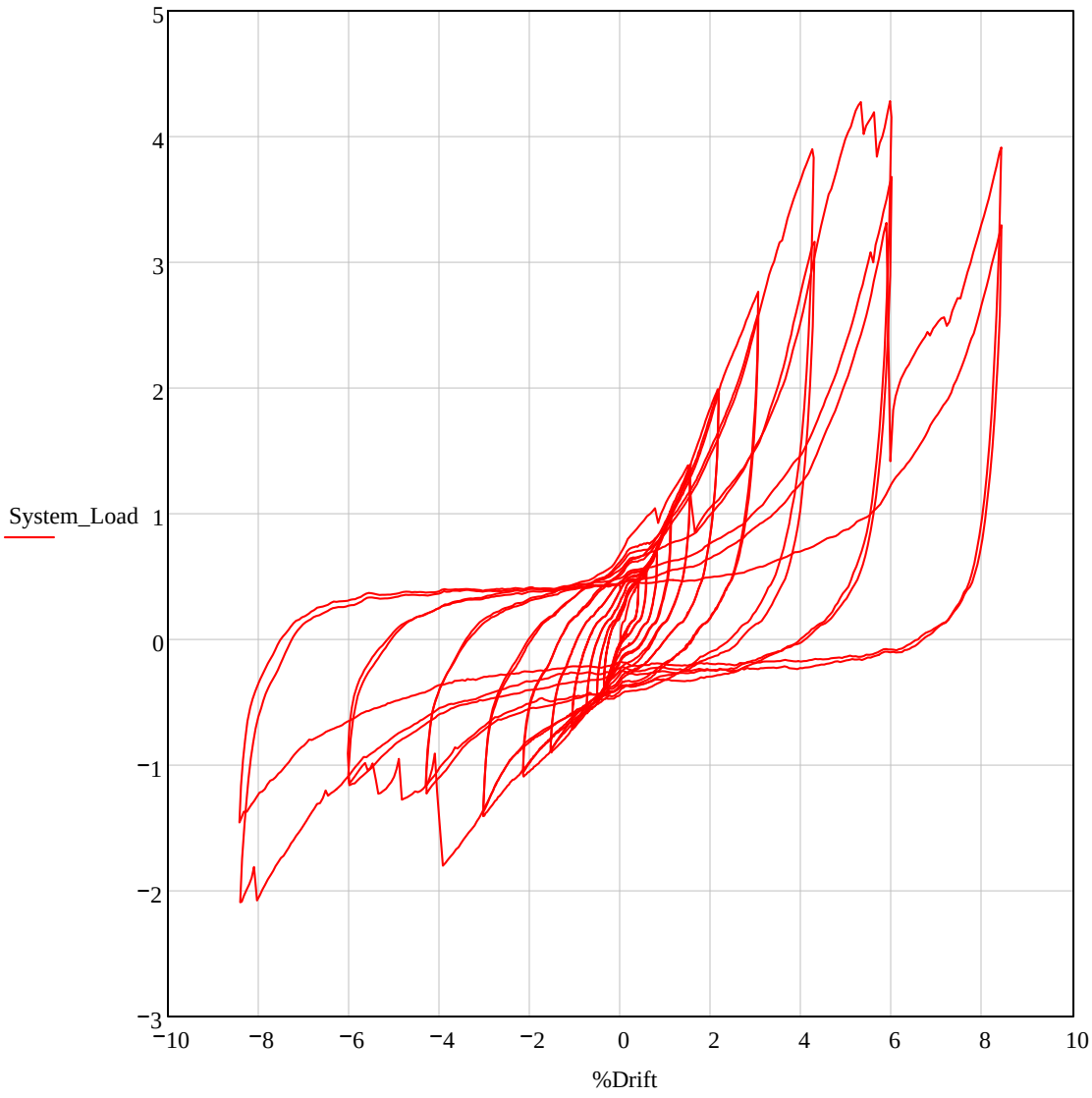

Force Distribution

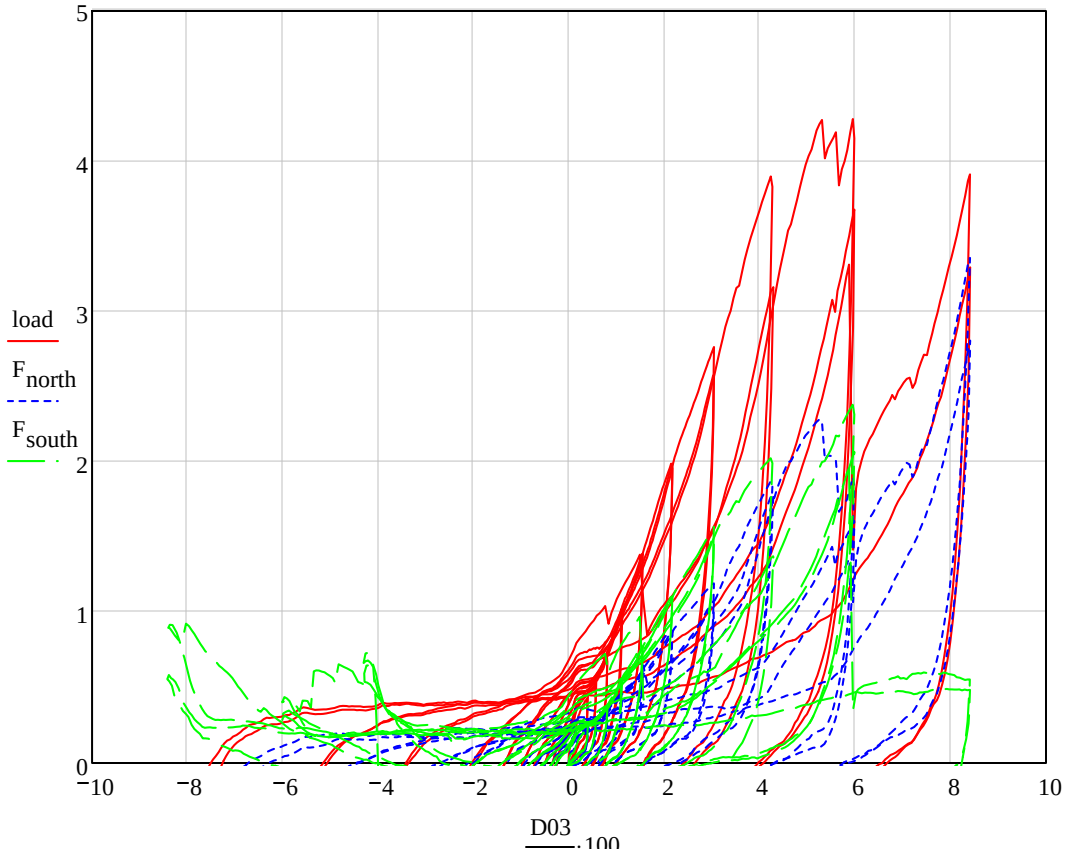

Percent Distribution

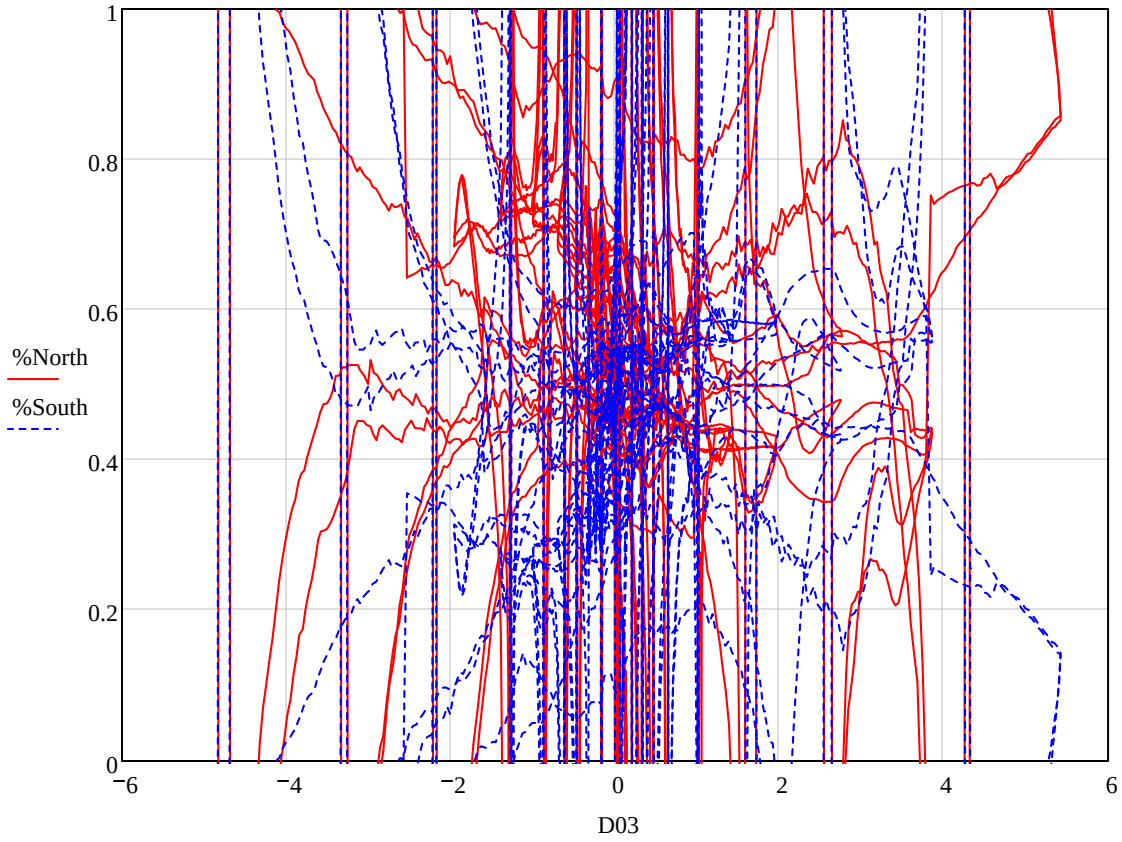

Glass Rotation

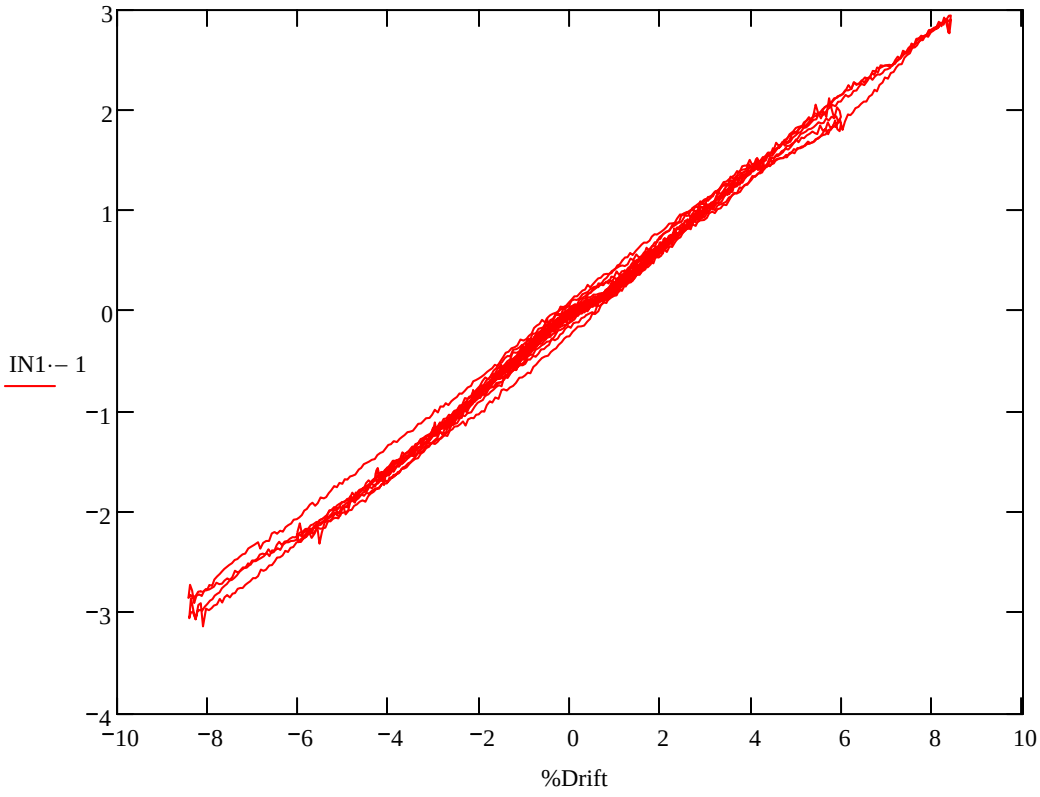

Critical Buckling Calculation - Full Scale

Geometry

$l_a := 58in$ Length of side A

$l_b := 58in$ Length of side B

$l_{diag} := \sqrt{l_a^2 + l_b^2}$ Diagonal length

$L_{unsup} := l_{diag} \cdot .45$ $L_{unsup} = 36.911\,in$ Assume Unsupported length as a function of Diagonal Length

$K := .75$

Column Effective Length Factor:
- Both ends pinned: 1.0
- Both ends fixed: 0.5
- One fixed other pined: 1/sqrt(2)
- One fixed other free: 2.0

Material Properties

$E := 10600000psi$ Modulous of Elasticity

Moment of inertia calculations

$I := \frac{(l_a) \cdot (0.25in)^3}{12}$ $I = 0.076\,in^4$ Moment of inertia

Critical Buckling Load

$L_b := \frac{\pi^2 \cdot E \cdot I}{(K \cdot L_{unsup})^2}$ $L_b = 10.31\,kip$

$\sin(45deg) \cdot L_b = 7.29\,kip$ convert to horizontal component

Critical Buckling Calculation - Small Scale

Geometry

$l_a := 12in$ Length of side A

$l_b := 12in$ Length of side B

$l_{diag} := \sqrt{l_a^2 + l_b^2}$ Diagonal length

$L_{unsup} := l_{diag} \cdot .75$ $L_{unsup} = 12.728\,in$ Assume Unsupported length as a function of Diagonal Length

$K := 1.0$

Column Effective Length Factor:
Both ends pinned: 1.0
Both ends fixed: 0.5
One fixed other pined: 1/sqrt(2)
One fixed other free: 2.0

Material Properties

$E := 10600000psi$ Modulous of Elasticity

Moment of inertia calculations

Need to take hexagon and convert into equivilant area rectangle

$I := \frac{(l_a) \cdot (0.25in)^3}{12}$ $I = 0.016\,in^4$ Moment of inertia

Critical Buckling Load

$L_b := \frac{\pi^2 \cdot E \cdot I}{(K \cdot L_{unsup})^2}$ $L_b = 10.09\,kip$

$\sin(45deg) \cdot L_b = 7.135\,kip$ convert to horizontal component